Volume 3, Issue 2, June 2023

COMPLEX ENGINEERING SYSTEMS

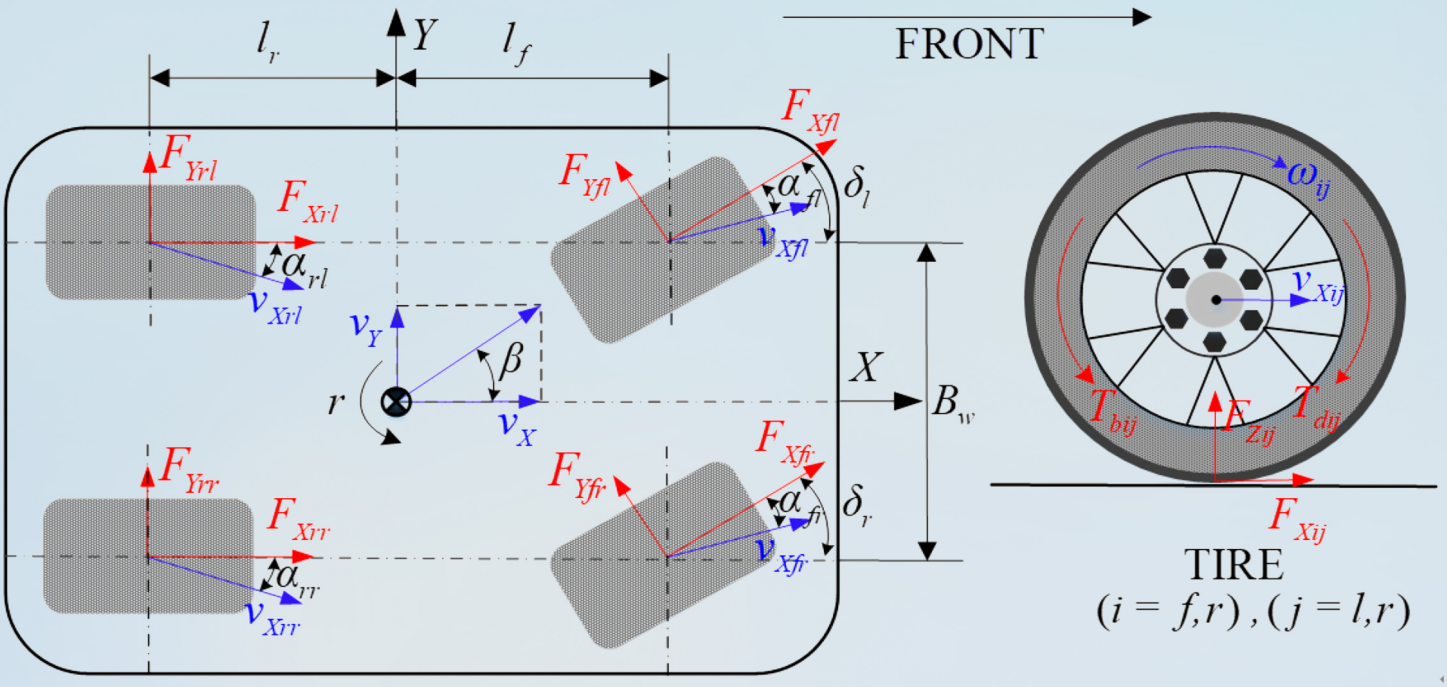

Nonlinear hierarchical control for four-wheel-independent-drive electric vehicle

Xiang Chen, Yuan Qu, Taowen Cui, Jin Zhao

Open Access
ISSN 2770-6249 (Online)
www.comengsys.com

EDITORIAL BOARD

GENERAL INFORMATION

About the Journal

Complex Engineering Systems (*CES*) are composed of a set of interconnected systems that their collective behaviors or properties are difficult to be predicted or managed. The context of *Complex Engineering Systems* (*CES*) is concerned with developing multi-component engineering systems, designs, or algorithms to exploit those unpredictable collective behaviors or properties. Complexity in engineering systems is in general manifested in component, product, system, interconnections of interacting subsystems or multidisciplinary system designs. In a broad sense, complexity is related to the expected amount of information may need to describe a dynamical system.

The primary objective of this journal is to provide a high-level platform for researchers and practitioners to disseminate theoretical- or engineering-oriented research output achievements within the context of *Complex Engineering Systems* (*CES*)that fosters knowledge sharing in different branches of engineering discipline. *Complex Engineering Systems* (*CES*) also publishes novel theoretical methods, algorithms, simulations, experiments, and case studies as applications of state-of-the-art research in *Complex Engineering Systems* (*CES*).

Information for Authors

Manuscripts should be prepared in accordance with Author Instructions.
Please check https://comengsys.com/pages/view/author_instructions for details.
All manuscripts should be submitted online at https://oaemesas.com/login?JournalId=comengsys.

Copyright

Permissions

Disclaimer

Publisher

OAE Publishing Inc.
245 E Main Street Ste 107, Alhambra CA 91801, USA
Website: www.oaepublish.com

Contacts

E-mail: editorial@comengsys.com
Website: https://comengsys.com/

Complex Engineering Systems

CONTENTS

Volume 3 / Issue 2 /

Research Article

Ma *et al. Complex Eng Syst* 2023;3:10
DOI: 10.20517/ces.2023.14

Complex Engineering Systems

Research Article

Open Access

Fixed-time integral sliding mode tracking control of a wheeled mobile robot

Ling Ma, Chenghu Wang, Cheng Ge, Hui Liu, Bo Li

Institute of Logistics Science and Engineering, Shanghai Maritime University, Shanghai 201306, China.

Correspondence to: Associate Prof. Bo Li, Institute of Logistics Science and Engineering, Shanghai Maritime University, Shanghai 201306, China. E-mail: libo@shmtu.edu.cn

How to cite this article: Ma L, Wang C, Ge C, Liu H, Li B. Fixed-time integral sliding mode tracking control of a wheeled mobile robot. *Complex Eng Syst* 2023;3:10. http://dx.doi.org/10.20517/ces.2023.14

Received: 1 May 2023 **First Decision:** 29 May 2023 **Revised:** 13 Jun 2023 **Accepted:** 20 Jun 2023 **Published:** 29 Jun 2023

Academic Editor: Mouquan Shen **Copy Editor:** Yanbing Bai **Production Editor:** Yanbing Bai

Abstract

This paper presents a fixed-time integral sliding mode control scheme for a nonholonomic wheeled mobile robot (WMR). To achieve the trajectory tracking mission, the dynamic model of a WMR is first transformed into a second-order attitude subsystem and a third-order position subsystem. Two novel continuous fixed-time disturbance observers are proposed to estimate the external disturbances of the two subsystems, respectively. Then, trajectory tracking controllers are designed for two subsystems by utilizing the reconstructed information obtained from the disturbance observers. Additionally, an auxiliary variable that incorporates the Gaussian error function is introduced to address the chattering problem of the control system. Finally, the proposed control scheme is validated by a wheeled mobile robotic experimental platform.

Keywords: Wheeled mobile robot, trajectory tracking, disturbance observer, fixed-time stability, integral sliding mode control

1. INTRODUCTION

During the past decades, the wheeled mobile robot (WMR) has attracted extensive attention as it is widely used in various fields. The research on the WMR mainly includes robot positioning, motion planning, and motion control, among which the motion control is a fundamental problem. There are three main parts of the motion control, including point stabilization, path planning, and trajectory tracking[1]. The trajectory

tracking control is a significant field in motion control, which has been studied extensively in recent years[2]. In practical engineering applications, a WMR is a highly coupled system with nonholonomic constraints and external disturbances. Hence, it is significant to design an anti-interference trajectory tracking control scheme with superior performance. At present, the design of the tracking controller of a WMR is mainly based on two types: one is to consider only the kinematic model[3], while the other is to design on the basis of kinematic and dynamic models[4]. The kinematic model-based control only considers the linear velocity and angular velocity as the control inputs. Compared with the kinematic model, the introduction of dynamic models can solve the external disturbance problem and the crucial nonholonomic constraint problem[5].

In[6], the system with nonhonolomic constraints was transformed into an extended chain system by coordinate transformation. On this basis, some scholars have designed the trajectory tracking control schemes by transforming the kinematic model of a WMR into a chain structure[7]. In practice, there is a problem called "excellent velocity tracking"[8] when designing a trajectory tracking controller only based on a kinematic system. Thus, it is more reasonable to take the force or torque as inputs of the control system instead of the speed. Meanwhile, external disturbances can be further taken into account. Nevertheless, the design process of the controller that simultaneously incorporates both the kinematic and dynamic models is complicated. The work of Zhai and Song[9] transformed the dynamic error system into second-order and third-order subsystems. And an intermediate variable related to the position error is introduced to tackle the problem of constructing a control method for a third-order system using the terminal sliding mode control. However, the aforementioned control schemes can only achieve finite time stability. It is noteworthy that the upper limit of the convergence time is unknown and dependent on the initial states of the control system. To overcome this problem, fixed-time stable control methods are proposed[10]. In reference[11], a new integral sliding mode-based control (ISMC) scheme was developed and applied on the dynamic model of the WMR to enable the WMR to track the desired trajectory in a fixed time. However, there exists the singularity problem, making the WMR unable to track the arbitrary trajectories and limiting its practical application when the desired angular velocity is zero.

In the practical motion environment, there are external disturbances and uncertainties that can deteriorate the performance of the control system. To cope with the problem, an observer-based control scheme is an efficient method with disturbance-rejection performance[12]. The traditional observers can only achieve asymptotic stability of the observation errors, whereas the finite time disturbance observers were designed to improve the performance of the observer[13]. On this basis, the fault-tolerant attitude control problem of spacecraft under external disturbances was solved by the introduction of a continuous finite-time observer[14], which also restrains the chattering phenomenon. Zhang *et al.* put forward a novel continuous practical fixed-time disturbance observer and applied it on a WMR, which can not only avoid the chattering problem but also improve the ability to attenuate disturbance[15]. Different from the work of Zhang, the Gaussian error function, which is sometimes called probability integral[16], can also be used to develop a control scheme that improves the chattering problem[17].

Motivated by the above discussions, an integral sliding mode-based fixed-time trajectory tracking control scheme is proposed by combining the kinematic model with the dynamic model of a WMR in this paper. **(1)** A continuous fixed-time disturbance observer using the Gaussian error function is proposed, which avoids the chattering problem and estimates the external disturbance of a WMR accurately. **(2)** An auxiliary variable incorporating variable exponential coefficients is introduced to simplify the design process of the controller for the third-order subsystem and avoid the singularity problem simultaneously. **(3)** The reliability and effectiveness of the designed control scheme are verified by a comparative experiment conducted on a wheeled mobile experimental platform.

2. PRELIMINARIES AND PROBLEM STATEMENT

2.1. Preliminaries

Lemma 1 [18] *Consider the following system as*

$$\dot{\boldsymbol{x}} = f(\boldsymbol{x}),\ \boldsymbol{x}(0) = \boldsymbol{x_0},\ \boldsymbol{x} \in R \tag{1}$$

If there exists a positive definite Lyapunov function $V(\boldsymbol{x})$*, which satisfies* $\dot{V}(\boldsymbol{x}) \leq -m_1 V^a(\boldsymbol{x}) - n_1 V^b(\boldsymbol{x}) + \varrho$*, where* m_1, n_1*, and* ϱ *are all positive constants.* $0 < a < 1, b > 1$ *are real numbers. Then the origin of the system (2) is fixed-time stable, and the settling time is bounded by* $t_1 \leq \frac{1}{m_1\vartheta(1-a)} + \frac{1}{n_1\vartheta(b-1)}$ *with* $0 < \vartheta < 1$.

Lemma 2 [16] *The Gaussian error function is defined as follows:*

$$\operatorname{erf}(x) = \frac{2}{\sqrt{\pi}} \int_0^x e^{-2t^2} \mathrm{dt} \tag{2}$$

where e is the natural constant. If $0 \leq x < 1$*, then the Gaussian error function will satisfy* $\frac{1}{2}x \leq \operatorname{erf}(x) \leq 2x$.

Lemma 3 [19] *For* $x \in \mathbf{R}$ *and* $\mu > 0$*, one gets the following chain of inequalities:* $x\tanh(\frac{x}{\mu}) < x\operatorname{erf}(\frac{x}{\mu}) < |x|$.

Lemma 4 [20] *The following inequality will hold* $|x| - \frac{\varepsilon}{\kappa} \leq x\tanh(\kappa x)$ *for any* $\kappa > 0$ *and for any* $\varepsilon \in \mathbf{R}$*, where* $\varepsilon = e^{-(\varepsilon+1)}$*. Then,* $\varepsilon = 0.2785$ *can be obtained.*

2.2. Dynamic model of WMR

A nonholonomic WMR system is shown in Figure 1. It consists of two balance wheels and two driving wheels, and the line between the balance wheels is perpendicular to the line between the driving wheels. The distance between the driving wheel and the barycentric coordinate is R, and r is the radius of the driving wheel. The position and attitude control is achieved by independent direct current motors, which provide the appropriate torques to the driving wheels. One assumes that the center of mass of the WMR coincides with the geometric center. Then, the dynamic model of the WMR is expressed in the form of[21]

$$\begin{cases} \dot{x} = v\cos\theta \\ \dot{y} = v\sin\theta \\ \dot{\theta} = \omega \\ J\dot{\omega} = u_1 + d_1 \\ m\dot{v} = u_2 + d_2 \end{cases} \tag{3}$$

with $u_1 = \frac{R}{r}(\tau_1 - \tau_2)$, and $u_2 = \frac{1}{r}(\tau_1 + \tau_2)$. τ_1 and τ_2 present the control torques. v and ω are the linear and angular velocities of the WMR, respectively. m denotes the mass, and J the moment of inertia. (x, y) is the actual coordinates. θ is the orientation of the vehicle counterclockwise from the positive direction of the X axis. $(\dot{x}, \dot{y}, \dot{\theta})$ denotes the motion of the WMR. d_1 and d_2 represent the external disturbances.

The reference trajectory is defined as

$$\begin{cases} \dot{x}_r = v_r\cos\theta_r \\ \dot{y}_r = v_r\sin\theta_r \\ \dot{\theta}_r = \omega_r \end{cases} \tag{4}$$

where x_r, y_r, and θ_r denote the position and attitude states of the virtual WMR, respectively.

Assumption 1: Suppose ω_r, $\dot{\omega}_r$, v_r, and $\dot{v}_r$ are satisfied with $|\omega_r| \leq \omega_{r_{\max}}$, $|\dot{\omega}_r| \leq \omega_{1_{\max}}$, $|v_r| \leq v_{r_{\max}}$, And $|\dot{v}_r| \leq v_{1_{\max}}$, where $\omega_{r_{\max}}$, $\omega_{1_{\max}}$, $v_{r_{\max}}$, and $v_{1_{\max}}$ are positive constants.

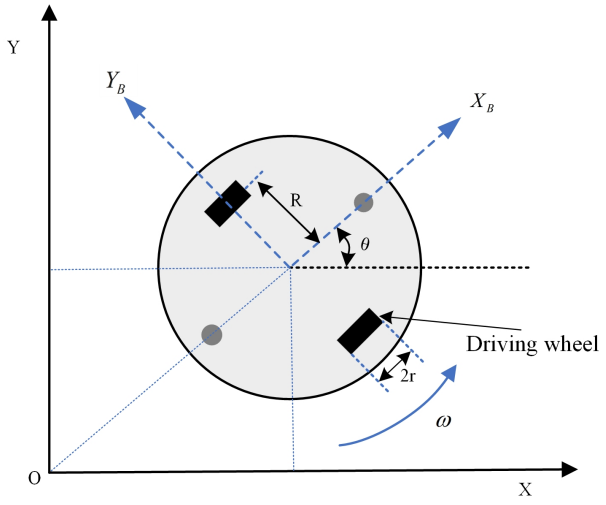

Figure 1. Physical model of a WMR. WMR: wheeled mobile robot.

Assumption 2: Suppose the d_1, d_2, and their derivatives exist with bounds, which is given by $|d_1| \leq k_{1m}$, $|d_2| \leq k_{2m}$, where k_{1m} and k_{2m} are all positive constants.

Then, the tracking errors of the WMR are expressed as

$$\begin{bmatrix} x_e \\ y_e \\ \theta_e \end{bmatrix} = \begin{bmatrix} \cos\theta & \sin\theta & 0 \\ -\sin\theta & \cos\theta & 0 \\ 0 & 0 & 1 \end{bmatrix} \begin{bmatrix} x - x_r \\ y - y_r \\ \theta - \theta_r \end{bmatrix}. \tag{5}$$

Furthermore, the error dynamics system could be transformed in the form of

$$\begin{cases} \dot{x}_e = \omega y_e - v + v_r \cos\theta_e \\ \dot{y}_e = v_r \sin\theta_e - \omega x_e \\ \dot{\theta}_e = \omega - \omega_r \\ J\dot{\omega} = u_1 + d_1 \\ m\dot{v} = u_2 + d_2 \end{cases} \tag{6}$$

To simplify the whole design process, the system (6) can be divided into two subsystems, which contain a second-order subsystem:

$$\begin{cases} \dot{\theta}_e = \omega - \omega_r \\ J\dot{\omega} = u_1 + d_1 \end{cases} \tag{7}$$

and a third-order subsystem:

$$\begin{cases} \dot{x}_e = \omega y_e - v + v_r \cos\theta_e \\ \dot{y}_e = v_r \sin\theta_e - \omega x_e \\ m\dot{v} = u_2 + d_2 \end{cases} \tag{8}$$

3. FIXED-TIME TRAJECTORY CONTROL

In this section, a fixed-time sliding mode control scheme is developed to realize the fast and high-accuracy trajectory tracking control of a WMR under external disturbances. Firstly, a fixed-time disturbance observer

and a new fixed-time sliding mode surface are proposed for the second-order subsystem (7). On this basis, a fixed-time controller is constructed to make the error variables, θ_e and $\dot{\theta}_e$, converge into a small region around the origin. Then, a fixed-time controller is developed for the third-order subsystem (8), which guarantees that the system state variables, x_e, y_e, and v, are all uniformly ultimately bounded, and the tracking errors, x_e and y_e, can converge into a small region around the origin in a fixed time.

3.1. Tracking control laws design for the second-order subsystem

3.1.1. Fixed-time disturbance observer

Firstly, for the attitude error subsystem (7), define an auxiliary variable as

$$\varsigma_1 = \omega - \varpi_1 \tag{9}$$

where ϖ_1 satisfies

$$\dot{\varpi}_1 = \frac{1}{J}u_1 + l_{11}\,\mathrm{erf}(\varsigma_1) + l_{12}|\varsigma_1|^{\gamma_1}\,\mathrm{erf}(\varsigma_1) \tag{10}$$

The parameters l_{11} and l_{12} are positive constants with $l_{11} > k_{1m}/J$. Let variable exponential coefficient $\gamma_1 = \frac{\lambda_0\varsigma_1^2}{1+\mu_0\varsigma_1^2}$ with λ_0 and μ_0 satisfying $0 < \mu_0 < 1$ and $1 + \mu_0 < \lambda_0$.

Theorem 1 *For the second-order subsystem (7), if the disturbance observer is constructed as*

$$\hat{d}_1 = J\Big(l_{11}\,\mathrm{erf}(\varsigma_1) + l_{12}|\varsigma_1|^{\gamma_1}\,\mathrm{erf}(\varsigma_1)\Big) \tag{11}$$

then it can estimate d_1 accurately in a fixed time. That is to say, the observation error $\tilde{d}_1 = d_1 - \hat{d}_1$ can converge into a small region within a fixed time.

Proof of Theorem 1 Select a Lyapunov function as $V_2 = \varsigma_1^2$, differentiating it, one has

$$\begin{aligned}
\dot{V}_2 &= 2\varsigma_1(\dot{\omega} - \dot{\varpi}_1)\\
&= 2\varsigma_1\Big(\frac{1}{J}(u_1 + d_1) - \big(\frac{1}{J}u_1 + l_{11}\,\mathrm{erf}(\varsigma_1) + l_{12}|\varsigma_1|^{\gamma_1}\,\mathrm{erf}(\varsigma_1)\big)\Big)\\
&= 2\varsigma_1\Big(-l_{11}\,\mathrm{erf}(\varsigma_1) - l_{12}|\varsigma_1|^{\gamma_1}\,\mathrm{erf}(\varsigma_1) + \frac{1}{J}d_1\Big)\\
&= -2\Big(l_{11}\varsigma_1\,\mathrm{erf}(\varsigma_1) - \frac{1}{J}\varsigma_1 d_1 + l_{12}\varsigma_1|\varsigma_1|^{\gamma_1}\,\mathrm{erf}(\varsigma_1)\Big)\\
&\le -2\Big(l_{11}\varsigma_1\tanh(\varsigma_1) - \frac{1}{J}\varsigma_1 d_1 + l_{12}\varsigma_1|\varsigma_1|^{\gamma_1}\,\mathrm{erf}(\varsigma_1)\Big)\\
&\le -2\Big(l_{11}|\varsigma_1| - l_{11}\epsilon_1 - \frac{k_{1m}}{J}|\varsigma_1| + l_{12}\varsigma_1|\varsigma_1|^{\gamma_1}\,\mathrm{erf}(\varsigma_1)\Big)\\
&\le -2l_{12}|\varsigma_1||\varsigma_1|^{\gamma_1}\,\mathrm{erf}(|\varsigma_1|) + 2l_{11}\epsilon_1\\
&= -2l_{12}|\varsigma_1|^{\gamma_1+1}\,\mathrm{erf}(|\varsigma_1|) + 2l_{11}\epsilon_1
\end{aligned} \tag{12}$$

where ϵ_1 is a positive constant.

Case 1 When $V_2 > 1$ and $|\varsigma_1| > 1$, one has $\mathrm{erf}(|\varsigma_1|) > \mathrm{erf}(1)$ and $\frac{\lambda_0\varsigma_1^2}{1+\mu_0\varsigma_1^2} \ge \frac{\lambda_0}{1+\mu_0} > 1$. Then (12) can be rewritten as

$$\begin{aligned}
\dot{V}_2 &\le -2(l_{12}\,\mathrm{erf}(1) - l_{11}\epsilon_1)|\varsigma_1|^{\frac{\lambda_0}{1+\mu_0}+1}\\
&\le -2(l_{12}\,\mathrm{erf}(1) - l_{11}\epsilon_1)V_2^{\frac{\lambda_0+\mu_0+1}{2(1+\mu_0)}}
\end{aligned} \tag{13}$$

As $l_{12}\,\mathrm{erf}(1) - l_{11}\epsilon_1 > 0$ and $\bar{\gamma}_1 = \frac{\lambda_0+\mu_0+1}{2(1+\mu_0)} > 1$, then all the solutions of $\{V_2 > 1\}$ will reach the set $\{V_2 \le 1\}$ within a fixed time $t_{f1} \le \frac{1}{2(l_{12}\,\mathrm{erf}(1)-l_{11}\epsilon_1)(\bar{\gamma}_1-1)}$.

Case 2 In the converse case $V_2 \leq 1$, one has

$$\dot{V}_2 \leq -2l_{12}|\varsigma_1||\varsigma_1|^{\gamma_1}\operatorname{erf}(|\varsigma_1|) + 2l_{11}\epsilon_1 \tag{14}$$

As $1+\mu_0\varsigma_1^2 \geq 1$ and $|\varsigma_1| \leq 1$, it can be obtained that $\min\left(|\varsigma_1|^{\gamma_1}\right) \geq \min\left(|\varsigma_1|^{\lambda_0\varsigma_1^2}\right) = e^{\frac{-\lambda_0}{2e}}$. Considering the Lemma 3, then (14) is converted into the following form

$$\begin{aligned}
\dot{V}_2 &\leq -2l_{12}|\varsigma_1||\varsigma_1|^{\gamma_1}\tanh(|\varsigma_1|) + 2l_{11}\epsilon_1 \\
&\leq 2l_{12}|\varsigma_1||\varsigma_1|^{\gamma_1} + 2l_{12}|\varsigma_1|^{\gamma_1}\epsilon_2 + 2l_{11}\epsilon_1 \\
&\leq -2l_{12}|\varsigma_1||\varsigma_1|^{\gamma_1} + 2l_{12}\epsilon_2 + 2l_{11}\epsilon_1 \\
&\leq -2l_{12}|\varsigma_1|^{\gamma_1+1} + 2l_{11}\epsilon_1 + 2l_{12}\epsilon_2 \\
&\leq -2l_{12}e^{\frac{-\lambda_0}{2e}}|\varsigma_1| + 2l_{11}\epsilon_1 + l_{12}\epsilon_2 \\
&\leq -b_1V_2^{\frac{1}{2}} + \tilde{\epsilon} \\
&\leq -l_{13}b_1V_2^{\frac{1}{2}} - (1-l_{13})b_1V_2^{\frac{1}{2}} + \tilde{\epsilon}
\end{aligned} \tag{15}$$

with $b_1 = 2l_{12}e^{\frac{-\lambda_0}{2e}}$, and $\tilde{\epsilon} = 2l_{11}\epsilon_1 + 2l_{12}\epsilon_2$. When $0 < l_{13} < 1$, and $\tilde{\epsilon} - (1-l_{13})b_1V_2^{\frac{1}{2}} \geq 0$, (15) can be simplified as $\dot{V}_2 \leq -l_{13}b_1V_2^{\frac{1}{2}}$. Then, the solution of V_2 will reach a small set Δ_1, which is defined as $\Delta_1 = \left\{\varsigma_1 | V_1(\varsigma_1) \leq (\frac{\tilde{\epsilon}}{b_1(1-l_{13})})^2\right\}$ within a settling time $t_{f2} \leq \frac{2}{b_1 l_{13}}$.

In view of the above two cases, the auxiliary variable ς_1 will converge into a small set $\Delta_1 = \left\{\varsigma_1 | V_1(\varsigma_1) \leq (\frac{\tilde{\epsilon}}{b_1(1-l_{13})})^2\right\}$ within settling time $t_f = t_{f1} + t_{f2}$.

Then, the disturbance observation error

$$\begin{aligned}
\tilde{d}_1 &= d_1 - \hat{d}_1 \\
&= d_1 - J\left(l_{11}\operatorname{erf}(\varsigma_1) + l_{12}|\varsigma_1|^{\gamma_1}\operatorname{erf}(\varsigma_1)\right)
\end{aligned} \tag{16}$$

The disturbance d_1 is bounded according to Assumption 1. Thus, the disturbance observer (11) can estimate d_1 accurately, and the observation error $\tilde{d}_1$ can remain in a small set $\Delta_2 = \left\{\varsigma_1 \middle| |\varsigma_1| \leq k_{1m} + J\left(l_{11}\operatorname{erf}(\Delta_1) + l_{12}|\Delta_1|^{\bar{\gamma}_1}\operatorname{erf}(\Delta_1)\right)\right\}$ after a fixed time, where $\bar{\gamma}_1 = \frac{\lambda_0\Delta_1^2}{1+\mu_0\Delta_1^2}$.

3.1.2. Fixed-time sliding mode controller

For the subsystem (7), define $\omega_e = \omega - \omega_r$. A fixed-time integral sliding mode surface is introduced as follows[22]

$$s_1 = \omega_e + \int_0^t \left(k_{11}(\lceil\theta_e\rfloor^{p_1} + \lceil\theta_e\rfloor^{q_1}) + k_{12}(\lceil\omega_e\rfloor^{p_2} + \lceil\omega_e\rfloor^{q_2})\right)\mathrm{d}\tau \tag{17}$$

with $0 < p_i < 1$, $q_i > 1$, and $(i = 1, 2)$. For any $x \in \mathrm{R}$, $\alpha \in \mathrm{R}^+$, the notation is defined as $\lceil x\rfloor^\alpha = |x|^\alpha \operatorname{sign}(x)$. Based on the sliding mode surface as (17), the fixed-time controller is designed as follows:

$$u_1 = -J\left(k_{11}(\lceil\theta_e\rfloor^{p_1} + \lceil\theta_e\rfloor^{q_1}) + k_{12}(\lceil\omega_e\rfloor^{p_2} + \lceil\omega_e\rfloor^{q_2}) + \alpha_1\lceil s_1\rfloor^{p_3} + \alpha_2\lceil s_1\rfloor^{q_3} + \alpha_3\operatorname{erf}(s_1) - \dot{\omega}_r\right) - \hat{d}_1 \tag{18}$$

where $\alpha_i, k_{1i}, (i = 1, 2)$ are positive constants, α_3 satisfies $\alpha_3 \geq \frac{k_{1m}}{J}$. In addition, $p_i, q_i, (i = 1, 2, 3)$ are all positive odd integers with $0 < p_i < 1, q_i > 1$.

Theorem 2 *For the second-order system (7), if the fixed-time controller is constructed in the form of (18), then the real sliding mode variable will converge into a small set within a fixed time.*

Proof of Theorem 2 Choose a Lyapunov function as $V_3 = \frac{1}{2}s_1^2$ and refer to Lemma 2 to Lemma 4, the time derivative of V_3 is

$$\begin{aligned}\dot{V}_3 &= s_1\Big(\dot{\omega}_e + k_{11}(\lceil\theta_e\rfloor^{p_1} + \lceil\theta_e\rfloor^{q_1}) + k_{12}(\lceil\omega_e\rfloor^{p_2} + \lceil\omega_e\rfloor^{q_2})\Big)\\ &= s_1\Big(\frac{1}{J}(u_1 + d_1) - \dot{\omega}_r + k_{11}(\lceil\theta_e\rfloor^{p_1} + \lceil\theta_e\rfloor^{q_1}) + k_{12}(\lceil\omega_e\rfloor^{p_2} + \lceil\omega_e\rfloor^{q_2})\Big)\\ &= s_1\Big(-\alpha_1\lceil s_1\rfloor^{p_3} - \alpha_2\lceil s_1\rfloor^{q_3} - \alpha_3\,\mathrm{erf}(s_1) + \frac{1}{J}\tilde{d}_1\Big)\\ &\le -\alpha_1|s_1|^{p_3+1} - \alpha_2|s_1|^{q_3+1} - \alpha_3 s_1\tanh(s_1) + \frac{1}{J}|s_1||\tilde{d}_1|\\ &\le -2^{\bar{p}_3}\alpha_1 V_2^{\bar{p}_3} - 2^{\bar{q}_3}\alpha_2 V_2^{\bar{q}_3} + \bar{\vartheta}_1\end{aligned} \tag{19}$$

where $\bar{p}_3 = \frac{p_3+1}{2}, \bar{q}_3 = \frac{q_3+1}{2}, \bar{\vartheta}_1 = \alpha_3\vartheta_1$ with ϑ_1 being a positive constant. By using Lemma 4, the second-order system (7) is fixed-time stable. The sliding mode surface s_1 will converge into a small region $\Delta_3 = \Big\{s_1|V(s_1) \le \min\Big\{\big(\frac{c_2}{\alpha_1 2^{\bar{p}_3}}\big)^{\frac{1}{\bar{p}_3}}, \big(\frac{c_2}{\alpha_2 2^{\bar{q}_3}}\big)^{\frac{1}{\bar{p}_3}}\Big\}\Big\}$ around the origin in a fixed time t_{s_1}, which is determined by $t_{s_1} \le \frac{1}{\alpha_1 2^{\bar{p}_3}\phi_1(1-\bar{p}_3)} + \frac{1}{\alpha_2 2^{\bar{q}_3}\phi_1(\bar{q}_3-1)}$. Then, one can obtain that variables θ_e and ω_e converge to zero along the real sliding mode in a fixed time[23].

3.2. Tracking control laws design for the third-order subsystem

After the angular error θ_e converges to zero according to Theorem 2, one can obtain that $\sin\theta_e$ equals zero, and $\cos\theta_e$ equals 1. The system (8) can be simplified as

$$\begin{cases}\dot{x}_e = \omega_r y_e - v + v_r\\ \dot{y}_e = -\omega_r x_e\\ m\dot{v} = u_2 + d_2\end{cases} \tag{20}$$

3.2.1. Fixed-time disturbance observer

Introduce the following auxiliary variable for the simplified third-order subsystem (20)

$$\varsigma_2 = v - \varpi_2 \tag{21}$$

where ϖ_2 satisfies

$$\dot{\varpi}_2 = \frac{1}{m}u_2 + l_{21}\mathrm{erf}(\varsigma_2) + l_{22}|\varsigma_2|^{\gamma_2}\,\mathrm{erf}(\varsigma_2) \tag{22}$$

where $\gamma_2 = \frac{\lambda_3\varsigma_1^2}{1+\mu_3\varsigma_1^2}$, and λ_3 and μ_3 are integers satisfying the constraints: $0 < \mu_3 < 1$, $1 + \mu_3 < \lambda_3$. The parameters l_{21} and l_{22} are positive constants with $l_{21} > k_{2m}$ and $l_{22} > 0$.

Theorem 3 *For the simplified third-order subsystem (20), a fixed-time disturbance observer is developed in the form of*

$$\hat{d}_2 = m\Big(l_{21}\,\mathrm{erf}(\varsigma_2) + l_{22}|\varsigma_2|^{\gamma_2}\,\mathrm{erf}(\varsigma_2)\Big) \tag{23}$$

then it can estimate d_2 in a fixed time, and the observation error $\tilde{d}_2 = d_2 - \hat{d}_2$ can converge into a small region around the origin within a fixed time t_{d_2}.

Proof of Theorem 3 Similar to the proof of Theorem 1.

3.2.2. Fixed-time sliding mode controller

For the third-order subsystem (20), introduce the following auxiliary variable:

$$\xi = x_e + \int_0^t \Big(\lambda_1\,\mathrm{erf}(x_e) - \lambda_2\,\mathrm{erf}(y_e) + \lambda_3 x_e y_e\,\mathrm{erf}(y_e) + k_1|x_e|^{\gamma_3}\,\mathrm{erf}\big(\frac{x_e}{\epsilon_3}\big)\Big)\mathrm{d}\tau \tag{24}$$

where λ_1 λ_2, k_1, and ϵ_3 are positive constants, $\lambda_2 \leq \lambda_1 \operatorname{erf}(1)$. Let $\gamma_3 = \frac{\lambda_4 x_e^{\,2}}{1+\mu_4 x_e^{\,2}}$, with λ_4 and μ_4 being integers and $0 < \mu_4 < 1$, $1 + \mu_4 < \lambda_4$.

Select a fixed-time sliding mode surface as:

$$s_2 = \dot{\xi} + \int_0^t \left(k_{21} \left(\lceil \xi \rfloor^{p_4} + \lceil \xi \rfloor^{q_4} \right) + k_{22} \left(\lceil \dot{\xi} \rfloor^{p_5} + \lceil \dot{\xi} \rfloor^{q_5} \right) \right) \mathrm{d}\tau \tag{25}$$

where k_{21} and k_{22} are positive constants, $0 < p_i < 1$ and $q_i > 1$, $i = 4, 5$ are positive odd integers.

Theorem 4 *For the third-order subsystem (20), if the fixed-time sliding mode surface is chosen as (25) and the fixed-time controller is designed as (26),*

$$\begin{aligned} u_2 =& m \Big(\dot{v}_r + \dot{\omega}_r y_e + \omega_r \dot{y}_e + \dot{h}(x_e, y_e) + k_{21} \left(\lceil \xi \rfloor^{p_4} + \lceil \xi \rfloor^{q_4} \right) \\ &+ k_{22} \left(\lceil \dot{\xi} \rfloor^{p_5} + \lceil \dot{\xi} \rfloor^{q_5} \right) + \beta_1 \lceil s_2 \rfloor^{p_6} + \beta_2 \lceil s_2 \rfloor^{q_6} + \beta_3 \operatorname{erf}(s_2) \Big) + \hat{d}_2 \end{aligned} \tag{26}$$

then the sliding mode surface s_2 is fixed-time stable, which will converge into a small region of origin within settling time $t_{s_2} \leq \frac{1}{\alpha_4 2^{\bar{p}_6} \phi_2 (1-\bar{p}_6)} + \frac{1}{\alpha_5 2^{\bar{q}_6} \phi_2 (\bar{q}_6 - 1)}$. $h(x_e, y_e) = \lambda_1 \operatorname{erf}(x_e) - \lambda_2 \operatorname{erf}(y_e) + \lambda_3 x_e y_e \operatorname{erf}(y_e) + k_1 |x_e|^{\gamma_3} \operatorname{erf}\left(\frac{x_e}{\epsilon_2}\right)$, in which β_1, β_2 are positive constants, and p_6, q_6 are positive odd integers satisfying $0 < p_6 < 1$, $q_6 > 1$.

Proof of Theorem 4 The proof process will be conducted in 3 steps: (1) After the angular error θ_e converges to zero according to Theorem 2, s_2 and the auxiliary variable ξ can converge into a small region around the origin within a fixed time; (2) The error variables x_e, y_e can converge into a small region around the origin within a fixed time; (3) It should be proved that x_e and y_e do not escape to infinity before the angular error θ_e converges to zero.

Step 1 Select a positive Lyapunov function $V_4 = \frac{1}{2} s_2^2$, differentiating it and substituting (24)-(26) yields to

$$\begin{aligned} \dot{V}_4 &= s_2 \dot{s}_2 \\ &= s_2 \Big(-\beta_1 \lceil s_2 \rfloor^{p_6} - \beta_2 \lceil s_2 \rfloor^{q_6} - \beta_3 \operatorname{erf}(s_2) + \frac{1}{m} (\hat{d}_2 - d_2) \Big) \\ &\leq -\beta_1 |s_2|^{p_6+1} - \beta_2 |s_2|^{q_6+1} - \beta_3 s_2 \operatorname{erf}(s_2) + \frac{1}{m} s_2 \tilde{d}_2 \\ &\leq -\beta_1 |s_2|^{p_6+1} - \beta_2 |s_2|^{q_6+1} - \beta_3 s_2 \tanh(s_2) + \frac{1}{m} s_2 \tilde{d}_2 \\ &\leq -\beta_1 |s_2|^{p_6+1} - \beta_2 |s_2|^{q_6+1} - \beta_3 |s_2| + \frac{1}{m} |s_2| |\tilde{d}_2| \\ &\leq -2^{\bar{p}_6} \beta_1 V_3^{\bar{p}_6} - 2^{\bar{q}_6} \beta_2 V_3^{\bar{q}_6} + \bar{\vartheta}_2 \end{aligned} \tag{27}$$

where $\bar{p}_6 = \frac{p_6+1}{2}$, $\bar{q}_6 = \frac{q_6+1}{2}$, $\bar{\vartheta}_2 = \beta_3 \vartheta_2$ with ϑ_2 being a positive constant. Using the Lemma 4, the third-order subsystem (14) is fixed-time stable, and s_2 will converge into a small set $\Delta_4 = \left\{ s_2 | V(s_2) \leq \min\left\{ \left(\frac{c_3}{\alpha_1 2^{\bar{p}_6}}\right)^{\frac{1}{\bar{p}_6}}, \left(\frac{c_3}{\alpha_2 2^{\bar{q}_6}}\right)^{\frac{1}{\bar{p}_6}} \right\} \right\}$ around zero in the fixed time t_{s_2}, which is determined by

$$t_{s_2} \leq \frac{1}{\alpha_4 2^{\bar{p}_6} \phi_2 (1 - \bar{p}_6)} + \frac{1}{\alpha_5 2^{\bar{q}_6} \phi_2 (\bar{q}_6 - 1)} \tag{28}$$

Then, s_2 will hold in a small region of origin, which guarantees a real sliding mode surface[23]. Therefore, the auxiliary variable ξ and its derivative $\dot{\xi}$ will also converge into the origin along the sliding mode surface[24].

Step 2 According to (25), when the auxiliary $\dot{\xi} = 0$, one has

$$\dot{x}_e = -\lambda_1 \operatorname{erf}(x_e) + \lambda_2 \operatorname{erf}(y_e) - \lambda_3 x_e y_e \operatorname{erf}(y_e) - k_1 |x_e|^{\gamma_3} \operatorname{erf}\left(\frac{x_e}{\epsilon_3}\right) \tag{29}$$

Choose a Lyapunov function as $V_5 = x_e^2$, the time derivative of V_5 is

$$\begin{aligned}\dot{V}_5 &= 2x_e\dot{x}_e \\ &= -2\Big(\lambda_1 x_e \operatorname{erf}(x_e) - \lambda_2 x_e \operatorname{erf}(y_e) + \lambda_3 x_e^2 y_e \operatorname{erf}(y_e) + k_1|x_e|^{\gamma_3}\operatorname{erf}(\frac{x_e}{\epsilon_3})\Big) \\ &\le -2\Big(\lambda_1|x_e| - \lambda_2|x_e| - \lambda_1\epsilon_4 + k_1 x_e|x_e|^{\gamma_3}\operatorname{erf}(\frac{x_e}{\epsilon_3})\Big) \\ &\le -2\Big(k_1\epsilon_3|x_e||x_e|^{\gamma_3}\operatorname{erf}(|\frac{x_e}{\epsilon_3}|) - \lambda_1\epsilon_4\Big)\end{aligned} \tag{30}$$

where ϵ_4 is a positive constant. The rest of the proof is similar to the proof of Theorem 2. There exists a constant $0 < \vartheta_3 < 1$ such that the variable x_e will reach and keep in a small region Δ_5 around the origin within a fixed time T_2:

$$T_2 \le \frac{1}{k_1\vartheta_3 e^{-\frac{\lambda_4}{2e}}} + \frac{1}{2k_1\epsilon_3(\frac{\lambda_4}{1+\mu_4} - 1)} \tag{31}$$

Then, it can be obtained that the $\dot{x}_e$ is a uniformly continuous form (29). Employ Barbalat Lemma [25] to prove $\dot{x}_e \to 0$ as $t \to \infty$, then $\dot{x}_e$ is bounded after the variable x_e converges. Hence, there exists a small region Δ_5 around the origin that y_e can converge into Δ_5.

Step 3 Before the angular error θ_e converges to zero, $\theta_e \neq 0$, such that subsystem (13) cannot be simplified as (19). It should be proved that system state variables x_e, y_e, and v are bounded before the angular error θ_e converges to zero.
Consider the following bounded function:

$$V_6 = \frac{1}{2}x_e^2 + \frac{1}{2}y_e^2 + |v| \tag{32}$$

The time derivative of V_6 is

$$\begin{aligned}\dot{V}_6 &\le |x_e||\dot{x}_e| + |y_e||\dot{y}_e| + |\dot{v}| \\ &\le |x_e||\dot{x}_e| + |y_e||\dot{y}_e| + m\Big(\omega_r\dot{y}_e + |\dot{h}(x_e, y_e)| + k_{21}\big(|\xi|^{p_4} + |\xi|^{q_4}\big) + k_{22}\big(|\dot{\xi}|^{p_5} + |\dot{\xi}|^{q_5}\big) \\ &\quad +\beta_1|s|_2^{p_6} + \beta_2|s|_2^{q_6}\Big) + \frac{|\tilde{d}_2|}{m} \\ &\le |x_e||\dot{x}_e| + |y_e||\dot{y}_e| + m\Big(|\dot{y}_e| + k_{21}\big(|\xi|^{p_4} + |\xi|^{q_4}\big) + k_{22}\big(|\dot{\xi}|^{p_5} + |\dot{\xi}|^{q_5}\big) + \beta_1|s|_2^{p_6} + \beta_2|s|_2^{q_6} \\ &\quad +\lambda_3\big(|\dot{x}_e||y_e| + |x_e||\dot{y}_e| + |x_e||y_e||\dot{y}_e|\big) + \frac{k_1\lambda_4|x_e||\dot{x}_e|}{1+\mu_0 x_e^2}|x_e|^{\gamma_3}\Big(1 + \frac{2|x_e|}{1+\mu_4 x_e^2}\Big) \\ &\quad +\frac{2k_1}{\epsilon_2\sqrt{\pi}}|x_e|^{\gamma_3}|\dot{x}_e|\Big) + \frac{|\tilde{d}_2|}{m} \\ &\le |x_e||\dot{x}_e| + |y_e||\dot{y}_e| + m\Big(|\dot{y}_e| + k_{21}\big(|\xi|^{p_4} + |\xi|^{q_4}\big) + k_{22}\big(|\dot{\xi}|^{p_5} + |\dot{\xi}|^{q_5}\big) + \beta_1|s|_2^{p_6} + \beta_2|s|_2^{q_6} \\ &\quad +\lambda_3\big(|\dot{x}_e||y_e| + |x_e||\dot{y}_e| + |x_e||y_e||\dot{y}_e|\big) + \frac{k_1\lambda_4}{\mu_4}(1 + 2|x_e|)|x_e|^{\frac{\lambda_4}{\mu_4}-1}|x_e| \\ &\quad +\frac{2k_1}{\epsilon_2\sqrt{\pi}}|x_e|^{\frac{\lambda_4}{\mu_4}}|x_e|\Big) + \frac{|\tilde{d}_2|}{m}\end{aligned} \tag{33}$$

Let $\eta_1 = \sqrt{x_e^2 + y_e^2 + |v|} \ge \eta > 1$, then one has the following inequalities: $|x_e| \le \eta_1, |y_e| \le \eta_1, |v| \le \eta_1$. Furthermore, there exist positive constants $a_i (i = 3, 4), b_l, c_l, (l = 4, 5, ..., 9)$, which satisfy $|x_e|^{\frac{\lambda_4}{\mu_4}} \le a_3\eta_1$, $|x_e|^{\frac{\lambda_4}{\mu_4}-1} \le a_4\eta_1$, $|s_2|^{p_6} < b_4 + c_4\eta_1$, $|s_2|^{q_6} < b_5 + c_5\eta_1$, $|\xi|^{p_4} < b_6 + c_6\eta_1$, $|\xi|^{q_4} < b_7 + c_7\eta_1$, $|\dot{\xi}|^{p_5} < b_8 + c_8\eta_1$,

$|\dot{\xi}|^{q_5} < b_9 + c_9\eta_1$. According to Theorem 3, the state variable θ_e, ω will converge into the origin within a fixed time t_{s_1}, then one has $\theta_e \le \theta_m$, $|\omega| \le \omega_m$, $|\tilde{d}_2| < k_d$. Further $|\dot{y}_e| < |\dot{x}_e| \le v_{1_{\max}} + \omega_m\eta_1$ can be obtained. Then, (33) can be simplified as

$$\begin{aligned}\dot{V}_6 \le\ & (2\eta_1 + 2m\lambda_3 + \eta_1^2 + m)(v_{1_{\max}} + \omega_m\eta_1) + \frac{mk_1\lambda_4}{\mu_4}(v_{1_{\max}} + \omega_m\eta_1)a_4\eta_1 \\ & + \frac{2mk_1}{\epsilon_2\sqrt{\pi}}a_3\eta_1(v_{1_{\max}} + \omega_m\eta_1) + \frac{k_d}{m} \\ \le\ & \frac{\eta_1^2}{2}2\Big(2v_{1_{\max}} + 3\omega_m + 2m\lambda_3 + m + \frac{2mk_1a_4\lambda_4}{\mu_4}(v_{1_{\max}} + \omega_m) + \frac{2ma_3k_1}{\epsilon_2\sqrt{\pi}}(v_{1_{\max}} + \omega_m)\Big) \\ & + 2m\lambda_3 v_{1_{\max}} + \frac{k_d}{m} \\ \le\ & KV_6 + \varrho_1\end{aligned} \tag{34}$$

where K and ϱ_1 satisfy the following constraints:

$$K = 2\Big(2v_{1_{\max}} + 3\omega_m + 2m\lambda_3 + m + \frac{2mk_1a_4\lambda_4}{\mu_4}(v_{1_{\max}} + \omega_m) + \frac{2ma_3k_1}{\epsilon_2\sqrt{\pi}}(v_{1_{\max}} + \omega_m)\Big) \tag{35}$$

$$\varrho_1 = 2m\lambda_3 v_{1_{\max}} + \frac{k_d}{m} \tag{36}$$

On the contrary, if $\eta_1 > 1$, there exists a positive constant ϱ_2, which satisfies $\dot{V}_6 \le \varrho_2$. One has $\dot{V}_6 \le KV_6 + \varrho_3$ for the state variable x_e, y_e, v. Further, before the angular error θ_e converges to zero, one can obtain

$$V_6 \le \big(V_6(0) + \frac{\varrho_3}{K}\big)e^{Kt} - \frac{\varrho_3}{K} \tag{37}$$

Remark 1 The auxiliary variable ξ in (24) can reduce the order of the third-order subsystem, which simplifies the process of the controller design. In addition, the controller developed in this paper can guarantee that the system state variables converge in a fixed time and the chattering problem is solved by using the error function erf(·). Furthermore, utilizing the variable exponent coefficient in (24) avoids the common singularity problem.

4. EXPERIMENT RESULTS

To verify the effectiveness of the proposed control scheme, the trajectory tracking experiment is implemented on a Quanser QBot 2e mobile robot platform composed of a QBot 2e mobile robot, an OptiTrack system with 12 infrared cameras, and a computer. The experimental platform is presented in Figure 2. The whole closed-loop experiment structure is as follows: The simulation diagram is compiled on the host computer equipped with MATLAB/Simulink to transform the simulation into an executable file. And the control scheme is written to the Gumstix computer embedded in the QBot 2e through wireless communication protocol. The real-time position information of the QBot 2e is obtained by the OptiTrack positioning system. Then the host computer calculates the information and transmits them to the embedded computer of a WMR for the input of real-time calculation of executable files. So as to complete the trajectory experiment of the mobile robot.

In the experiment, the physical parameters of the QBot 2e are chosen as follows: $m = 4$ kg, $J = 2.5$ kg $\cdot$ m^2. The desired reference trajectory is set as $x_r = \cos(0.2t)$ m, $y_r = \sin(0.2t)$ m. The initial values of the reference and practical trajectories are $[x_r(0), y_r(0), \theta_r(0)]^{\mathrm{T}} = [1, 0, \pi/2]^{\mathrm{T}}$, $[x(0), y(0), \theta(0)]^{\mathrm{T}} = [0.7, -0.02, \pi/6]^{\mathrm{T}}$, respectively. The main relevant parameters of the proposed control scheme are as follows: $k_1 = 0.001$, $k_{11} = k_{12} = 0.9$, $k_{21} = 0.05$, $k_{22} = 0.06$, $\epsilon_2 = 0.00001$. Choose the parameters $\alpha_1 = 2$, $\alpha_2 = 0.5$, $\beta_1 = \beta_2 = 1$ for the sliding mode surface s_1 in (17) and s_2 in (25), respectively.

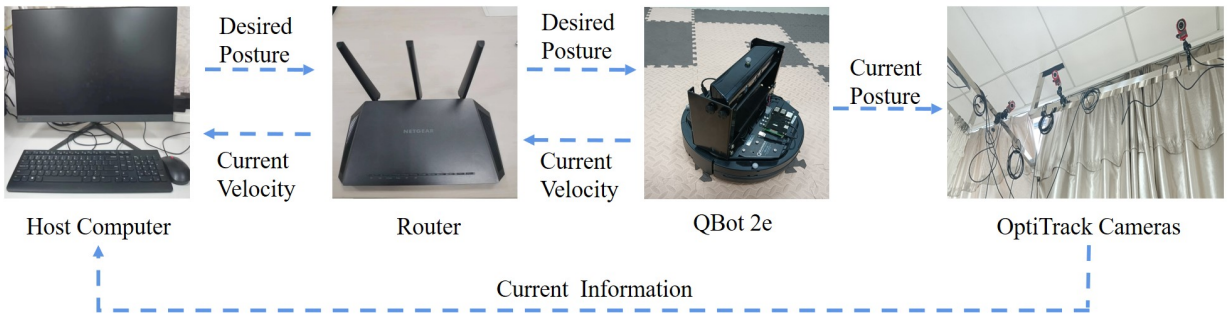

Figure 2. The Quanser QBot 2e Mobile Robot Platform.

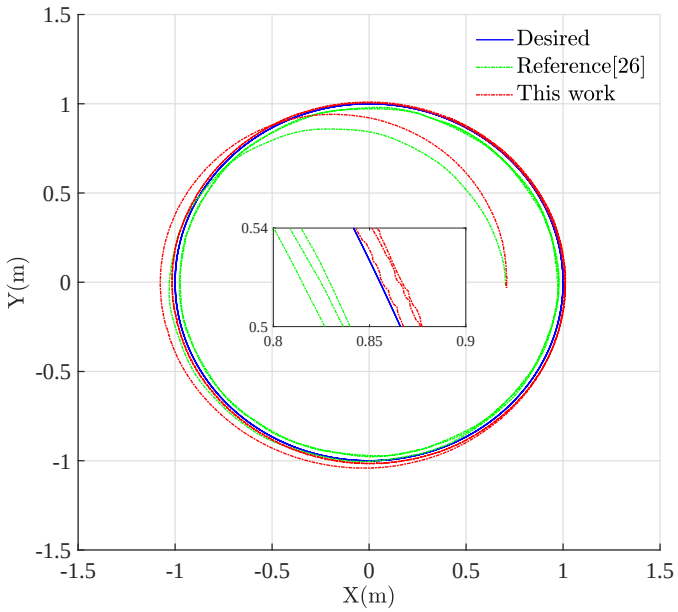

Figure 3. The comparative trajectory tracking experiment results of the WMR. WMR: wheeled mobile robot.

It is obvious that the WMR trajectory tracking mission can be achieved by the designed control method as plotted in the red track in Figure 3. The time response curves of the sliding mode surfaces, s_1 and s_2, are shown in Figure 4, which converge very quickly. To illustrate the excellence of the proposed control method, a comparative experiment on the trajectory tracking of WMRs is conducted between this work and reference [26]. The control inputs of the designed control scheme and reference are shown in Figure 5, which are nonsingular and continuous. Figure 6 illustrates the tracking errors in this experiment, which have a big fluctuation due to the influence of external disturbances. In the experiment, the external disturbance is from the experimental environment, such as uneven ground. The observed disturbance values are shown in Figure 7, which indicates the effectiveness of the proposed disturbance observer in this work. From the experimental results, it can be concluded that the designed control scheme has the robustness against the external disturbance and high tracking accuracy.

5. DISCUSSION

In this paper, a universal control scheme for fixed-time trajectory tracking based on ISMC is put forward. The dynamic model of the WMR has been transformed into two error subsystems. Then utilizing the fixed-time technology and ISMC, a new fixed-time disturbance observer has been proposed and applied on the two error subsystems. Furthermore, an observer-based tracking control method has been proposed to achieve

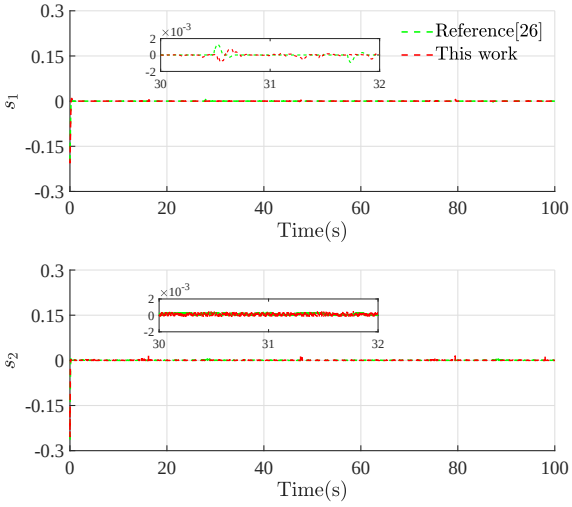

Figure 4. Comparative results of sliding mode surfaces in the experiment.

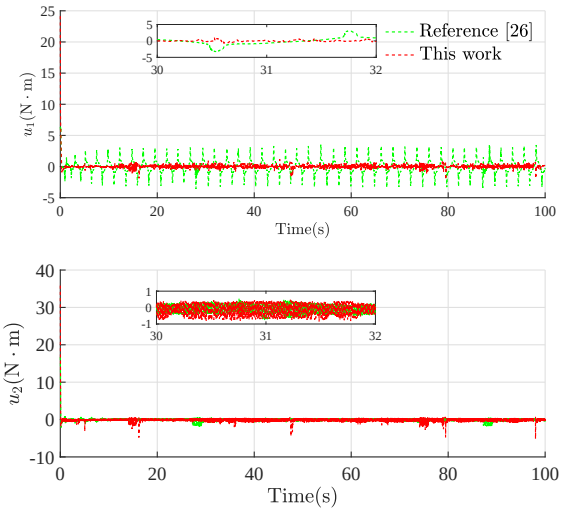

Figure 5. Comparative results of control torques in the experiment.

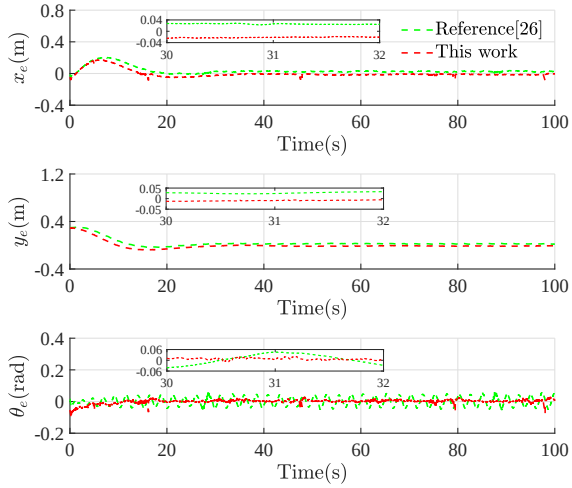

Figure 6. Comparative results of tracking errors x_e, y_e, θ_e in the experiment.

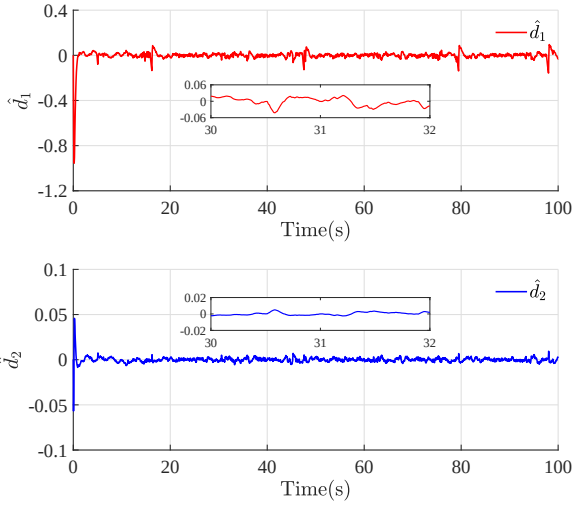

Figure 7. Disturbance estimation $\hat{d}_1$ and $\hat{d}_2$ in the experiment.

a trajectory tracking mission for the WMR, and guarantee the tracking error converges within a fixed time. Finally, the proposed control approach has been verified by a mobile robotic platform, and the experimental results show fine control performances. Our future work will focus on how to realize the formation tracking control of multi-wheeled mobile robots in both theory and experiment.

DECLARATIONS

Acknowledgments

The authors would like to thank the editors and reviewers for their valuable comments dedicated to this article.

Authors' contributions

Made significant contributions in writing, methodology, review: Li B
Executed writing-original draft, experiment verification: Ma L
Methodology validation: Wang C

Data result analysis: Ge C
Supervision and modification: Liu H

Availability of data and materials
Not applicable.

Financial support and sponsorship
This work was supported in part by the National Natural Science Foundation of China (62073212), Natural Science Foundation of Shanghai (23ZR1426600), and Innovation Fund of Chinese Universities Industry-University-Research (2021ZYB05004).

Conflicts of interest
All authors declared that there are no conflicts of interest.

Ethical approval and consent to participate
Not applicable.

Consent for publication
Not applicable.

REFERENCES

1. Panahandeh P, Alipour K, Tarvirdizadeh B, Hadi A. A kinematic Lyapunov-based controller to posture stabilization of wheeled mobile robots. *Mech Syst Signal Pr* 2019;134:1–19. DOI
2. Huang H, Li Y, Bai Q. An improved a star algorithm for wheeled robots path planning with jump points search and pruning method. *Complex Eng Syst* 2022;2:11. DOI
3. Kanayama Y, Kimura Y, Miyazaki F, Noguchi T. A stable tracking control method for an autonomous mobile robot. In: Proceedings., IEEE International Conference on Robotics and Automation; 1990;1. pp. 384–89. DOI
4. Fierro R, Lewis F. Control of a nonholonomic mobile robot: backstepping kinematics into dynamics. In: Proceedings of 1995 34th IEEE Conference on Decision and Control; 1995;4. pp. 3805–10. DOI
5. Bloch A. Nonholonomic mechanics and control. Interdisciplinary Applied Mathematics. New York, NY: Springer; 2003. DOI
6. Murray R, Sastry S. Nonholonomic motion planning: steering using sinusoids. *IEEE Trans Automat Contr* 1993;38:700–16. DOI
7. Tayebi A, Tadjine M, Rachid A. Invariant manifold approach for the stabilization of nonholonomic chained systems: Application to a mobile robot. *Nonlinear Dynam* 2001;24:167–81. DOI
8. Wang X, Zhang G, Neri F, et al. Design and implementation of membrane controllers for trajectory tracking of nonholonomic wheeled mobile robots. *Integr Comput-Aid E* 2016;23:15–30. DOI
9. Zhai J, Song Z. Adaptive sliding mode trajectory tracking control for wheeled mobile robots. *Int J Control* 2019;92:2255–62. DOI
10. Ou M, Sun H, Zhang Z, Li L. Fixed-time trajectory tracking control for multiple nonholonomic mobile robots. *T I Meas Control* 2021;43:1596–608. DOI
11. Li B, Zhang H, Xiao B, Wang C, Yang Y. Fixed-time integral sliding mode control of a high-order nonlinear system. *Nonlinear Dynam* 2022;107:909–20. DOI
12. Liu Q, Cai Z, Chen J, Jiang B. Observer-based integral sliding mode control of nonlinear systems with application to single-link flexible joint robotics. *Complex Eng Syst* 2021;1:8. DOI
13. Zhang Z, Leibold M, Wollherr D. Integral sliding-mode observer-based disturbance estimation for euler–lagrangian systems. *IEEE Trans Contr Syst T* 2020;28:2377–89. DOI
14. Li B, Hu Q, Yang Y. Continuous finite-time extended state observer based fault tolerant control for attitude stabilization. *Aerosp Sci Technol* 2019;84:204–13. DOI
15. Zhang H, Li B, Xiao B, Yang Y, Ling J. Nonsingular recursive-structure sliding mode control for high-order nonlinear systems and an application in a wheeled mobile robot. *ISA T* 2022;130:553–64. DOI
16. Chevillard S. The functions erf and erfc computed with arbitrary precision and explicit error bounds. *Inform Comput* 2012;216:72–95. DOI
17. Eltayeb A, Rahmat M, Basri MAM, Mahmoud MS. An improved design of integral sliding mode controller for chattering attenuation and trajectory tracking of the quadrotor UAV. *Arab J Sci Eng* 2020;45:6949–61. DOI

18. Ba D, Li Y, Tong S. Fixed-time adaptive neural tracking control for a class of uncertain nonstrict nonlinear systems. *Neurocomputing* 2019;363:273–80. DOI
19. Bagul Y, Chesneau C. Sigmoid functions for the smooth approximation to the absolute value function. *MJPAA* 2021;7:12–19. DOI
20. Polycarpou M, Ioannou P. A robust adaptive nonlinear control design. *Automatica* 1996;32:423–27. DOI
21. Jiang Z, Nijmeijer H. Tracking control of mobile robots: A case study in backstepping. *Automatica* 1997;33:1393–99. DOI
22. Wang C, Wen G, Peng Z, Zhang X. Integral sliding-mode fixed-time consensus tracking for second-order non-linear and time delay multi-agent systems. *J Franklin I* 2019;356:3692–710. DOI
23. Plestan F, Shtessel Y, Brégeault V, Poznyak A. New methodologies for adaptive sliding mode control. *Int J Control* 2010;83:1907–19. DOI
24. Song T, Fang L, Wang H. Model-free finite-time terminal sliding mode control with a novel adaptive sliding mode observer of uncertain robot systems. *Asian J of Control* 2022;24:1437–51. DOI
25. Li B, Gong W, Yang Y, Xiao B, Ran D. Appointed fixed time observer-based sliding mode control for a quadrotor UAV under external disturbances. *IEEE Trans Aero Elec Sys* 2022;58:290–303. DOI
26. Tian B, Liu L, Lu H, et al. Multivariable finite time attitude control for quadrotor UAV: Theory and experimentation. *IEEE Trans Ind Electron* 2018;65:2567–77. DOI

Zander *et al. Complex Eng Syst* 2023;3:9
DOI: 10.20517/ces.2023.11

Complex Engineering Systems

Research Article

Open Access

Reinforcement learning with Takagi-Sugeno-Kang fuzzy systems

Eric Zander, Ben van Oostendorp, Barnabas Bede

DigiPen Institute of Technology, Redmond, WA 98012, USA.

Correspondence to: Eric Zander, DigiPen Institute of Technology, 9931 Willows Rd. NE.Redmond, WA 98012, USA.
E-mail: eric.zander@digipen.edu

How to cite this article: Zander E, van Oostendorp B, Bede B. Reinforcement learning with Takagi-Sugeno-Kang fuzzy systems. *Complex Eng Syst* 2023;3:9. http://dx.doi.org/10.20517/ces.2023.11

Received: 17 Mar 2023 **First Decision:** 12 Apr 2023 **Revised:** 16 May 2023 **Accepted:** 19 May 2023 **Published:** 14 Jun 2023

Academic Editor: Hamid Reza Karimi **Copy Editor:** Fanglin Lan **Production Editor:** Fanglin Lan

Abstract

We propose reinforcement learning (RL) architectures for producing performant Takagi-Sugeno-Kang (TSK) fuzzy systems. The first employs an actor-critic algorithm to optimize existing TSK systems. An evaluation of this approach with respect to the Explainable Fuzzy Challenge (XFC) 2022 is given. A second proposed system applies Deep Q-Learning Network (DQN) principles to the Adaptive Network-based Fuzzy Inference System (ANFIS). This approach is evaluated in the CartPole environment and demonstrates comparability to the performance of traditional DQN. In both applications, TSK systems optimized via RL performed well in testing. Moreover, the given discussion and experimental results highlight the value of exploring the intersection of RL and fuzzy logic in producing explainable systems.

Keywords: Explainable AI, Fuzzy systems, Takagi-Sugeno-Kang fuzzy systems, Adaptive neuro-fuzzy inference systems, Reinforcement learning

1. INTRODUCTION

Fuzzy sets have been introduced in [1] as a mathematical framework for modeling under uncertainty. Fuzzy systems employ a fuzzy inference engine to solve control problems in various frameworks and applications [2,3]. In a majority of fuzzy control applications, a dynamic model joins a fuzzy system to create a dynamic fuzzy control system [4]. However, there are various applications where dynamic models are either not available or

too complex for effective use in the fuzzy setting. Such applications tend to include video games and other interactive environments[5].

Reinforcement learning (RL) comprises a collection of learning algorithms that allow optimization of various control systems. RL trains agents to adapt to a given environment via a reward system[6]. The agent takes action by assessing the state of the environment, and RL allows the agent to maximize the expected reward. Such algorithms are well suited for complex environments; RL has shown great success in games[7] and industrial applications[8].

Deep RL[9] has recently seen significant developments as agents have successfully outperformed humans in games such as Go[7], Poker[10], and video games[11]. This approach also finds effective employment in applications such as autonomous vehicles[12], UAVs[13], and fine-tuning of large language models[14]. However, RL models and related deep learning architectures, in particular, tend to have a significant drawback in their relative lack of explainability.

Explainable machine learning is a subject of extensive research[15–17] concerned with rendering relevant algorithms more understandable, transparent, and trustworthy. Explainable fuzzy AI has afforded significant developments in this domain due to characteristics such as amenability to visualization and expression in natural language[18–20]. Notably, literature discussing directed RL in the setting of explainable fuzzy AI proves scarce despite recent advancements in the former and a capacity for mutual benefit; exploration of genetic algorithms proves more common historically[21–23].

To aid in developing RL algorithms capable of producing explainable models, fuzzy RL-based architectures[24] show promise. Fuzzy Q-learning was proposed and studied in a series of research papers[25–27] primarily concerned with performance in control applications rather than explainability in general. Additionally, these explorations are disconnected from recent developments in deep RL. This presents a gap in the literature. However, in[28], the author developed Takagi-Sugeno-Kang (TSK) fuzzy systems with successful applications in various environments where Deep Q-Learning Network (DQN)[29] has illustrated effectiveness. Similar to an Adaptive Network-Based Fuzzy Inference System (ANFIS)[30], this approach leverages RL to train an agent in these environments and shows the promise of such experimentation.

This paper offers further practical study of RL-based TSK fuzzy systems and ANFIS architectures as solutions for developing explainable AI. The latter is compared to traditional Deep Q-learning algorithms. After a preliminary section where we provide an overview of the conceptual building blocks of our systems, we discuss the successful and winning application of RL-based TSK systems to the Asteroid Smasher framework and corresponding 2023 Explainable AI competition[31]. Additionally, we offer a comparison of ANFIS and DQN in the CartPole environment. The value of the relationship between RL and fuzzy systems to explainability is highlighted and discussed in both cases.

2. PRELIMINARIES

2.1. Fuzzy systems

Fuzzy sets are defined as functions $A : X \to [0, 1]$ and are interpreted as sets with a continuum of membership grades[1]. They are used in modeling under uncertainty, especially in a rule-based environment.

Fuzzy rules describe an imprecise cause-effect relationship between certain variables controlling a given system. Fuzzy rules are of the form

$$\text{If } x \text{ is } A \text{ then } y \text{ is } B$$

where A and B are fuzzy sets on domains X and Y, respectively. Fuzzy rules can be organized into fuzzy rule

bases

$$\text{If } x \text{ is } A_i \text{ then } y \text{ is } B_i$$

with antecedents A_i and consequences B_i, $i = 1, ..., n$ being fuzzy sets.

Mamdani fuzzy systems were introduced in [2], with the goal of developing fuzzy rule-based control systems. Mamdani fuzzy systems defined by the above rule base evaluate a fuzzy output as

$$B'(y) = \vee_{i=1}^{n} A_i(x) \wedge B_i(y).$$

The output of the system is then calculated using a defuzzification as an example

$$COG(B') = \frac{\int_Y B'(y) \cdot y dy}{\int_Y B'(y) dy}$$

To model more complex systems, one can define systems with multiple antecedents and connect them with an aggregation operator.

TSK Fuzzy Systems have been introduced in [3,32] and are based on rules with a fuzzy antecedent and a singleton consequence

$$\text{If } x \text{ is } A_i \text{ then } y = y_i.$$

In this paper, we are using a rule with a singleton consequence; however, TSK systems can also be defined with linear or higher-order consequences. The output of a TSK fuzzy system can be calculated as

$$TSK(x) = \frac{\sum_{i=1}^{n} A_i(x) \cdot y_i}{\sum_{i=1}^{n} A_i(x)}.$$

In the case of multiple antecedents, the rule base is modified as an example

$$\text{If } x \text{ is } A_i \text{ and } y \text{ is } B_i \text{ then } z = z_i.$$

with the evaluation of the output being

$$TSK(x, y) = \frac{\sum_{i=1}^{n} A_i(x) \cdot B_i(y) \cdot z_i}{\sum_{i=1}^{n} A_i(x) \cdot B_i(y)}.$$

In the present paper, we use TSK fuzzy systems in the context of RL.

2.2. Reinforcement learning

2.2.1. Bellman's Equation

Bellman equation, named after Richard E. Bellman for his work in [33], is an equation for controlling systems based on states, rewards, and actions, which altogether allow us to compute the value for the state, i.e., the total expected reward in a given state, given by

$$V(s) = \max_a (R(s, a) + \gamma \sum P(s, a, s')V(s').$$

$V(s)$ is called the value of a state s. This function gets updated as the agent learns more information about the state, especially which actions (a) yield the highest cumulative reward. The reward r is given for a state-action pair and is not bound by any restrictions. γ is a discount factor, typically specified between 0 and 1, with a common value of 0.99. γ is tuned to balance "near" and "far" rewards with lower values prioritizing immediate rewards and higher values valuing future rewards more. P is the probability of ending in state s' (next state) by taking action a when starting from state s. $V(s')$ is the value of the next state. This recursive definition allows policies to learn which actions to take on a given state to maximize the cumulative reward of future states.

2.2.2. Q-learning

Q-learning[34] is a model-free RL algorithm, which will learn the Q-values or the expected reward for a state. Rather than attempt to model the environment, Q-learning aims to predict preferable actions to take in a specific state by extending the Bellman Equation as

$$Q^{new}(s,a) = Q(s,a) + \alpha \cdot (R(s,a) + \gamma \max_a Q(s',a) - Q(s,a)).$$

Q^{new} are the new Q-values of the state-action pair. These new values get updated from the previous Q-values and added to α, a learning rate, multiplied by the temporal difference (TD). The TD is the current reward of the state-action pair added to the discount factor γ multiplied by the maximum reward that can be earned from the next state before the current value of the state-action pair is subtracted. The Q-function aims to update the action that should be taken for a given state to maximize the cumulative reward.

2.2.3. Deep Q-learning

Common techniques for Q-learning include creating a Deep Neural Network (NN) for predicting the Q-function followed by optimization via backpropagation. This model is known as a Deep Q-Learning Network[29] and is a particular case of Q-learning that relies on a Deep NN architecture. This allows the agent to learn continuous states, learn continuous values in discrete states, and generalize to states not yet seen. For example, a simple Q-learning algorithm could involve creating a lookup table where each element is a state of an environment such as Grid World[6]. However, such an approach does not generalize to more complex environments such as StarCraft II[35]; the practically countless number of possible states renders their storage in an extremely inefficient table, and Deep Q-learning handles these tasks elegantly.

2.2.4. Improvements to Q-learning and Deep Q-learning

One very common problem with Q-learning is sampling inefficiency and over-estimation of the Q-values. There are several methods to address these problems. Here, we will discuss experience replay, double Q-learning, and actor-critic architectures.

Experience replay[36] allows Q-learning agents to be more sample efficient by storing transitions or collections of states, actions, rewards, and next states. Instead of exclusively learning from a current state, agents sample prior experiences. This allows the agent to revisit states it has already visited and learn more to speed up convergence of the agent's current policy. Popular and powerful extensions to experience replay for improving sample efficiency include prioritized experience replay (PER)[37] and hindsight experience replay (HER)[38].

Double Deep Q-Learning (DDQN)[39] is another technique to aid in the stability of training. A second model, which is a copy of the original network, is offline (frozen) for a set number of training iterations. The target Q-values are then sampled from the target network and used to compute the Q-values for the online (unfrozen) network. One issue with DDQN is the tendency of the online model to move too aggressively towards optimal performance and negatively impact the stability of training. To address this, a soft update, known commonly as Polyak Updating[40], is performed on the target network using the weights of the online model multiplied by a small value. This form of weight regularization allows the target model to slowly improve over time and prevents harsh updates to the learning.

An actor-critic RL architecture consists of an actor that acts out the current policy and estimates the current value policy and a critic that evaluates the current policy and estimates the policy gradient using a TD evaluation[41]. The system also encompasses a supervisor that controls the balance between exploration (performed by the actor) and exploitation (performed by the critic).

3. REINFORCEMENT LEARNING WITH FUZZY SYSTEMS

RL in the context of fuzzy logic was introduced in [24] and based on the Mamdani framework. It was successfully used in the CartPole problem. RL TSK fuzzy systems have been developed for various applications [28,42].

3.1. Reinforcement learning TSK fuzzy system

As learned behaviors in complex systems are often the result of intricate optimization processes, explainable RL constitutes a challenging problem. However, the interpretability of fuzzy systems indicates the potential value of a method of TSK fuzzy system optimization inspired by traditional Q-learning. In other words, a system in which one approximates the Q function with a TSK fuzzy system [28] stands to offer some unique benefits. This approach was successfully employed in applications such as a simulation in a simple discrete grid-world environment or in continuous environments such as CartPole or Lunar Lander [28].

The idea in the setting of a TSK-based Q-learning is to set the Q function to be approximated by a TSK fuzzy system, i.e.,

$$Q(s,a) = TSK(s,a).$$

TD Q-learning equation is given by

$$Q(s,a) = Q(s,a) + \alpha(R(s') + \gamma Q(s',a) - Q(s,a))$$

When updating the parameters of a system in RL we can use the general equation

$$w_i = w_i + \alpha(R(s') + \gamma Q(s',a) - Q(s,a))\frac{\partial Q}{\partial w_i}$$

with $w_i, i = 1, ..., n$ being parameters of the system. As a result, we can update the parameters of the fuzzy system using this approach in the context of a TSK fuzzy system as

$$w_i = w_i + \alpha(R(s') + \gamma TSK(s',a) - TSK(s,a))\frac{\partial TSK(s,a)}{\partial w_i}.$$

Here, w_i are the parameters of the fuzzy system. Just as in the case of RL, one may wish to mitigate instability via techniques such as experience replay and the usage of an actor-critic environment.

To give a theoretical foundation to our proposed algorithm, we include here an initial discussion on convergence. First, we observe that the Q-learning algorithm is known to be convergent [43,44] under standard assumptions on the given Markov Decision Process (MDP). Additionally, NNs with various membership functions are known to be universal approximators [45,46]. Combining the above results and the conclusions in [47,48], we can approximate the Q function by the output of the NN, which leads to the convergence of Deep Q-learning models. It is known that TSK fuzzy systems are universal approximators [49,50], i.e., they have similar approximation properties to those of NNs. Together, the ideas above allow the conclusion that replacing the NN in a DQN architecture with a TSK fuzzy system will retain the same properties as DQNs. In summary, the TSK fuzzy system is an approximator of the Q function. Therefore, the Q-learning algorithm with TSK fuzzy systems is convergent. The above theoretical motivation warrants a deeper investigation of the approximation properties of RL TSK fuzzy systems as a topic for future research.

3.2. Case study: Reinforcement learning TSK system for Asteroid Smasher

3.2.1. Problem description

To test the algorithm, we created optimized TSK fuzzy systems through RL to play a variant of the game Asteroids called Asteroid Smasher (see Figure 1). Developed by the University of Cincinnati for the Explainable Fuzzy AI Challenge (XFC 2022), the game environment incorporates additional complexities to increase both the difficulty and value of explainable automation. These include the addition of multiple agents, screen-wrap for ships and hazards, and unique scenarios to test edge cases.

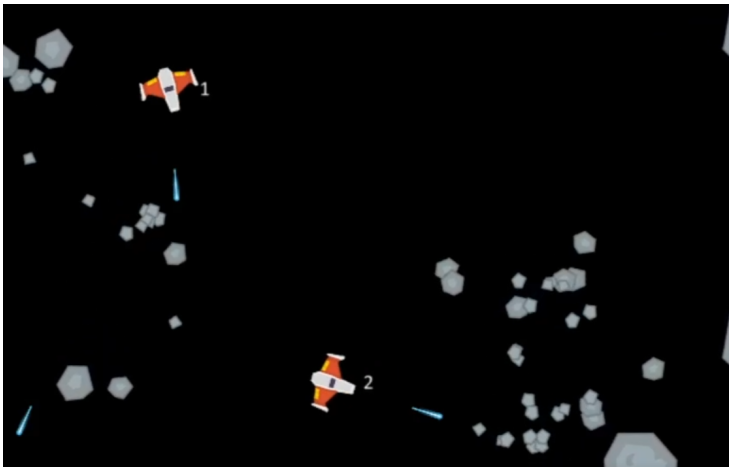

Figure 1. Example of the Asteroid Smasher environment.

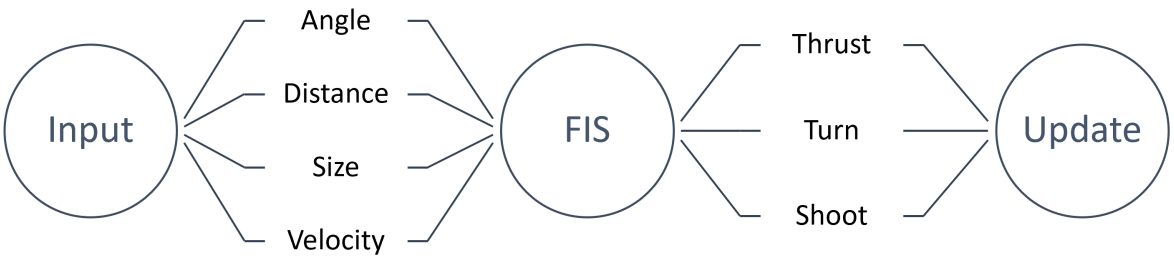

Figure 2. Simplified overview of the fuzzy inference system's threat inputs and behavioral output.

While the primary metric for performance concerned the total number of asteroids destroyed, other metrics included accuracy, number of lives lost, and execution speed. More importantly, the explainability of the system proved crucial as the motivating factor for the test case. In pursuit of balancing AI explainability with performance, TSK systems lending themselves to visualization and descriptions through natural language were developed and optimized via the described learning algorithm.

3.2.2. System description

We created a base model comprised of fuzzy systems to serve as a foundation for optimization.

To balance score and execution time, each ship tracks distances and angles to immediate threats and potential targets. These values take into account considerations such as screen wrap and object size. More importantly, they serve as inputs to fuzzy systems that determine shooting, turning, and thrust behavior. A general overview of this process is shown in Figure 2.

3.2.3. Learning algorithm

The employed algorithm for optimization approximates gradient descent by iteratively running scenarios and altering TSK outputs to more closely resemble the best performer. This requires establishing a performant objective function and additional hyperparameter tuning; the range of possible TSK output values, number of iterations, and learning rate all vary based on configuration. However, the theoretical upside is a more systematic approach to optimal performance when compared to approaches such as genetic algorithms. The approach used for this project is described in Algorithm 1.

Algorithm 1 Asteroid Smasher Iterative Learning

```
Initialize FIS
Set learning rate α
for each epoch do
    Create/choose a scenario
    Test scenario with the current FIS and save score in the interval [0, 1]
    for i in range(k) do
        Create a alteration vector h with adjustments to each TSK output parameter
        Create a new fuzzy system by adding h to the baseline's parameters
        Test scenario with altered fuzzy system and save score in the interval [0, 1]
    end for
    Calculate maximum score difference s = best − baseline
    Create the new current FIS with currentFIS = currentFIS + (α ∗ s ∗ h)
end for
```

In other words, we created a number of slightly modified fuzzy systems per scenario and borrowed slightly from the alterations made to the best performer. The degree to which the modification is added to the baseline is a product of the alteration, the given learning rate, and the difference between the maximum score and baseline. Some stability was gained by adding the last condition; scores that were only slightly better appeared to warrant proportionally smaller adjustments.

Scenario creation constitutes an important component of this process. For some problems, this may be trivial, but others may require consideration of the problem, goal, and available resources. To train for the competition, highly difficult and random scenarios with a very large number of asteroids were generated in lieu of a battery of scenarios for reasons primarily related to ease of implementation.

3.2.4. Experimental results

Applying the discussed iterative learning method resulted in a story of minor but noticeable performance increase across key competition metrics such as score, win rate in difficult scenarios, and number of successful hits on asteroids.

Performance comparisons of the base model, the product of optimization, and a model where TSK outputs were randomly initialized are shown in Figure 3 and Figure 4. It is important to note that, in this application, a manually tuned agent served as the starting point of optimization rather than the randomly initialized one.

Even a sizable rolling average across epochs still illustrates notable instability. Part of this is likely attributable to the randomness innate to the extreme training scenarios. However, testing methods similar to those described previously for increasing the stability of RL may constitute a key area of further research.

3.2.5. Explainability

An advantage of the FIS is its ability to encapsulate complex behavior in an interface that deals in partial truths and natural language; functions and interactions that would prove difficult to interpret otherwise are meaningfully organized in comprehensible fuzzy sets and rules. More fundamentally, dealing with partial truths can prove more familiar and intuitive than crisp logic to a human expert.

In this case, the developed systems are comprised of a natural language rule set and associated fuzzy sets that lend themselves to visualization. Figure 5 illustrates this with plots of antecedent fuzzy sets and 0^{th} order outputs describing varying levels of ship thrust. Included is the associated rule set in which the relationships

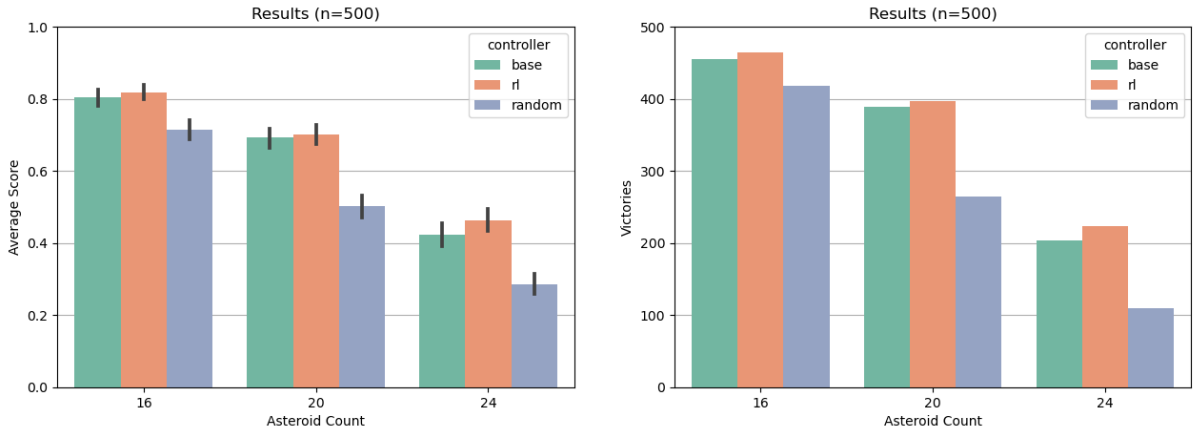

Figure 3. Comparisons of average game score and number of victories in challenging scenarios for the manually tuned model (base), the product of reinforcement learning (RL), and randomly initialized models (random).

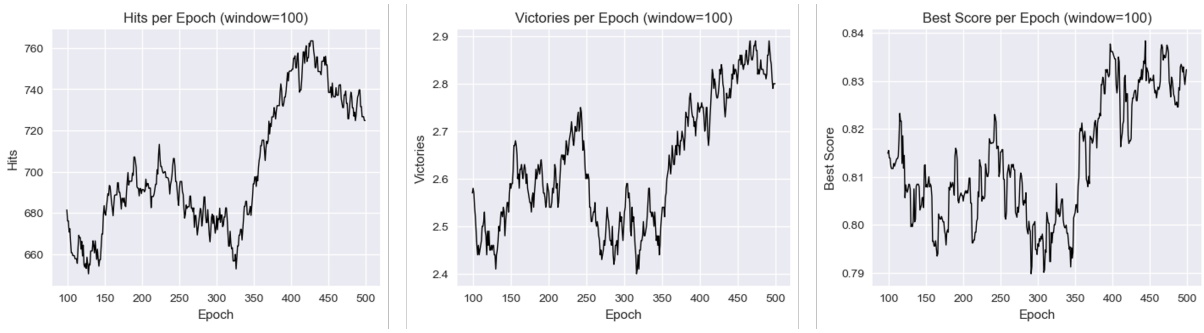

Figure 4. Rolling averages of several performance metrics throughout training.

between inputs and outputs are encoded in natural language. Similar systems were employed to determine the relative value of asteroids as targets and dictating turning and shooting behaviors.

As previously discussed, the explainability of the FIS in applications such as control systems is already well established. Rather than further clarifying this, the described algorithm and Asteroid Smasher example instead serve to delineate and test an alternative to more commonly employed methods for the optimization of existing FIS-based architectures. Successful application here offers experimental evidence to join the relatively scarce literature on developing fuzzy systems with RL as opposed to historically prevalent approaches such as genetic algorithms.

3.3. Case study: reinforcement learning ANFIS for classic control environments

3.3.1. Introduction to ANFIS

The intersection of fuzzy logic and RL stands to offer more than an alternative method of post-hoc optimization for the former: notoriously opaque NN architectures also stand to benefit from integration with explainable fuzzy systems. In other words, neuro-fuzzy systems offer a means for taking advantage of the strengths of artificial NNs while peering a little further into the black-box models that find widespread use in RL applications and elsewhere.

To bolster experimental results in this domain, we tested an ANFIS[30] (Figure 6) on OpenAI's classical control environment CartPole[51]. An example of the environment is shown in Figure 7. The ANFIS extends the TSK system by allowing the parameters of the fuzzy rules to be learned via gradient descent optimization rather

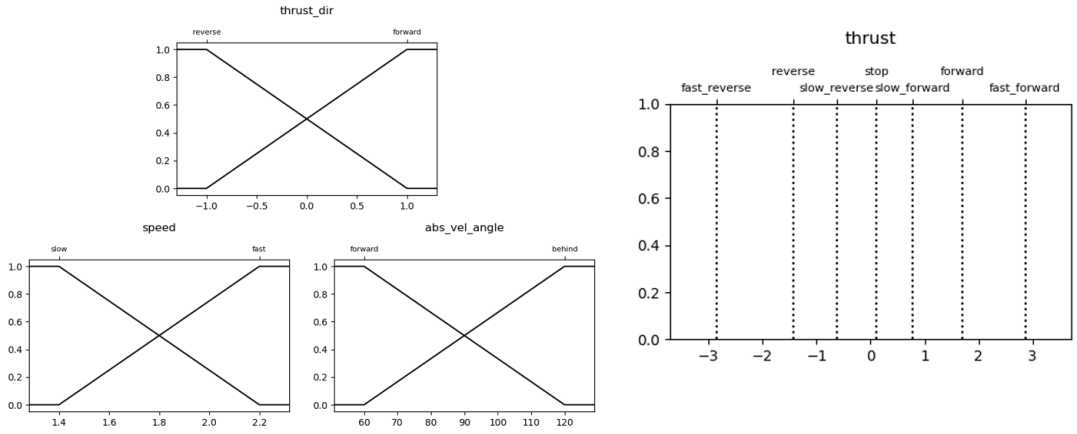

if thrust-dir is reverse and abs-vel-angle is forward and speed is fast then thrust is fast-reverse
if thrust-dir is reverse and abs-vel-angle is forward and speed is slow then thrust is reverse
if thrust-dir is reverse and abs-vel-angle is behind and speed is slow then thrust is slow-reverse
if thrust-dir is reverse and abs-vel-angle is behind and speed is fast then thrust is stop

if thrust-dir is forward and abs-vel-angle is forward and speed is fast then thrust is stop
if thrust-dir is forward and abs-vel-angle is forward and speed is slow then thrust is slow-forward
if thrust-dir is forward and abs-vel-angle is behind and speed is slow then thrust is forward
if thrust-dir is forward and abs-vel-angle is behind and speed is fast then thrust is fast-forward

Figure 5. Antecedent fuzzy sets, optimized TSK consequents, and associated rules for determining ship thrust.

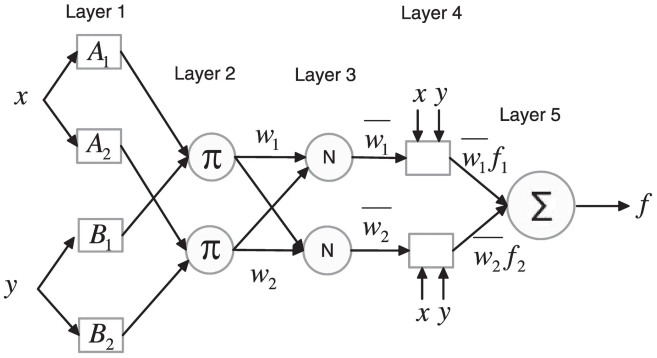

Figure 6. Example ANFIS Structure [53] with 2 antecedents and 1 consequent.

than using fixed constants for the parameters of the antecedents and the consequences. Towards this end, the ANFIS is combined with a NN to learn representations from the inputs, which are then fuzzified by the network. Outputs of the ANFIS layers are calculated by multiplying the fuzzified output of the NN by antecedents of rules. Then, the antecedents are multiplied by learnable parameters and summed to form the consequences. In the case of multiple-consequent models where the output dimension is more than a single value, we used a modified ANFIS structure: the Multioutput Adaptive Neuro-Fuzzy Inference System (MANFIS) [52]. This method creates a separate rule base for each output dimension but follows the defuzzification process as a typical ANFIS. This process is shown in Figure 8.

A NN of abstract shape is used and can be configured as desired. After passing the input through the NN, the

(a) Example of starting position.

(b) Example of state that would terminate the episode.

Figure 7. Snapshots of states for the CartPole [51] environment.

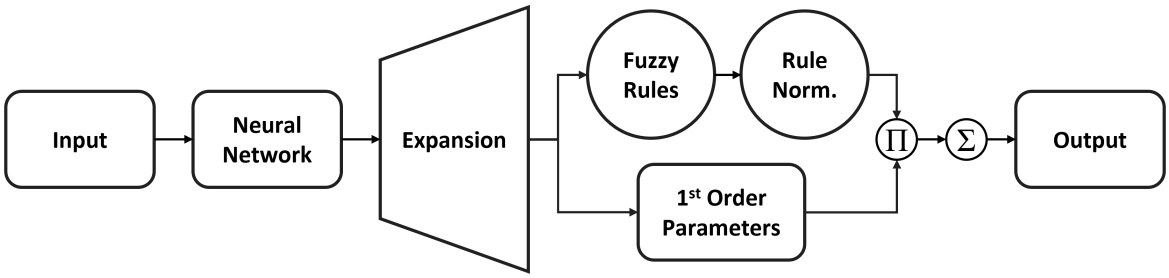

Figure 8. Flowchart for ANFIS model. NN output undergoes fuzzy rule evaluation and normalization. Separately, network output is transformed according to learned 1^{st} order parameters and multiplied by the normalized rule outputs. These values are summed and given as output.

output is expanded in dimensions to match the number of rules. This is then passed through the fuzzy rules to calculate their firing levels prior to normalization along each output dimension. Then, in the case of a 1^{st} order ANFIS, the input is multiplied by a parameter, and a bias is added. If the 0^{th} order ANFIS is used, the input is passed along to the next layer. Next, the normalized firing levels are multiplied by the inputs to form the rule evaluation. Finally, the output is summed along each rule base to form the final output with the correct dimension.

3.3.2. CartPole-v1

The CartPole-v1 environment has four variables for the input: the position of the cart, the velocity of the cart, the angle of the pole, and the angular velocity of the pole. The expected output has two actions: move left and move right. The job of the models is to learn and maximize the Q-values for each state to achieve a maximum possible reward of 500, where, in each frame, the agent gets a reward of 1 if the cart and pole are within the min and max values for each respective field. A reward of 500 means that during 500 frames, the agent is able to balance the pole. To perform an action in the environment, we take the action with the maximum Q-value.

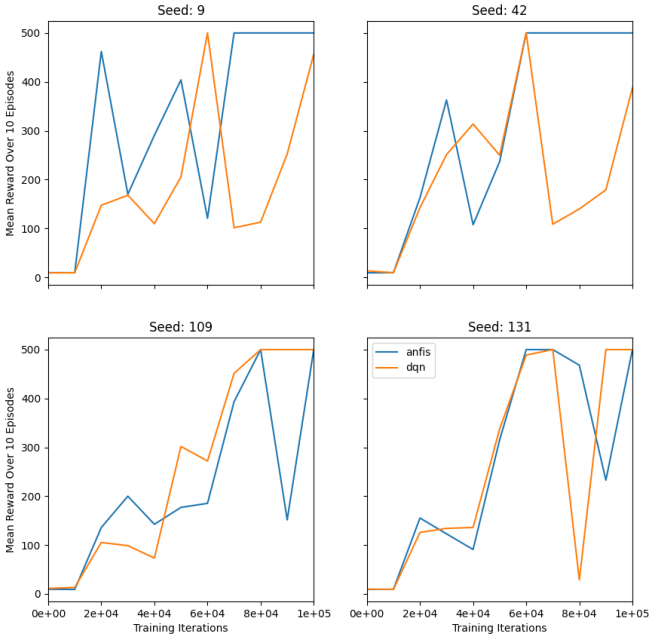

Figure 9. Comparisons between ANFIS DQN and DQN.

3.3.3. ANFIS DQN vs DQN

We compare the ANFIS DQN architecture proposed above with a standard DQN architecture. Both models are equipped with a Double DQN structure with soft updates and have a similar number of trainable parameters; 17,410 for the DQN and 17,407 for the ANFIS DQN. Both models are also equipped with the same optimization method, learning rate, etc., and trained for 100,000 iterations. The appendix contains parameters and hyperparameters.

3.3.4. Experimental results

For testing the results of the two models, we look at the mean reward of 10 testing environments every 10,000 iterations. The goal is to have the agent hit a mean reward of 500 for all 10 test environments.

From Figure 9, we can see that both models can learn the environment. In some cases, we can see that the ANFIS DQN model learns the environment quicker, such as in seed 9 and seed 42. While in other cases, it seems to perform about as well as the DQN, such as in seeds 109 and 131. The most interesting case is in seed 42, where the ANFIS DQN and DQN solve the environment in the same number of steps, but the ANFIS DQN learns it with more stability while not falling off after learning and continues to have a solution after 60,000 iterations. This trend also appears in seed 9, where after 70,000 iterations, the ANFIS DQN has a stable solution. From these tests, we can see that the ANFIS DQN is able to match, if not slightly outperform, the DQN agent.

3.3.5. Explainability

As suggested, a primary advantage of this approach over non-fuzzy DQN concerns the capacity for explainability; one may visualize the fuzzy rule components before and after training to help in understanding the changes made during optimization and the resulting behavior.

To illustrate this, an example concerning the approximation of a mathematical function is shown in Figure 10. In this case, Gaussian functions corresponding to fuzzy rules expand and contract following gradient descent

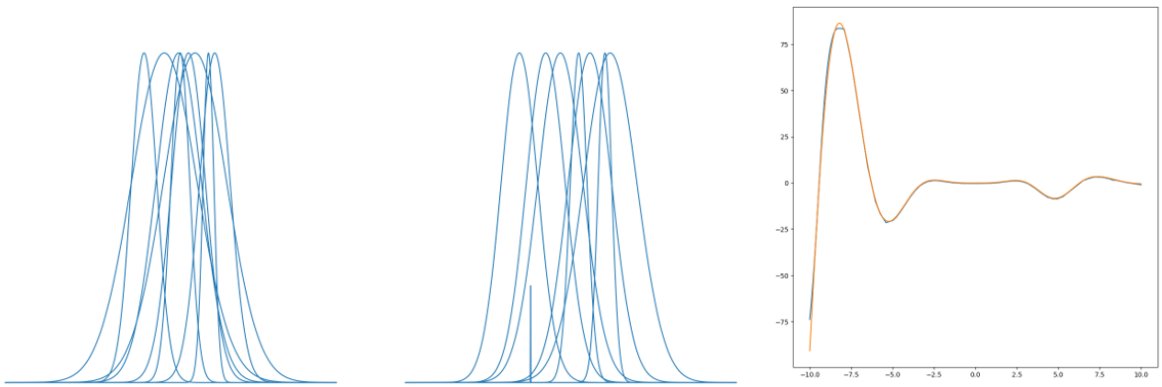

(a) Rule base before training **(b)** Rule base after training **(c)** Results of function approximation

Figure 10. Comparison of rules for approximating a function before and after optimization. The straight line represents a rule that becomes insignificant after training.

to afford a close estimate of the function. Notably, one Gaussian function depicted by the straight line in Figure 10b becomes insignificant after training. Not only does this indicate potential robustness to network overparameterization, but the ability to visualize the components of the system in this way also highlights a propensity for troubleshooting architectural design and training.

The CartPole example represents a jump in complexity that corresponds with increased challenges to helpful visualization; the 32 rules for movement in either direction stand to benefit from a more directed form of presentation. However, the same principles of visual feedback for training and resulting behavior apply. Both before and after training, one may observe the rule base of the ANFIS DQN and extract important information about the decisions of the agent.

We can see how some of the behaviors are shaped by analyzing the distribution and coverage of antecedents in Figure 11. In the current visualization, it may be hard to explain all aspects of interaction, but we can investigate some possible behaviors. The blue curves indicate the rules for moving the cart to the left, and the red curves describe movement to the right. The domain is the domain for input space from CartPole. Each input that is passed into the rules comes from the output of a NN. The blue curves are related to moving the cart to the left, and the red curves for moving the cart to the right. While we cannot see exactly what inputs the rules are related to, we can see some trends that indicate what each rule may be impacting. In the beginning, both sets of colored curves are fairly uniform around the origin. After training, we can see that they have spread out to cover more domains, and some curves are wider. Some interesting things to note are there are two inputs in the observation space for cart velocity and pole angle. Negative values are associated with the pole and the cart moving to the left. We can see how some of the blue curves moved further to the left, and the red curves moved further to the right. This is because the intelligent action of moving the cart the opposite way the pole is moving can help correct the position of the pole. These small insights can give us some explanation as to what the network is doing when making decisions. With a better visualization, we could see what each rule is specifically looking at in the input related to the output.

It should be noted that there is also much unique potential for experimentation with novel explainability mechanisms. Further research of ANFIS DQN in this vein could support efforts in quantifying changes to rules after training, identifying rules that become insignificant, highlighting substantial activations for any one state, and exploring aggregations that describe overall trends in behavior. While similar ideas have certainly been explored to aid the interpretability of traditional NNs, the capacity for visualization offered by FIS-based ar-

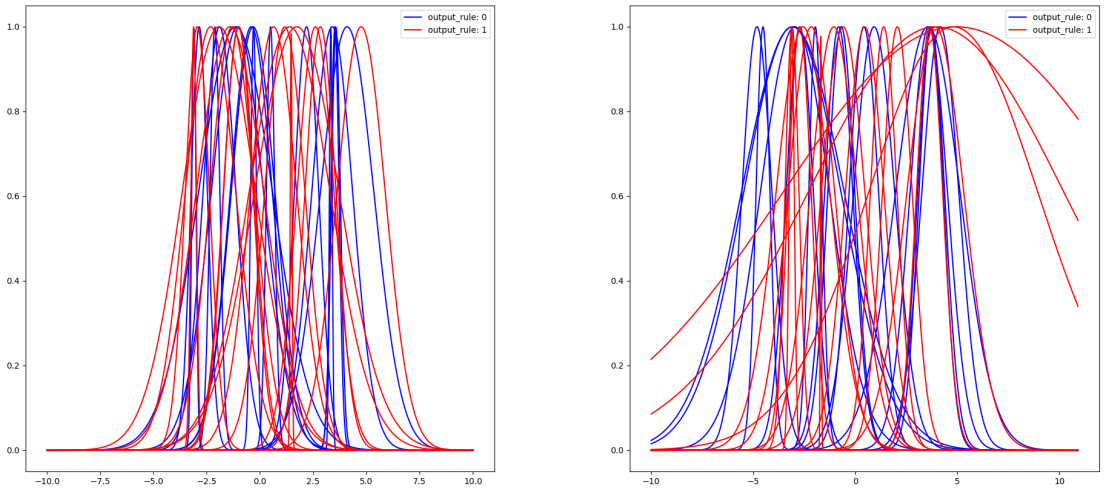

(a) Rule base before training **(b)** Rule base after training

Figure 11. Comparison of rule antecedent distributions for moving left (blue) and right (red) in the CartPole environment. Input consists of encoded cart position, cart velocity, pole angle, and pole angular velocity.

chitectures represents a significant opportunity due to the reasons discussed and the relative lack of existing literature in this domain specifically.

4. CONCLUSION

In the present paper, we study fuzzy systems controlled via RL and multiple applications of this framework. The first environment considered is the Asteroid Smasher game in which the associated agent made use of fuzzy systems trained via an actor-critic RL algorithm. This agent won XFC 2022, an Explainable AI competition emphasizing fuzzy logic. We also compared ANFIS DQN architectures with classic DQN architectures and demonstrated that the fuzzy systems perform similarly or, in some cases, better than DQN systems. More significantly, we highlighted the amenability of TSK-based architectures to explainability and visualization when compared to more traditional NNs.

Grounds for further research include an exploration of possible improvements to the stability of the RL algorithm used to tackle the Asteroid Smasher environment. With respect to ANFIS architectures, additional exploration of applications, network architectures, membership functions, and unique explainability mechanisms could also prove valuable for both performance and explainability. In both cases, there are extensions such as improved experience replay, dueling DQN, and distributional learning that could afford improved results.

The most significant takeaway concerns the relatively underinvestigated and mutually beneficial relationship between RL and fuzzy logic. Despite trends in the former and the value that each stands to offer the other, alternative methods are more commonly employed to optimize fuzzy systems. Moreover, promising neuro-fuzzy frameworks face relative obscurity in light of the steadfast need for trust and interpretability in domains where NNs are pervasive. Consequently, additional experimentation serves to afford value when building performant and explainable applications.

DECLARATIONS

Authors' contributions

Wrote and reviewed the paper: Zander E, van Oostendorp B, Bede B

Availability of data and materials

There are no applicable datasets, but the implementation of a PyTorch compatible ANFIS layer is available here if relevant: https://github.com/Squeemos/pytorch_anfis.

Financial support and sponsorship

None.

Conflicts of interest

All authors declared that there are no conflicts of interest.

Ethical approval and consent to participate

Not applicable.

Consent for publication

Not applicable.

REFERENCES

1. Zadeh LA. Fuzzy sets. *Inf Contr* 1965;8:338–53. DOI
2. Mamdani EH, Assilian S. An experiment in linguistic synthesis with a fuzzy logic controller. *Int J Man-Mac Studies* 1975;7:1–13. DOI
3. Takagi T, Sugeno M. Fuzzy identification of systems and its applications to modeling and control. In: *IEEE Trans Syst , Man, Cybern* 1985;8:116–32. DOI
4. Precup RE, Hellendoorn H. A survey on industrial applications of fuzzy control. *Comput Industry* 2011;62:213–26. DOI
5. Pirovano M. The use of fuzzy logic for artificial intelligence in games. *University of Milano, Milano* 2012. Available from: https://www.michelepirovano.com/pdf/fuzzy_ai_in_games.pdf [Last accessed on 6 Jun 2023]
6. Russell SJ. Artificial intelligence a modern approach. Pearson Education, Inc.; 2010.
7. Silver D, Schrittwieser J, Simonyan K, et al. Mastering the game of Go without human knowledge. *Nature* 2017;550:354–59. DOI
8. Lakhani AI, Chowdhury MA, Lu Q. Stability-preserving automatic tuning of PID control with reinforcement learning. *Complex Eng Syst* 2022;2:3. DOI
9. Li Y. Deep reinforcement learning: an overview. *arXiv preprint arXiv:170107274* 2017. DOI
10. Zhao E, Yan R, Li J, Li K, Xing J. AlphaHoldem: high-Performance artificial intelligence for heads-up no-limit poker via end-to-end reinforcement learning. In: Proceedings of the AAAI Conference on Artificial Intelligence. vol. 36; 2022. pp. 4689–97. DOI
11. Shao K, Tang Z, Zhu Y, Li N, Zhao D. A survey of deep reinforcement learning in video games. *arXiv preprint arXiv:191210944* 2019. DOI
12. Chen J, Yuan B, Tomizuka M. Model-free deep reinforcement learning for urban autonomous driving. In: 2019 IEEE intelligent transportation systems conference (ITSC). IEEE; 2019. pp. 2765–71. DOI
13. Walker O, Vanegas F, Gonzalez F, Koenig S. A deep reinforcement learning framework for UAV navigation in indoor environments. In: 2019 IEEE Aerospace Conference. IEEE; 2019. pp. 1–14. DOI
14. Ouyang L, Wu J, Jiang X, et al. Training language models to follow instructions with human feedback. *J Inf Process Syst* 2022;35:27730–44. DOI
15. Mundhenk TN, Chen BY, Friedland G. Efficient saliency maps for explainable AI. *arXiv preprint arXiv:191111293* 2019. DOI
16. Borys K, Schmitt YA, Nauta M, et al. Explainable AI in medical imaging: an overview for clinical practitioners–Beyond saliency-based XAI approaches. *Eur J Radiol* 2023:110786. DOI
17. Holzinger A, Saranti A, Molnar C, Biecek P, Samek W. Explainable AI methods-a brief overview. In: xxAI-Beyond Explainable AI: International Workshop, Held in Conjunction with ICML 2020, July 18, 2020, Vienna, Austria, Revised and Extended Papers. Springer; 2022. pp. 13–38. DOI
18. Hagras H. Toward human-understandable, explainable AI. *Computer* 2018;51:28–36. DOI
19. Mencar C, Alonso JM. Paving the way to explainable artificial intelligence with fuzzy modeling. In: Fuzzy Logic and Applications.

Springer; 2019. pp. 215–27. DOI
20. Viaña J, Ralescu S, Cohen K, Ralescu A, Kreinovich V. Extension to Multidimensional Problems of a Fuzzy-Based Explainable and Noise-Resilient Algorithm. In: Decision Making Under Uncertainty and Constraints: A Why-Book. Springer; 2023. pp. 289–96. DOI
21. Pickering L, Cohen K. Genetic Fuzzy Controller for the Homicidal Chauffeur Differential Game. In: Applications of Fuzzy Techniques: Proceedings of the 2022 Annual Conference of the North American Fuzzy Information Processing Society NAFIPS 2022. Springer; 2022. pp. 196–204. DOI
22. Pickering L, Cohen K. Toward explainable AI—genetic fuzzy systems—a use case. In: Explainable AI and Other Applications of Fuzzy Techniques: Proceedings of the 2021 Annual Conference of the North American Fuzzy Information Processing Society, NAFIPS 2021. Springer; 2022. pp. 343–54. DOI
23. Fernandez A, Herrera F, Cordon O, del Jesus MJ, Marcelloni F. Evolutionary fuzzy systems for explainable artificial intelligence: Why, when, what for, and where to? *IEEE Comput Intell Mag* 2019;14:69–81. DOI
24. Berenji HR. A reinforcement learning—based architecture for fuzzy logic control. *Int J Approx Reason* 1992;6:267–92. DOI
25. Glorennec PY, Jouffe L. Fuzzy Q-learning. In: Proceedings of 6th international fuzzy systems conference. vol. 2. IEEE; 1997. pp. 659–62. DOI
26. Er MJ, Deng C. Online tuning of fuzzy inference systems using dynamic fuzzy Q-learning. *IEEE Trans Syst Man Cybern B Cybern* 2004;34:1478–89. DOI
27. Jamshidi P, Sharifloo AM, Pahl C, Metzger A, Estrada G. Self-learning cloud controllers: Fuzzy q-learning for knowledge evolution. In: 2015 International Conference on Cloud and Autonomic Computing. IEEE; 2015. pp. 208–11. DOI
28. Kumar S. Learning of Takagi-Sugeno Fuzzy Systems using Temporal Difference methods. DigiPen Institute of Technology; 2020.
29. Mnih V, Kavukcuoglu K, Silver D, et al. Human-level control through deep reinforcement learning. *Nature* 2015 Feb;518:529–33. DOI
30. Jang JSR. ANFIS: adaptive-network-based fuzzy inference system. *IEEE Trans Syst , Man, Cybern* 1993;23:665–85. DOI
31. King SD. Explainable AI competition; 2023. Accessed on 2/15/2023. Available from: https://xfuzzycomp.github.io/XFC/. [Last accessed on 6 Jun 2023]
32. Sugeno M, Kang G. Structure identification of fuzzy model. *Fuzzy Sets Syst* 1988;28:15–33. DOI
33. Bellman R. A markovian decision process. *Indiana Univ Math J* 1957;6:679–84. Available from: https://www.jstor.org/stable/24900506 [Last accessed on 6 Jun 2023]
34. Watkins CJCH, Dayan P. Q-learning. *Mach Learn* 1992 May;8:279–92. DOI
35. Vinyals O, Babuschkin I, Czarnecki WM, et al. Grandmaster level in StarCraft II using multi-agent reinforcement learning. *Nature* 2019;575:350–54. DOI
36. Lin LJ. Self-improving reactive agents based on reinforcement learning, planning and teaching. *Mach Learn* 1992;8:293–321. DOI
37. Schaul T, Quan J, Antonoglou I, Silver D. Prioritized experience replay. arXiv; 2015. DOI
38. Andrychowicz M, Wolski F, Ray A, et al. Hindsight Experience Replay. arXiv; 2018. DOI
39. van Hasselt H, Guez A, Silver D. Deep reinforcement learning with double Q-learning. arXiv; 2015. DOI
40. Polyak BT, Juditsky AB. Acceleration of Stochastic Approximation by Averaging. *SIAM J Control Optim* 1992 Jul;30:838–55. DOI
41. Rosenstein MT, Barto AG, Si J, et al. Supervised actor-critic reinforcement learning. *Learning and Approximate Dynamic Programming: Scaling Up to the Real World* 2004:359–80. Available from: https://citeseerx.ist.psu.edu/document?repid=rep1&type=pdf&doi=ec4de9c9729f9301aefa713ac42f194a364a4406 [Last accessed on 6 Jun 2023]
42. Yan X, Deng Z, Sun Z. Competitive Takagi-Sugeno fuzzy reinforcement learning. In: Proceedings of the 2001 IEEE International Conference on Control Applications (CCA'01)(Cat. No. 01CH37204). IEEE; 2001. pp. 878–83. DOI
43. Jaakkola T, Jordan M, Singh S. Convergence of stochastic iterative dynamic programming algorithms. *Adv Neural Inf Proces Syst* 1993;6. Available from: https://proceedings.neurips.cc/paper/1993/file/5807a685d1a9ab3b599035bc566ce2b9-Paper.pdf [Last accessed on 6 Jun 2023]
44. Melo FS. Convergence of Q-learning: a simple proof. *Inst Syst Robot, Tech Rep* 2001;1–4. Available from: https://d1wqtxts1xzle7.cloudfront.net/55970511/ProofQlearning-libre.pdf?1520268288=&response-content-disposition=inline%3B+filename%3DConvergence_of_Q_learning_a_simple_proof.pdf&Expires=1686128725&Signature=SZMvoQSM3Z7UPmyXfT4QOw8Co0pUvQM1h3NfUwa3aJXBPsj8ox1O9WI~QaTZrpZ5~Cr4NcfcDmsh~IUjT101xNeKR2-PCvewznfNXB38~UEGN736l3lniIQLKe1QdebMTHgvtL7iDOivntOKxrLAnzUx0I4dYlAuYUf3qBNk37aqJtIH6WTpCuJUKeH3pW282tY11MVEK0P~Czp-WsOkY8wtMOu8~NCNcS2sR6d1rhV1JeWPv1BuTAg6-hBUFFhbqLIY7SvJ8j6IWA0bJy~Miaz4Q2C37sOi2eo2~y819e3F3jiby3mMWeEpf1WYPUWK~0hB475dafC5FGZcEKTVjA__&Key-Pair-Id=APKAJLOHF5GGSLRBV4ZA [Last accessed on 6 Jun 2023]
45. Cybenko G. Approximation by superpositions of a sigmoidal function. *Math Control Signal Systems* 1989;2:303–14. DOI
46. Yarotsky D. Error bounds for approximations with deep ReLU networks. *Neural Netw* 2017;94:103–14. DOI
47. Melo FS, Ribeiro MI. Q-learning with linear function approximation. In: Learning Theory: 20th Annual Conference on Learning Theory, COLT 2007, San Diego, CA, USA; June 13-15, 2007. Proceedings 20. Springer; 2007. pp. 308–22. DOI
48. Papavassiliou VA, Russell S. Convergence of reinforcement learning with general function approximators. In: IJCAI. vol. 99; 1999. pp. 748–55. Available from: http://people.eecs.berkeley.edu/~russell/papers/ijcai99-bridge.pdf [Last accessed on 6 Jun 2023]
49. Ying H. General Takagi-Sugeno fuzzy systems are universal approximators. In: 1998 IEEE International Conference on Fuzzy Systems Proceedings. IEEE World Congress on Computational Intelligence (Cat. No. 98CH36228). vol. 1. IEEE; 1998. pp. 819–23. DOI
50. Bede B. Mathematics of Fuzzy Sets and Fuzzy Logic. Springer; 2013.
51. Brockman G, Cheung V, Pettersson L, et al. Openai gym. *arXiv preprint arXiv:160601540* 2016. DOI
52. Benmiloud T. Multioutput Adaptive Neuro-Fuzzy Inference System. In: Proceedings of the 11th WSEAS International Conference on

Nural Networks and 11th WSEAS International Conference on Evolutionary Computing and 11th WSEAS International Conference on Fuzzy Systems. NN'10/EC'10/FS'10. Stevens Point, Wisconsin, USA: World Scientific and Engineering Academy and Society (WSEAS); 2010. p. 94–98.

53. Al-Hmouz A, Shen J, Al-Hmouz R, Yan J. Modeling and simulation of an adaptive neuro-Fuzzy inference system (ANFIS) for mobile learning. *IEEE Trans Learning Technol* 2012;5:226–37. DOI

APPENDIX: ANFIS AND DQN HYPERPARAMETERS

Most hyperparameters were taken from previous work/recommended defaults of libraries

1. DQN Structure
    - 2 linear layers with 128 nodes and ReLU activation functions
2. ANFIS Structure
    - 2 linear layers with 128, 127 nodes, respectively, and ReLU activation functions
    - 16 rules, with the mean of the Gaussian membership function sampled from the Normal distribution and scaled by 2 to increase rule-base coverage, and the standard deviations sampled from the uniform distribution
    - Learnable parameters/biases for summation sampled from the Normal distribution and scaled by 2
3. Optimizer: ADAM
4. Learning rate: .001
5. Gamma discount factor: 0.99
6. Max replay memory size: 10,000
7. Batch Size: 128
8. Begin training after: 1,000 iterations
9. Epsilon start: 1.0
10. Epsilon end: .01
11. Epsilon decay: After 20,000 iterations in a linear fashion
12. Gradient clipping norm: 10
13. Target network update iterations: 100
14. Tau soft update parameter: .001

Chen *et al*. *Complex Eng Syst* 2023;3:8
DOI: 10.20517/ces.2022.50

Complex Engineering Systems

Research Article

Open Access

Nonlinear hierarchical control for four-wheel-independent-drive electric vehicle

Xiang Chen[1,2], Yuan Qu[1], Taowen Cui[1], Jin Zhao[1]

[1]Vehicle Lab of Intelligent Vector Control Technology, Chery Automobile Company Limited, Wuhu 241000, Anhui, China.
[2]College of Energy and Power Engineering, Nanjing University of Aeronautics and Astronautics, Nanjing 210016, Jiangsu, China.

Correspondence to: Dr./Associate Prof. Xiang Chen, College of Energy and Power Engineering, Nanjing University of Aeronautics and Astronautics, 29 Yudao Street, Nanjing 210016, Jiangsu, China. E-mail: jluchenxiang@163.com

How to cite this article: Chen X, Qu Y, Cui T, Zhao J. Nonlinear hierarchical control for four-wheel-independent-drive electric vehicle. *Complex Eng Syst* 2023;3:8. http://dx.doi.org/10.20517/ces.2022.50

Received: 28 Nov 2022 **First Decision:** 31 Jan 2023 **Revised:** 26 Mar 2023 **Accepted:** 25 Apr 2023 **Published:** 20 May 2023

Academic Editor: Hamid Reza Karimi **Copy Editor:** Fangling Lan **Production Editor:** Fangling Lan

Abstract

As under-constrained systems, four-wheel-independent-drive (4WID) electric vehicles have more driving degrees of freedom. In this context, reasonable control and distribution of driving or braking torque to each wheel is extremely important from the vehicle safety perspective. However, it is difficult to provide the optimal wheel torque because of the time-varying characteristics and typical over-actuated nature of the system. In light of these challenges, a novel hierarchical control scheme comprising a top- and bottom-level controller is proposed herein. First, for the top-level controller, a time-varying model-predictive-control (TV-MPC) controller is designed based on an extended 3-degree-of-freedom (3-DOF) reference vehicle model. The total driving force and additional yaw moment can be obtained using the TV-MPC. Second, for the bottom-level controller, the torque expression of each wheel is determined using the equal-adhesion-rate-rule -based algorithm. The co-simulation results obtained herein indicate that the proposed control scheme can effectively improve vehicle safety.

Keywords: Safety, four-wheel-independent-drive electric vehicle, time-varying model-predictive-control, equal adhesion allocation

1. INTRODUCTION

Worldwide, energy crises and environmental pollution are the fundamental reasons driving the development of electric vehicles (EVs)[1,2]. For any type of vehicle, vehicle handling stability, which determines driving safety, is a significant performance measure. Among various types of EVs, four-wheel independent drive (4WID) EVs come with four in-wheel motors that can simultaneously reduce energy consumption and increase vehicle stability[3,4]. Given that the use of independent in-wheel motors facilitates independent installation of drive systems, this approach allows each wheel to regulate its driving force, which provides more possibilities to enhance vehicle performance in terms of maneuverability and stability[5,6]. However, because of the time-varying nonlinear characteristics of vehicles, 4WID EV stability and effective torque distribution algorithms remain suboptimal.

The greatest advantage of 4WID vehicles is that the four hub motors can be controlled independently, meaning that the motors can work in their respective high efficient range and optimal attachment range to the extent possible. Given that vehicle stability is essential for traffic safety, many scholars have focused on the key issues related to vehicle stability. In this context, the understeer coefficient in quasi-steady-state maneuvers has been studied extensively, with a focus on typical lateral dynamics controls, such as active front steering and yaw moment control[7–9]. Lenzo *et al*. derived a relationship between the understeer coefficient and yaw moment, and they obtained an apparently surprising result at low speeds: the rear-wheel-drive (RWD) architecture provided the highest level of understeer, and the yaw moment due to the longitudinal forces of the front tires was significant under high lateral accelerations and steering angles[10]. Analogously, the concept of relaxed static stability (RSS) was proposed and utilized to guide the configuration of the 4WID configuration and to design the overall 4WID vehicle structure with the aim of improving vehicle stability" without affecting the intended meaning[11]. In Ref.[12], the influences of the electric motor's output power limit, road friction coefficient, and torque response of each wheel on stability control were elucidated. Chen *et al*. used a double-layer control algorithm to determine the desired yaw moment and longitudinal forces of four tires with the aim of improving vehicle stability[13]. The authors of[14] added a layer to the aforementioned algorithm[13] to judge whether a vehicle is in a stable state by implementing the phase plane method before the two layers. For stability control of 4WID vehicles, sliding mode control and its improved version are the most commonly used methods[15,16]. An integral sliding mode control (ISMC) approach was proposed for 4WID vehicles to generate differential drive force to assist the steering process in the absence of adequate lateral tire force[17]. However, sliding mode control tends to oscillate near the sliding surface. Peng *et al*. proposed a 7-degree-of-freedom (DoF) model-predictive control (MPC) method to improve vehicle stability[18]. However, in their case, discrete MPC linearization was slightly rough, which may lead to inaccurate results.

Although a few researchers have drawn attention toward this knowledge, the problems of ensuring vehicle stability and torque allocation still cannot be solved quickly and accurately for the following reasons: (1) 4WID EVs are highly nonlinear and time-varying system, and the use of simple processes will reduce the system accuracy; (2) The four in-wheel motors are not decoupled and need to be coordinated simultaneously; and (3) Unpredictability of the iteration steps in the traditional optimization algorithm may lead to a scenario where the torques applied to the four tires do not reach the respective optimal values in real time. In Ref.[16], the minimum total adhesion rate algorithm was used to allocate torque to each wheel. However, this method may lead to local optimization or large differences in the adhesion rates of different tires. For this reason, we propose a hierarchical control algorithm that includes a nonlinear-MPC-based upper algorithm for obtaining the total longitudinal force and direct yaw moment, and an equal-adhesion-rate-rule-based lower torque allocation algorithm. The main contributions of this study are as follows: (1) an extended 3-DOF reference vehicle model is built that can be integrated with the traditional 2-DOF reference vehicle model; (2) Exact expressions are derived for the first-order derivatives of TV-MPC; and (3) A torque allocation algorithm based on the equal adhesion rate rule of the bottom-level controller is proposed to ensure full utilization of the adhesion rate. The structure of the hierarchical control algorithm proposed herein is illustrated in Figure 1.

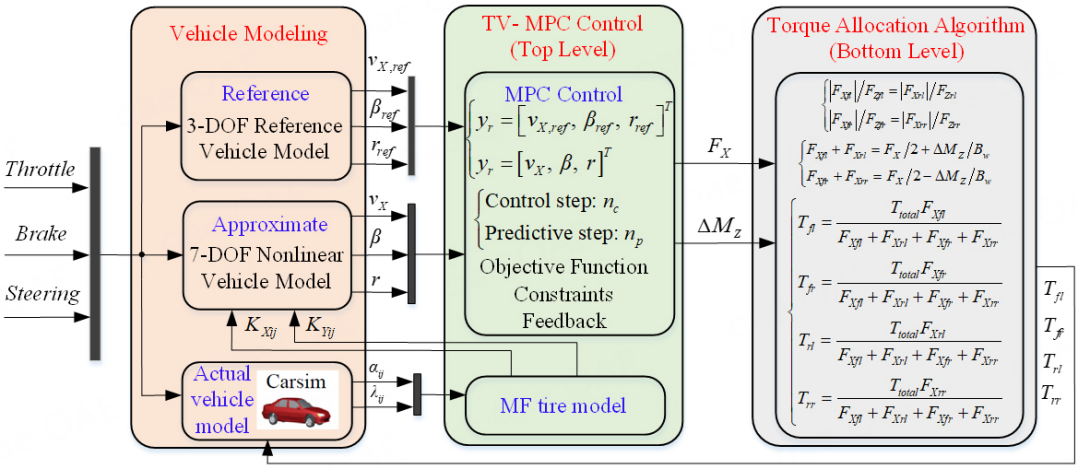

Figure 1. Structure of hierarchical control algorithm proposed herein.

The remainder of this paper is organized as follows. In Section 2, three models related to the vehicle are built. In Section 3, a time-varying MPC controller is designed. In Section 4 the equal-adhesion-rate-rule-based torque allocation algorithm is elaborated. In Section 5, the proposed method is demonstrated by conducting a Carsim–Simulink co-simulation. Finally, our concluding remarks are presented in Section 6.

2. VEHICLE MODEL

By considering the nonlinear and time-varying dynamic characteristics of 4WID EVs and the related control problems, an extended 3-DOF reference vehicle model and a nonlinear 7-DOF vehicle model are established in this section. In addition, a magic formula (MF) tire model is developed.

2.1. 3-DOF reference vehicle model

In this study, a single-track vehicle model is used as the 3-DOF reference vehicle model. According to [19], the actual and desired longitudinal accelerations of the vehicle satisfy the following first-order relationship:

$$a = \frac{K}{1+\tau s} a_{des} \tag{1}$$

where a and a_{des} represent the actual and desired longitudinal accelerations of the vehicle, respectively; $K = 1$ is the system gain; and τ is the time constant that ranges from 0.2 to 0.5. Therefore, the relationship between the actual and desired longitudinal velocities can be expressed as

$$v_X = \frac{v_{X,des}}{1+\tau s} \tag{2}$$

Here, $v_{X,des}$ can be calculated as follows:

$$\dot{v}_{X,des} = \frac{F_{Xf} + F_{Xf} - F_{total}}{m} \tag{3}$$

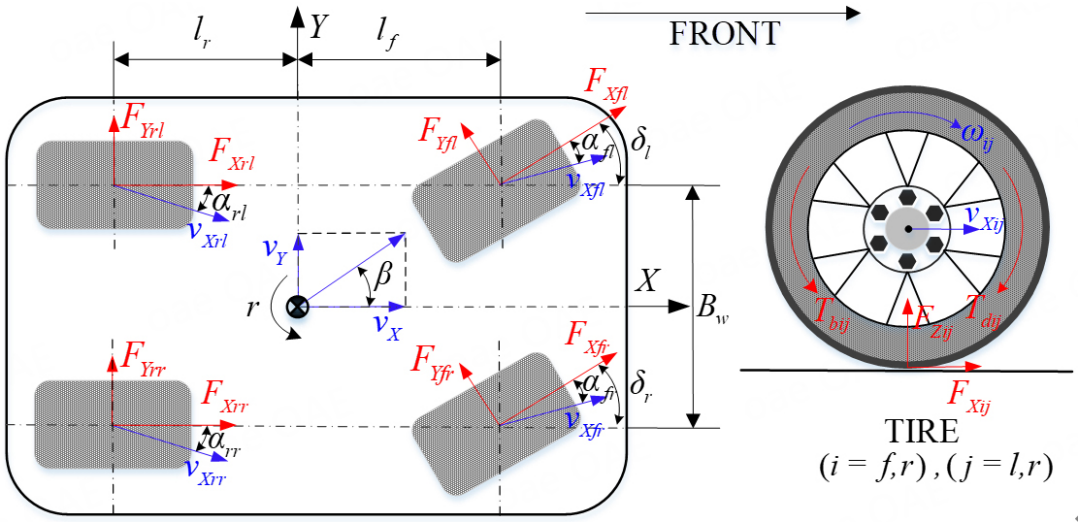

Figure 2. 7-DOF nonlinear vehicle dynamic model.

where m denotes the vehicle mass; F_{Xf} and F_{Xf} denote the longitudinal front and rear tire forces, respectively; F_{total} is the total resistance force; and $v_{X,des}$ and $v_{X,des}$ denote the actual and desired longitudinal vehicle velocities, respectively. Combined with the traditional 2-DOF linear vehicle model, the transfer function of the 3-DOF reference vehicle model can be expressed as follows:

$$\begin{cases} v_{X,ref} = v_{X,des}/(1+\tau s) \\ \beta_{ref} = G_{\beta,des}\delta_f/(1+Ts) \\ r_{ref} = G_{r_r,des}\delta_f/(1+Ts) \end{cases} \tag{4}$$

where

$$\begin{cases} G_{\beta,des} = \dfrac{K_f K_r l_r (l_f+l_r)+mv_{X,des}^2 K_f l_f}{K_f K_r (l_f+l_r)^2+(K_f l_f-K_r l_r)mv_{X,des}^2} \\ G_{r,des} = \dfrac{K_f K_r (l_f+l_r)v_{X,des}}{K_f K_r (l_f+l_r)^2+(K_f l_f-K_r l_r)mv_{X,des}^2} \\ T = \dfrac{ml_f v_{X,des}}{K_r (l_f+l_r)} - \dfrac{\left[m\left(K_f l_f^2+K_r l_r^2\right)+I_Z (K_f+K_r)\right]v_{X,des}}{K_f K_r (l_f+l_r)^2+(K_f l_f-K_r l_r)mv_{X,des}^2} \end{cases}$$

Here, δ_f is the steering angle of the front wheel; I_Z is the yaw moment of the vehicle inertia; l_f and l_r are the distances from the mass center to the front and rear axles; K_f and K_r denote the front and rear wheel cornering stiffnesses; β and r are the sideslip angle and yaw rate of the vehicle, respectively.

2.2. 7-DOF nonlinear vehicle model

To obtain an accurate model for MPC control in the process of predicting the vehicle state, a 7-DOF nonlinear vehicle model, illustrated in Figure 2, is established, and it allows for free longitudinal motion, lateral motion, yaw motion, and rotation of the four wheels. The dynamic equilibrium equations of vehicle longitudinal, lateral, and yaw motions can be expressed as follows:

$$\begin{cases} m\left(\dot{v}_X - r\beta v_X\right) = \left(F_{Xfl} + F_{Xfl}\right)\cos\delta_f + F_{Xrl} + F_{Xir} - \left(F_{Yfl} + F_{Yfi}\right)\sin\delta_f \\ m(\dot{\beta} + r)v_X = \left(F_{Xfl} + F_{Xfi}\right)\sin\delta_f + \left(F_{Yfl} + F_{Yfi}\right)\cos\delta_f + F_{Yrl} + F_{Yrr} \\ I_Z\dot{r} = \left(F_{Xfl} + F_{Xff}\right)l_f\sin\delta_f + \left[\left(F_{Xfi} - F_{Xf}\right)\cos\delta_f + \left(F_{Xir} - F_{Xrl}\right)\right]\frac{B_w}{2} \\ \quad + \left(F_{Yfl} + F_{Yff}\right)l_f\cos\delta_f + \left(F_{Yfl} - F_{Yfi}\right)\frac{B_w}{2}\sin\delta_f - \left(F_{Yrl} + F_{Yrr}\right)l_r \end{cases} \tag{5}$$

In this equation, m and I_Z denote the vehicle's sprung mass and its moment of inertia around the Z axis, respectively; B_w is the vehicle's wheelbase; δ_f is the steering angle of the front axle, and it can be approximated as $\delta_l = \delta_r = \delta_f$; F_{Xij} and F_{Yij} denote longitudinal and lateral tire forces (where $i = f$ or r, $j = l$ or r; fl means front left, fr means front right, rl means rear left, and rr means rear right), respectively. The meanings of the other parameters are given in Section 2.1.

The rotational dynamic equilibrium equation of each wheel is expressed as follows:

$$I_w\dot{\omega}_{ij} = T_{ij} - F_{Xij}R_w \quad (i = f, r \quad j = l, r) \tag{6}$$

where I_w is the moment of wheel inertia around each axis of rotation, R_w is the effective radius of each wheel, ω_{ij} denotes the rotation rate of each wheel, and T_{ij} is the driving torque T_{dij} or braking torque T_{bij} of each in-wheel motor.

2.3. MF tire model

The general form of the MF tire model[20] is as follows:

$$Y(x) = D\sin\{C\arctan[Bx - E(Bx - \arctan(Bx))]\} \tag{7}$$

where x is either the longitudinal slip ratio λ_{ij} or lateral slip angle α_{ij}. B, C, D, and E denote the stiffness factor, shape factor, peak value, and curvature factor, respectively. The tire longitudinal slip ratio of each wheel is expressed as follows:

$$\lambda_{ij} = \begin{cases} \frac{\omega_{ij}R - v_{Xij}}{\omega_{ij}R_w} & \text{Driving Conditon} \\ \frac{v_{X_{ij}} - \omega_{ij}R}{v_{Xij}} & \text{Braking Conditon} \end{cases} \quad (i = f, r \quad j = l, r) \tag{8}$$

where v_{Xxy} denotes the longitudinal translational velocity of each wheel, which can be calculated as follows:

$$\begin{cases} v_{Xfi} = (v_X - rB_w/2)\cos\delta_f + \left(v_X\beta + rl_f\right)\sin\delta_f \\ v_{Xfr} = (v_X + rB_w/2)\cos\delta_f + \left(v_X\beta + rl_f\right)\sin\delta_f \\ v_{Xrl} = v_X - rB_w/2 \\ v_{Xrr} = v_X + rB_w/2 \end{cases} \tag{9}$$

The tire lateral sideslip angle of each wheel can be expressed as follows:

Table 1. MF tire model parameters a_0–a_8 and b_0–b_6

Parameter	a_0	a_1	a_2	a_3	a_4	a_5	a_6	a_7	a_8
Value	1.37	-0.0039	8.78	0.0076	5.1	-0.00016	0	0.0001	0.3
Parameter	b_0	b_1	b_2	b_3	b_4	b_5	b_6		
Value	1.388	-0.049	99.7	2,311	8.97	0.662	-1,323		

$$\begin{cases} \alpha_{fl} = \frac{\beta v_X + r l_f}{v_X - r B_w/2} - \delta_f & \alpha_{rl} = \frac{\beta v_X - r l_r}{v_X - r B_w/2} \\ \alpha_{fr} = \frac{\beta v_X + r l_f}{v_X + r B_w/2} - \delta_f & \alpha_{rr} = \frac{\beta v_X - r l_r}{v_X + r B_w/2} \end{cases} \tag{10}$$

The parameters B, C, D, and E in the longitudinal MF tire model are given as follows:

$$C = a_0, \quad D = \mu\left(a_1 F_Z^2 + a_2 F_Z\right), \quad B = \left(a_3 F_Z^2 + a_4 F_Z\right) e^{\sigma_5 F_z}/(CD), \quad E = a_6 F_Z^2 + a_7 F_Z + a_8$$

The parameters B, C, D, and E in the lateral MF tire model are given as follows:

$$C = b_0, \quad D = \mu\left(b_1 F_Z^2 + b_2 F_Z\right), \quad B = b_3 \sin\left[2\arctan\left(F_Z/b_4\right)\right]/(CD), \quad E = b_5 F_Z + b_6$$

where a_0–a_8 and b_0–b_6 can be calibrated by conducting tire force tests, and their values are listed in Table 1.

F_Z is the tire vertical force, and the vertical force of each tire can be expressed as follows:

$$\begin{cases} F_{Zfl} = m_w g + m g l_r/\left(l_f + l_r\right) - m\dot{v}_X h/\left(l_f + l_r\right) - m(r + \dot{\beta}) v_X h l_r/\left[B_w\left(l_f + l_r\right)\right] \\ F_{Zfr} = m_w g + m g l_r/\left(l_f + l_r\right) - m\dot{v}_X h/\left(l_f + l_r\right) + m(r + \dot{\beta}) v_X h l_r/\left[B_w\left(l_f + l_r\right)\right] \\ F_{Zrl} = m_w g + m g l_f/\left(l_f + l_r\right) + m\dot{v}_X h/\left(l_f + l_r\right) - m(r + \dot{\beta}) v_X h l_f/\left[B_w\left(l_f + l_r\right)\right] \\ F_{Zrr} = m_w g + m g l_f/\left(l_f + l_r\right) + m\dot{v}_X h/\left(l_f + l_r\right) + m(r + \dot{\beta}) v_X h l_f/\left[B_w\left(l_f + l_r\right)\right] \end{cases} \tag{11}$$

where m_w denotes tire mass, and g denotes gravitational acceleration. h is the distance between the roll center and sprung mass center. The longitudinal and lateral tire forces are limited in the adhesion ellipse. Therefore, the tire force calculated using the MF model can be modified using the following expressions:

$$\begin{cases} F_X = \frac{|\sigma_X|}{\sigma} Y(\lambda) & F_Y = \frac{|\sigma_Y|}{\sigma} Y(\alpha) \\ K_X = \frac{\partial F_X}{\partial \lambda} & K_Y = \frac{\partial F_Y}{\partial \alpha} \\ \sigma_X = \frac{\lambda}{1+\lambda} \quad \sigma_Y = \frac{\tan\alpha}{1+\lambda} & \sigma = \sqrt{\sigma_X^2 + \sigma_Y^2} \end{cases} \tag{12}$$

3. TIME-VARYING MPC

Model accuracy is the basis and key advantage of the MPC control method. To reflect the accuracy of the vehicle model to the extent possible, we utilize the nonlinear 7-DOF vehicle model developed in Section 2 as the basis of our MPC control strategy.

The longitudinal speed, sideslip angle, and yaw rate of the vehicle are set as the state variables of the predictive state space equation, which is expressed as $x = [v_X, \beta, r]^T$. The longitudinal total force and the yaw moment due to differences between the longitudinal forces of the four tires are set as the control variables:

$u = [F_X, \Delta M_Z]^T$. The output variables of this system are the same as the state variables, that is, $y = [v_X, \beta, r]^T$. The two control variables can be expressed approximately in terms of the longitudinal force of each tire, as follows:

$$\begin{cases} F_X = F_{Xfl} + F_{Xfr} + F_{Xrl} + F_{Xrr} \\ \Delta M_Z = \left(F_{Xfr} - F_{Xfl} + F_{Xrr} - F_{Xrl}\right) B_w/2 \end{cases} \tag{13}$$

According to Eq. (5), the state-space representation of this control system is as follows:

$$\dot{x} = f(x, u) \tag{14}$$

To reduce computational cost, the system state-space equation is linearized as follows:

$$\begin{cases} \dot{x} = Ax + Bu \\ y = Cx \end{cases} \tag{15}$$

where $A = \frac{\partial f(x,u)}{\partial x} = \begin{bmatrix} \frac{\partial f}{\partial v_X} & \frac{\partial f}{\partial \beta} & \frac{\partial f}{\partial r} \end{bmatrix}$, $B = \frac{\partial f(x,u)}{\partial u} = \begin{bmatrix} 1/m & 0 & 0 \\ 0 & 0 & 1/I_z \end{bmatrix}^T$, $C = \mathrm{diag}(1, 1, 1)$

$$\frac{\partial f}{\partial v_X} = \begin{bmatrix} r\beta + \frac{1}{m}\left[\left(\frac{\partial F_{Xfl}}{\partial v_X} + \frac{\partial F_{Xfr}}{\partial v_X}\right)\cos\delta_f + \frac{\partial F_{Xrl}}{\partial v_X} + \frac{\partial F_{Xrr}}{\partial v_X} - \left(\frac{\partial F_{Yfl}}{\partial v_X} + \frac{\partial F_{Yfr}}{\partial v_X}\right)\sin\delta_f\right]; \\ \frac{1}{mv_X}\left[\left(\frac{\partial F_{Xfl}}{\partial v_X} + \frac{\partial F_{Xfr}}{\partial v_X}\right)\sin\delta_f + \left(\frac{\partial F_{Yfl}}{\partial v_X} + \frac{\partial F_{Yfr}}{\partial v_X}\right)\cos\delta_f + \frac{\partial F_{Yrl}}{\partial v_X} + \frac{\partial F_{Yrr}}{\partial v_X}\right] \\ -\frac{1}{mv_X^2}\left[\left(F_{Xfl} + F_{Xfr}\right)\sin\delta_f + \left(F_{Yfl} + F_{Yfr}\right)\cos\delta_f + F_{Yrl} + F_{Yrr}\right]; \\ \frac{1}{I_Z}\left[\left(\frac{\partial F_{Xfl}}{\partial v_X} + \frac{\partial F_{Xfr}}{\partial v_X}\right) l_f \sin\delta_f + \left[\left(\frac{\partial F_{Xfr}}{\partial v_X} - \frac{\partial F_{Xfl}}{\partial v_X}\right)\cos\delta_f + \left(\frac{\partial F_{Xrr}}{\partial v_X} - \frac{\partial F_{Xrl}}{\partial v_X}\right)\right]\frac{B_w}{2}\right] \\ +\frac{1}{I_Z}\left[\left(\frac{\partial F_{Yfl}}{\partial v_X} + \frac{\partial F_{Yfr}}{\partial v_X}\right) l_f \cos\delta_f + \left(\frac{\partial F_{Yfl}}{\partial v_X} - \frac{\partial F_{Yfr}}{\partial v_X}\right)\frac{B_w}{2}\sin\delta_f - \left(\frac{\partial F_{Yrl}}{\partial v_X} + \frac{\partial F_{Yrr}}{\partial v_X}\right) l_r\right] \end{bmatrix} \tag{16a}$$

$$\frac{\partial f}{\partial \beta} = \begin{bmatrix} rv_X + \frac{1}{m}\left[\left(\frac{\partial F_{Xfl}}{\partial \beta} + \frac{\partial F_{Xfr}}{\partial \beta}\right)\cos\delta_f + \frac{\partial F_{Xrl}}{\partial \beta} + \frac{\partial F_{Xrr}}{\partial \beta} - \left(\frac{\partial F_{Yfl}}{\partial \beta} + \frac{\partial F_{Yfr}}{\partial \beta}\right)\sin\delta_f\right]; \\ \frac{1}{mv_X}\left[\left(\frac{\partial F_{Xfl}}{\partial \beta} + \frac{\partial F_{Xfr}}{\partial \beta}\right)\sin\delta_f + \left(\frac{\partial F_{Yfl}}{\partial \beta} + \frac{\partial F_{Yfr}}{\partial \beta}\right)\cos\delta_f + \frac{\partial F_{Yrl}}{\partial \beta} + \frac{\partial F_{Yrr}}{\partial \beta}\right]; \\ \frac{1}{I_z}\left[\left(\frac{\partial F_{Xfl}}{\partial \beta} + \frac{\partial F_{Xfr}}{\partial \beta}\right) l_f \sin\delta_f + \left[\left(\frac{\partial F_{Xfr}}{\partial \beta} - \frac{\partial F_{Xfl}}{\partial \beta}\right)\cos\delta_f + \left(\frac{\partial F_{Xrr}}{\partial \beta} - \frac{\partial F_{Xrl}}{\partial \beta}\right)\right]\frac{B_w}{2}\right] \\ +\frac{1}{I_z}\left[\left(\frac{\partial F_{Yfl}}{\partial \beta} + \frac{\partial F_{Yfr}}{\partial \beta}\right) l_f \cos\delta_f + \left(\frac{\partial F_{Yfl}}{\partial \beta} - \frac{\partial F_{Yfr}}{\partial \beta}\right)\frac{B_w}{2}\sin\delta_f - \left(\frac{\partial F_{Yrl}}{\partial \beta} + \frac{\partial F_{Yrr}}{\partial \beta}\right) l_r\right] \end{bmatrix} \tag{16b}$$

$$\frac{\partial f}{\partial r} = \begin{bmatrix} \beta v_X + \frac{1}{m}\left[\left(\frac{\partial F_{Xfl}}{\partial r} + \frac{\partial F_{Xfr}}{\partial r}\right)\cos\delta_f + \frac{\partial F_{Xrl}}{\partial r} + \frac{\partial F_{Xrr}}{\partial r} - \left(\frac{\partial F_{Yfl}}{\partial r} + \frac{\partial F_{Yfr}}{\partial r}\right)\sin\delta_f\right]; \\ -1 + \frac{1}{mv_X}\left[\left(\frac{\partial F_{Xfl}}{\partial r} + \frac{\partial F_{Xfr}}{\partial r}\right)\sin\delta_f + \left(\frac{\partial F_{Yfl}}{\partial r} + \frac{\partial F_{Yfr}}{\partial r}\right)\cos\delta_f + \frac{\partial F_{Yrl}}{\partial r} + \frac{\partial F_{Yrr}}{\partial r}\right]; \\ \frac{1}{I_z}\left[\left(\frac{\partial F_{Xfl}}{\partial r} + \frac{\partial F_{Xfr}}{\partial r}\right) l_f \sin\delta_f + \left[\left(\frac{\partial F_{Xfr}}{\partial r} - \frac{\partial F_{Xfl}}{\partial r}\right)\cos\delta_f + \left(\frac{\partial F_{Xrr}}{\partial r} - \frac{\partial F_{Xrl}}{\partial r}\right)\right]\frac{B_w}{2}\right] \\ +\frac{1}{I_Z}\left[\left(\frac{\partial F_{Yfl}}{\partial r} + \frac{\partial F_{Yfr}}{\partial r}\right) l_f \cos\delta_f + \left(\frac{\partial F_{Yfl}}{\partial r} - \frac{\partial F_{Yfr}}{\partial r}\right)\frac{B_w}{2}\sin\delta_f - \left(\frac{\partial F_{Yrl}}{\partial r} + \frac{\partial F_{Yrr}}{\partial r}\right) l_r\right] \end{bmatrix} \tag{16c}$$

The partial derivative in Eq. (15) can be calculated as follows:

$$\left[\frac{\partial F_{Xij}}{\partial v_X}\ \frac{\partial F_{Xij}}{\partial \beta}\ \frac{\partial F_{Xij}}{\partial r}\right] = K_{Xij}\left[\begin{array}{ccc} \frac{\lambda_{Xij}}{\dot{v}_X} & \frac{\lambda_{Xij}}{\dot{\beta}} & \frac{\lambda_{Xij}}{\dot{r}} \end{array}\right] \tag{17a}$$

$$\left[\begin{array}{ccc} \frac{\partial F_{Yfl}}{\partial v_X} & \frac{\partial F_{Yfl}}{\partial \beta} & \frac{\partial F_{Yfl}}{\partial r} \\ \frac{\partial F_{Yfr}}{\partial v_X} & \frac{\partial F_{Yfr}}{\partial \beta} & \frac{\partial F_{Yfr}}{\partial r} \\ \frac{\partial F_{Yrl}}{\partial v_X} & \frac{\partial F_{Yrl}}{\partial \beta} & \frac{\partial F_{Yrl}}{\partial r} \\ \frac{\partial F_{Yrr}}{\partial v_X} & \frac{\partial F_{Yrr}}{\partial \beta} & \frac{\partial F_{Yrr}}{\partial r} \end{array}\right] = \left[\begin{array}{ccc} K_{Yfl}\frac{-r\left(\beta B_w/2+l_f\right)}{\left(v_X-rB_w/2\right)^2} & K_{Yfl}\frac{v_X}{v_X-rB_w/2} & K_{Yfl}\frac{v_X l_f+\beta v_X B_w/2}{\left(v_X-rB_w/2\right)^2} \\ K_{Yfr}\frac{r\left(\beta B_w/2-l_f\right)}{\left(v_X+rB_w/2\right)^2} & K_{Yfr}\frac{v_X}{v_X+rB_w/2} & K_{Yfr}\frac{v_X l_f-\beta v_X B_w/2}{\left(v_X+rB_w/2\right)^2} \\ K_{Yfl}\frac{-r\left(\beta B_w/2-l_f\right)}{\left(v_X-rB_w/2\right)^2} & K_{Yfl}\frac{v_X}{v_X-rB_w/2} & K_{Yfl}\frac{-v_X l_r+\beta v_X B_w/2}{\left(v_X-rB_w/2\right)^2} \\ K_{Yfl}\frac{r\left(\beta B_w/2+l_f\right)}{\left(v_X+rB_w/2\right)^2} & K_{Yfl}\frac{v_X}{v_X+rB_w/2} & K_{Yfl}\frac{-v_X l_f-\beta v_X B_w/2}{\left(v_X+rB_w/2\right)^2} \end{array}\right] \tag{17b}$$

The parameters K_{Xij} and K_{Yij} can be obtained from the MF tire model by using Eq. (12). The parameters in matrix A, which is detailed in Eqs. (16) and (17), can be expressed using the results of the k-th step. Then, Eq. (15) can be discretized as follows:

$$\begin{cases} x(k+1) = G(k)x(k) + H(T)u(k) \\ y(k) = Cx(k) \end{cases} \tag{18}$$

where

$$\begin{cases} G(k) = e^{A(k)T} \approx TA(k) + I \\ H(T) = \int_0^T e^{AT}dt \cdot B \approx TB \end{cases}$$

The discrete linear equation for MPC control can be rewritten in the following form:

$$\begin{cases} \Delta x(k+1) = G(k)\Delta x(k) + H\Delta u(k) \\ y(k) = y(k-1) + C\Delta x(k) \end{cases} \tag{19}$$

where $\Delta u(k) = u(k) - u(k-1)$, and $\Delta x(k) = x(k) - x(k-1)$. The predictive time domain of this system is composed of n_p steps, control time domain of this system is composed of n_c steps, and the relationship $n_c \le n_p$ holds. In this work, n_p and n_c are set to 8 and 3, respectively. The n_c-step control input vector and n_p-step predictive output vector can be expressed as follows:

$$\begin{cases} \Delta U(k) = \left[\begin{array}{cccc} \Delta u(k) & \Delta u(k+1) & \cdots & \Delta u(k+n_c-1) \end{array}\right]^T \\ Y(k) = \left[\begin{array}{ccccccc} y(k+1) & y(k+2) & \cdots & y(k+n_c) & \cdots & y(k+n_p) \end{array}\right]^T \end{cases} \tag{20}$$

Therefore, the output vector of each future predictive n_p steps is given as follows:

$$Y(k) = S_x(k)x(k) + I_y y(k) + S_u(k)\Delta U(k) \tag{21}$$

where $S_x(k) = \begin{bmatrix} CG \\ \sum_{i=1}^{2} CG^i \\ \vdots \\ \sum_{i=1}^{n_p} CG^i \end{bmatrix}_{(k)}$, $I_y = \begin{bmatrix} I_{n_c \times n_c} \\ I_{n_c \times n_c} \\ \vdots \\ I_{n_c \times n_c} \end{bmatrix}_{n_p \times 1}$,

$$S_u(k) = \begin{bmatrix} CH & 0 & 0 & \cdots & 0 \\ \sum_{i=1}^{2} CG^{i-1}H & CH & 0 & \cdots & 0 \\ \vdots & \vdots & \vdots & \ddots & \vdots \\ \sum_{i=1}^{n_c} CG^{i-1}H & \sum_{i=1}^{n_c-1} CG^{i-1}H & \cdots & \cdots & CH \\ \vdots & \vdots & \vdots & \ddots & \vdots \\ \sum_{i=1}^{n_p} CG^{i-1}H & \sum_{i=1}^{n_p-1} CG^{i-1}H & \cdots & \cdots & \sum_{i=1}^{n_p-n_c+1} CG^{i-1}H \end{bmatrix}_{(k)}$$

To track the reference vehicle model as well as possible, a 3-DOF vehicle model is designed as the reference model. According to Eq. (4), the reference discrete output vector can be obtained as follows:

$$y_r(k) = G_r(T)y_r(k-1) + H_r(T)u_r(k-1) \tag{22}$$

where $u_r(k) = \begin{bmatrix} v_{X,des}(k) & \beta_{des}(k) & r_{des}(k) \end{bmatrix}^T$, $y_r(k) = \begin{bmatrix} v_{X,ref}(k) & \beta_{ref}(k) & r_{ref}(k) \end{bmatrix}^T$,

$A_r = diag(1/\tau, 1/T, 1/T), G_r(T) = I - TA_r$, and $H_r(T) = TA_r$. The n_p-step predictive output vector of the reference system can be expressed as follows:

$$Y_r(k) = \begin{bmatrix} y_r(k+1) & y_r(k+2) & \cdots & y_r(k+n_c) & \cdots & y_r(k+n_p) \end{bmatrix}^T \tag{23}$$

Accordingly, the output vector of each future predictive n_p steps of the reference system is given as follows:

$$Y_r(k) = W_{yr}y_r(k) + W_{ur}u_r(k) \tag{24}$$

where $W_{yr} = \begin{bmatrix} G_r & G_r^2 & \cdots & G_r^{n_p} \end{bmatrix}^T$, and $W_{ur} = \begin{bmatrix} H_r & \sum_{i-1}^{2} G_r^{i-1}H & \cdots & \sum_{i-1}^{n_p} G_r^{i-1}H \end{bmatrix}^T$. In addition, the following relationship $u_r(k+1/k) = u_r(k)(i = 1, 2 \cdots n_p)$ holds.

The objective function of this MPC strategy has the following quadratic form:

$$J(k) = \sum_{i=1}^{n_p} \|y(k+i) - y_r(k+i)\|_{Q_i}^2 + \sum_{i=1}^{n_e} \|\Delta u(k+i-1)\|_{R_i}^2 + \Theta \tag{25}$$

where Q_i and R_i are the weighting matrices of the first and second items, respectively. Θ represents a positive relaxation factor. The objective of this function is to follow the ideal model smoothly and accurately. The first term of this function describes the ability of the actual vehicle model to track the reference model. The second term indicates the change in the input vector, which can restrict changes to the input variables. Meanwhile, the input, input increment, and output variables are constrained in a domain that can be expressed as follows:

$$\begin{cases} u_{\min}(k+i) \le u(k+i) \le u_{\max}(k+i) & (i = 0, 1, \cdots, n_c - 1) \\ \Delta u_{\min}(k+i) \le \Delta u(k+i) \le \Delta u_{\max}(k+i) & (i = 0, 1, \cdots, n_c - 1) \\ y_{\min}(k+i) \le y(k+i) \le y_{\max}(k+i) & (i = 0, 1, \cdots, n_p - 1) \end{cases} \tag{26}$$

Because of constraints, it is generally impossible to obtain the analytical solution to this problem. For this reason, it is necessary to transform it into a quadratic programming (QP) problem to obtain a numerical solution. Therefore, we convert the above constraint equations into the form $C_Z \ge b$, as follows.

$$\begin{cases} \begin{bmatrix} -L_{\Delta U} \\ L_{\Delta U} \end{bmatrix} \Delta U(k) \ge \begin{bmatrix} -\Delta U_{\max}(k) \\ \Delta U_{\min}(k) \end{bmatrix} \\ \begin{bmatrix} -L_U \\ L_U \end{bmatrix} \Delta U(k) \ge \begin{bmatrix} U'(k-1) - U_{\max}(k) \\ U_{\min}(k) - U'(k-1) \end{bmatrix} \\ \begin{bmatrix} -S_u \\ S_u \end{bmatrix} \Delta U(k) \ge \begin{bmatrix} Y'(k-1) - Y_{\max}(k) \\ Y_{\min}(k) - Y'(k-1) \end{bmatrix} \end{cases} \tag{27}$$

where $L_{\Delta U}$, $\Delta U_{\max}(k)$, $\Delta U_{\min}(k)$, L_U, $U'(k-1)$, $U_{\max}(k)$, $U_{\min}(k)$, $Y'(k-1)$, $Y_{\max}(k)$, and $Y_{\min}(k)$ can be calculated according as described in [21]. Then, this question can be described as a standard QP problem. In this manner, the solution of this problem without the constraint equation can be set as the initial solution, which can be expressed as follows:

$$\Delta U(k,0) = \left(S_u^T(k-1)Q^T Q S_u(k-1) + R^T R\right) S_u^T(k-1)Q^T Q E(k) \tag{28}$$

where $E(k) = Y_r(k) - S_x(k-1)\Delta x(k) - I_y y(k)$ he optimal solution of the input vector $\Delta U^*(k)$ can be calculated using the algorithm of the QP problem with constraints. Then, the closed-loop control input can be obtained as follows:

$$\Delta u(k) = \begin{bmatrix} I_{2\times 2} & 0 & \cdots & 0 \end{bmatrix}_{1\times n_e} \Delta U^*(k) \tag{29}$$

Table 2. Parameters of vehicle and in-wheel motors

Parameter	Description	Value/Unit	Parameter	Description	Value/Unit
m	Vehicle mass	812 kg	B_w	Wheelbase	1.65 m
m_w	Vehicle mass	20 kg	P_e	Rated power	7.5 KW
l_f	Distance from mass center to front axle	1.1 m	P_m	Peak power	12 KW
l_r	Distance from mass center to rear axle	1.25 m	n_e	Rated speed	750 rpm
I_Z	Moment of vehicle inertia around Z axis	808 kg ·m^2	n_m	Peak speed	1,000 rpm
I_w	Moment of tire inertia around rotation axis	0.5 kg ·m^2	T_e	Rated torque	150 Nm
h	Distance between roll center and center of sprung mass	0.27 m	T_m	Peak torque	250 Nm
R_w	Distance between roll center and center of sprung mass	0.29 m			

4. TORQUE ALLOCATION ALGORITHM

The proposed torque allocation algorithm based on the equal adhesion rate rule is described in this section. We adopt the equal adhesion rate rule by considering only the adhesion rate of longitudinal force because the deviations due to the lateral and longitudinal forces are excessive, meaning that no solution can be obtained. Therefore, the longitudinal forces on the left and right sides of the vehicle are expressed as follows.

$$\begin{cases} \left|F_{Xfl}\right| / F_{Zfl} = \left|F_{Xrl}\right| / F_{Zrl} \\ \left|F_{Xfr}\right| / F_{Zfr} = \left|F_{Xrr}\right| / F_{Zrr} \end{cases} \tag{30}$$

The total longitudinal forces on the left and right sides of the vehicle can be calculated as follows:

$$\begin{cases} F_{Xfl} + F_{Xrl} = F_X/2 + \Delta M_Z/B_w \\ F_{Xfr} + F_{Xrr} = F_X/2 - \Delta M_Z/B_w \end{cases} \tag{31}$$

Therefore, each longitudinal tire force can be solved quickly by using Eqs. (30) and (31). By using the solved longitudinal tire force and algorithm of equal-adhesion-rate-rule, the torque acting on each wheel can be determined as follows.

$$\begin{cases} T_{fl} = \left(T_{total}F_{Xfl}\right) / \left(F_{Xfl} + F_{Xrl} + F_{Xfr} + F_{Xrr}\right) \\ T_{fr} = \left(T_{total}F_{Xfr}\right) / \left(F_{Xfl} + F_{Xrl} + F_{Xfr} + F_{Xrr}\right) \\ T_{rl} = \left(T_{total}F_{Xrl}\right) / \left(F_{Xfl} + F_{Xrl} + F_{Xfr} + F_{Xrr}\right) \\ T_{rr} = \left(T_{total}F_{Xrr}\right) / \left(F_{Xfl} + F_{Xrl} + F_{Xfr} + F_{Xrr}\right) \end{cases} \tag{32}$$

5. CO-SIMULATION AND RESULTS

To verify the proposed control algorithm, we compared it to the proportional-integral-derivative (PID) control strategy. The co-simulation method was used for this purpose. Two main typical driving conditions, namely ① double lane change (DLC) maneuver under high-adhesion-coefficient condition (μ = 0.9) and ② DLC maneuver under low-adhesion-coefficient condition (μ = 0.3), were considered. The parameters of the vehicle and in-wheel motors are summarized in Table 2.

The consistency of human driving cannot be guaranteed, and it would be unsuitable for real drivers to drive a vehicle at dangerously high speeds or on low-adhesion roads. For this reason, we conducted a simulation to validate the effectiveness of the proposed control scheme.

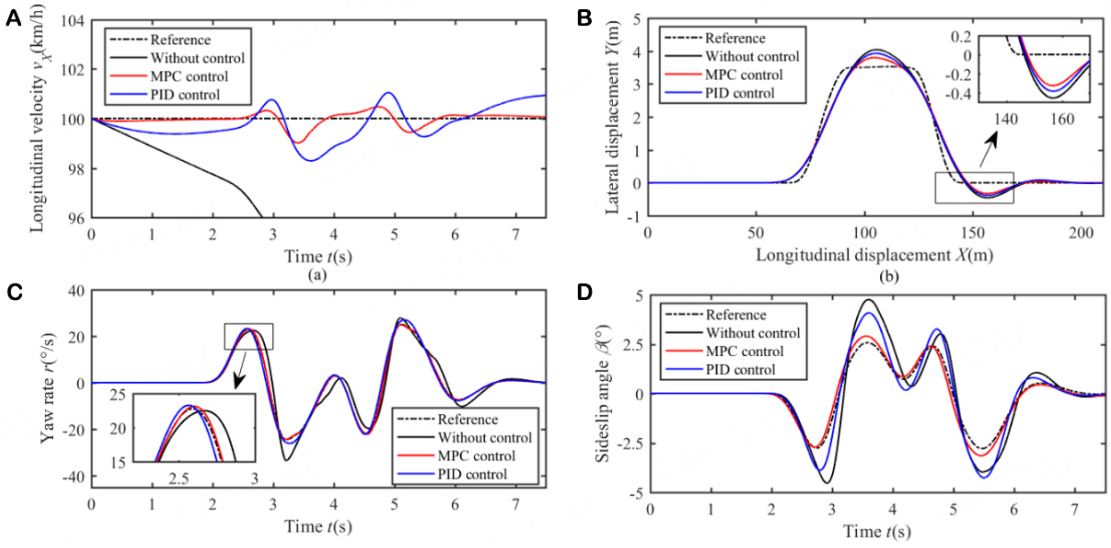

Figure 3. State comparison of different control modes during DLC maneuver. (μ = 0.9, v_x = 100 km/h).

5.1. DLC maneuver on high-adhesion road

The adhesion coefficient on the high-adhesion road was set to 0.9, and the reference vehicle velocity was set to 100 km/h. Figure 3. depicts a comparison of the typical state parameters by using different control methods, which are without active control, hierarchical time-varying MPC control, and PID control. According to Figure 3A, the velocity fluctuation due to the proposed hierarchical time-varying MPC control was smaller than that due to PID control. As shown in Figure 3B, compared to the without active control and PID control methods, the hierarchical time-varying MPC control method decreased the maximum lateral displacement by approximately 0.25 m and 0.11 m, respectively. The yaw rate and sideslip angle of the vehicle under MPC control were able to follow the ideal curve furthest, which effectively enhanced vehicle handling stability and safety, as depicted in Figure 3C and D.

The adhesion rate can be expressed as follows:

$$\varsigma_{ij} = \left|F_{Xij}\right| / F_{Zij} \tag{33}$$

where $i = f$ or r, $j = l$ or r, and fl denotes front left, fr denotes front right, rl denotes rear left, and rr denotes rear right.

The torque and adhesion rate of each tire are depicted in Figure 4. According to Figure 4A, the torque acting on each tire changed gently. Moreover, the torques acting on the left front and rear tires were similar but not equal. Likewise, the torques acting on the right front and rear tires were similar but not equal. However, the adhesion rates of the left two tires were almost equal, and the adhesion rates of the two right tires were almost equal, as depicted in Figure 4B. This indicates that the proposed algorithm can enhance vehicle safety and ensure that the adhesion rates of the two tires on the same side are as similar as possible.

5.2. DLC maneuver on low-adhesion road

Generally, a low-adhesion road can reflect the control effect more remarkably. The adhesion coefficient on a low-adhesion roads and the reference vehicle velocity were set to 0.3 and 70 km/h in this study. As illustrated in Figure 5A, the velocity fluctuation due to the hierarchical time-varying MPC control was smaller than that due

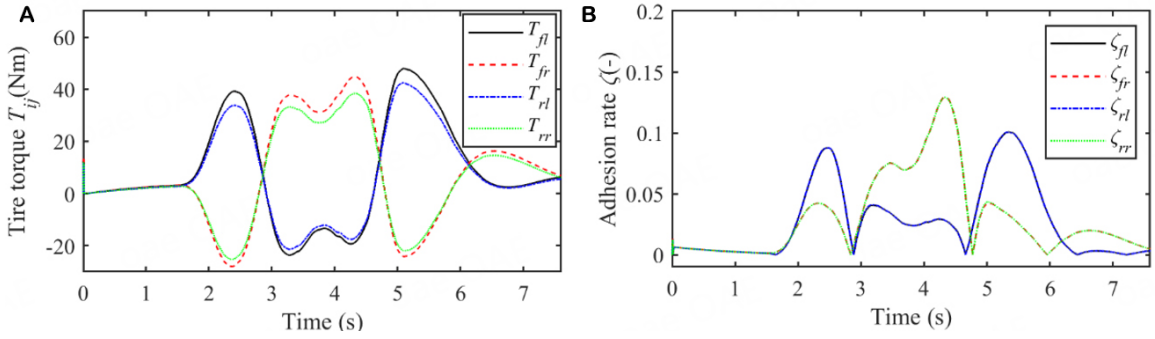

Figure 4. Torque and adhesion rate of each tire. (μ = 0.9, v_x = 100 km/h).

to PID control, and with both methods, velocity fluctuations occurred close to the reference line. However, without control, the velocity dropped considerably. As shown inFigure 5B, the vehicle without control lost stability and deviated from the designated trajectory. The hierarchical time-varying MPC control reduced the maximum lateral displacement by approximately 0.2 m compared to that achieved with PID control. As depicted in Figure 5C and D, under hierarchical time-varying MPC control, the yaw rate and sideslip angle tracked the reference curves very well. The performance of PID control was slightly inferior in comparison, while the case without control performed the worst and the vehicle diverged from the set trajectory. With both PID control and hierarchical time-varying MPC control, the yaw rate control effect was stronger than the sideslip angle control effect because the sideslip angle is more difficult to control than the yaw rate. However, with hierarchical time-varying MPC control, the sideslip angle was less than 2.5°, which is within the safety limit.

The torque and adhesion rate of each tire are shown in Figure 6. According to Figure 6A, the torques acting on the left front and rear tires are similar but not equal, and the torques acting on the right front and rear tires are similar but not equal. However, the adhesion rates of the two left tires are almost equal, and the adhesion rates of the two right tires are almost equal, as shown in Figure 6B. This finding indicates that the proposed algorithm can secure vehicle safety and ensure that the adhesion rates of the two tires on the same side of the vehicle are as close to each other as possible. Unlike on the high-adhesion road, the torques and adhesion rates of each of the tires are lower, which is consistent with the actual situation.

6. CONCLUSIONS

In this study, 3DOF reference vehicle model and a 7DOF nonlinear vehicle model were developed. A novel hierarchical time-varying MPC control strategy was proposed for 4WID EVs by considering vehicle stability and adhesion efficiency. A time-varying MPC controller was designed to reduce system error in the linearization process.

In the co-simulation, two typical conditions were adopted to demonstrate the performance of the proposed method. The DLC maneuver was performed on high- and low-adhesion roads to verify the effectiveness of the proposed control strategy. The results indicated that the proposed hierarchical time-varying MPC control strategy was able to enhance vehicle handling stability effectively. Furthermore, the lower torque allocation algorithm was able to improve the adhesion efficiency of each tire.

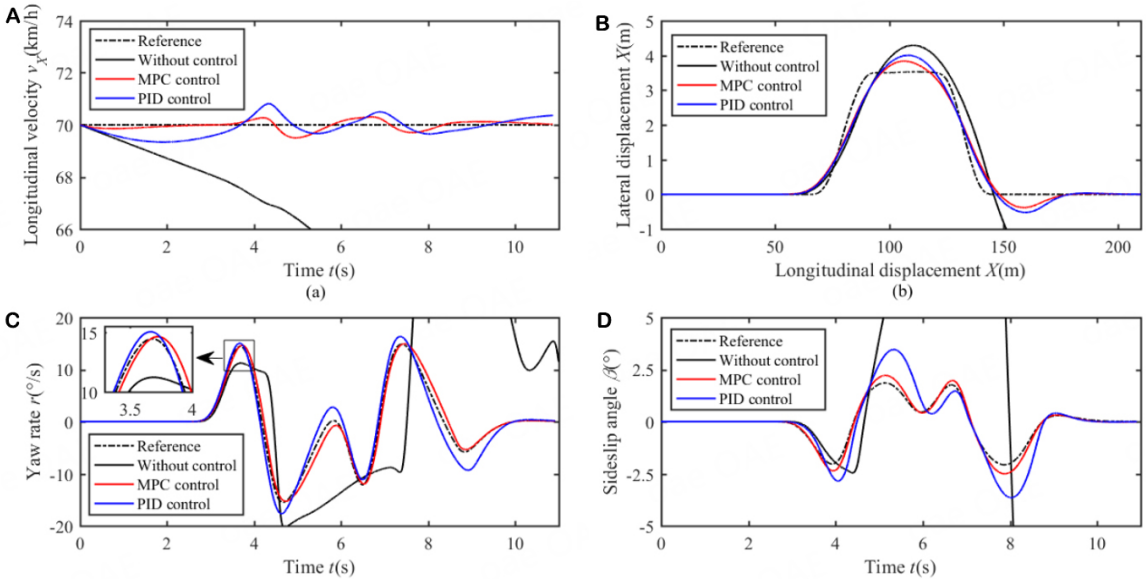

Figure 5. State comparison of different control modes during DLC maneuver (μ = 0.3, v_x = 70 km/h).

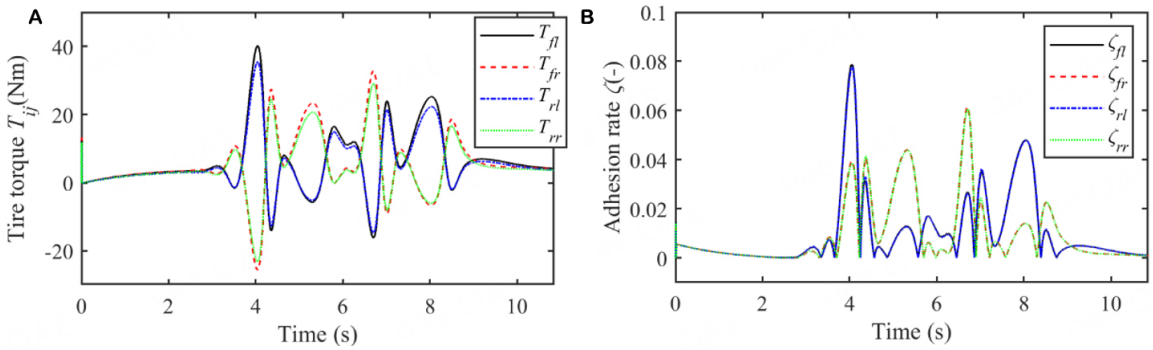

Figure 6. Torque and adhesion rate of each tire (μ = 0.3, v_x = 70 km/h).

DECLARATIONS

Authors' contributions

Conceptualization, methodology, writing-original Draft: Chen X
Supervision, project administration: Qu Y
Formal analysis: Cui T
Software, methodology: Zhao J

Availability of data and materials

Not applicable

Financial support and sponsorship

This work was supported by the National Natural Science Foundation of China (No. 52002211) and Key R&D Plan of Jiangsu Province (No. BE2022053-3).

Conflicts of interest

All authors declared that there are no conflicts of interest.

Ethical approval and consent to participate

Not applicable.

Consent for publication

Not applicable.

REFERENCES

1. Zhuang W, Li S, Zhang X, et al. A survey of powertrain configuration studies on hybrid electric vehicles. *Appl Energy* 2020;262:114553. DOI
2. Yang C, Shi Y, Li L, Wang X. Efficient mode transition control for parallel hybrid electric vehicle with adaptive dual-loop control framework. *IEEE Trans Veh Technol* 2020;69:1519-32. DOI
3. Jing H, Jia F, Liu Z. Multi-objective optimal control allocation for an over-actuated electric vehicle. *IEEE Access* 2018;6:4824-33. DOI
4. Liu J, Zhuang W, Zhong H, Wang L, Chen H, Tan C. Integrated energy-oriented lateral stability control of a four-wheel-independent-drive electric vehicle. *Sci China Technol Sci* 2019;62:2170-83. DOI
5. Ma Y, Chen J, Zhu X, Xu Y. Lateral stability integrated with energy efficiency control for electric vehicles. *Mech Syst Signal Process* 2019;127:1-15. DOI
6. Kobayashi T, Katsuyama E, Sugiura H, Ono E, Yamamoto M. Efficient direct yaw moment control: tyre slip power loss minimisation for four-independent wheel drive vehicle. *Veh Syst Dyn* 2018;56:719-33. DOI
7. Zhao J, Wong PK, Ma X, Xie Z. Chassis integrated control for active suspension, active front steering and direct yaw moment systems using hierarchical strategy. *Veh Syst Dyn* 2017;55:72-103. DOI
8. Song J. Active front wheel steering model and controller for integrated dynamics control systems. *Int J Automot Technol* 2016;17:265-72. DOI
9. Zhang H, Wang J. Robust gain-scheduling control of vehicle lateral dynamics through AFS/DYC. In Modeling, dynamics and control of electrified vehicles. Amsterdam, The Netherlands: Elsevier; 2018. pp. 339-68. DOI
10. Lenzo B, Bucchi F, Sorniotti A, Frendo F. On the handling performance of a vehicle with different front-to-rear wheel torque distributions. *Veh Syst Dyn* 2019;57:1685-704. DOI
11. Ni J, Wang W, Hu J, Xiang C. Relaxed static stability for four-wheel independently actuated ground vehicle. *Mech Syst Signal Process* 2019;127:35-49. DOI
12. Wu D, Ding H, Du C. Dynamics characteristics analysis and control of FWID EV. *Int J Automot Technol* 2018;19:135-46. DOI
13. Chen Y, Hedrick JK, Guo K. A novel direct yaw moment controller for in-wheel motor electric vehicles. *Veh Syst Dyn* 2013;51:925-42. DOI
14. Guo L, Ge P, Sun D. Torque Distribution Algorithm for Stability Control of Electric Vehicle Driven by Four In-Wheel Motors Under Emergency Conditions. *IEEE Access* 2019;7:104737-48. DOI
15. Alipour H, Bannae Sharifian MB, Sabahi M. A modified integral sliding mode control to lateral stabilisation of 4-wheel independent drive electric vehicles. *Veh Syst Dyn* 2014;52:1584-606. DOI
16. Chae M, Hyun Y, Yi K, Nam K. Dynamic Handling Characteristics Control of an in-Wheel-Motor Driven Electric Vehicle Based on Multiple Sliding Mode Control Approach. *IEEE Access* 2019;7:132448-58. DOI
17. Hu C, Wang R, Yan F, Huang Y, Wang H, Wei C. Differential Steering Based Yaw Stabilization Using ISMC for Independently Actuated Electric Vehicles. *IEEE Trans Intell Transport Syst* 2018;19:627-38. DOI
18. Peng H, Wang W, Xiang C, Li L, Wang X. Torque Coordinated Control of Four In-Wheel Motor Independent-Drive Vehicles With Consideration of the Safety and Economy. *IEEE Trans Veh Technol* 2019;68:9604-18. DOI
19. Zhu M, Chen H, Xiong G. A model predictive speed tracking control approach for autonomous ground vehicles. *Mech Syst Signal Process* 2017;87:138-52. DOI
20. Pacejka HB, Bakker E. The magic formula tyre model. *Veh Syst Dyn* 1992;21:1-18. DOI
21. Camacho EF, Alba CB. Model predictive control. Springer Science & Berlin, Germany: Business Media, 2013.

Ding *et al. Complex Eng Syst* 2023;3:7
DOI: 10.20517/ces.2023.06

Complex Engineering Systems

Research Article

Open Access

Secure consensus control for multi-agent systems under communication constraints via adaptive sliding mode technique

Meng Ding, Bei Chen

The School of Electric and Electronic Engineering, Shanghai University of Engineering Science, Shanghai 201620, China.

Correspondence to: Dr. Bei Chen, the School of Electric and Electronic Engineering, Shanghai University of Engineering Science, Shanghai 201620, China. E-mail: chenbei1631@163.com

How to cite this article: Ding M, Chen B. Secure consensus control for multi-agent systems under communication constraints via adaptive sliding mode technique. *Complex Eng Syst* 2023;3:xx. http://dx.doi.org/10.20517/ces.2023.06

Received: 20 Feb 2023 **First Decision:** 13 Mar 2023 **Revised:** 8 Apr 2023 **Accepted:** 15 Apr 2023 **Published:** 17 May 2023

Academic Editor: Hamid Reza Karimi **Copy Editor:** Fanglin Lan **Production Editor:** Fanglin Lan

Abstract

The consensus tracking problem is investigated for a class of multi-agent systems (MASs) under communication constraints. In particular, as a result of the impact of amplitude attenuation and random interference, communication among followers may inevitably suffer from the fading phenomenon. Meanwhile, the controllers may also be subject to malicious deception attacks, which will disrupt the correct operation of the MASs. Thus, the agents can only update their states based on fading information exchanged with their neighbors and the false control input under attacks. The consensus tracking error variables are first designed via the fading signal received from neighbors. Then, an online estimation strategy is introduced to estimate the unknown attacks, based on which the adaptive sliding mode controller is designed to attenuate the effect of the time-varying attacks on MASs. Convergence analysis of the MASs under the designed control strategy is provided by using the Lyapunov stability theory and adaptive sliding mode control method. Finally, the effectiveness of the theoretical results is verified via numerical simulations.

Keywords: Multi-agent systems, consensus tracking, adaptive mechanism, sliding mode control, deception attacks, channel fading

1. INTRODUCTION

As typical autonomous cyber-physical systems, multi-agent systems (MASs) provide an effective means to coordinate spatially distributed and networked agents, where agents interact together to optimize decisions and achieve system objectives. In recent decades, the development of cluster control has motivated more and more research on the consensus problem for MASs, such as multi-UAVs (Unmanned Aerial Vehicles) control[1–3], underwater cooperative operations[4], robot formation control[5–8], wireless sensors collaboration[9], microgrids control[10] and so on. As a key issue in the research of MASs, the consensus problem has received extensive attention in the past few decades. For example, Hu et al. proposed a new consensus protocol for complex networks composed of multiple subnetworks to ensure convergence[11]. Yao *et al.* considered the finite-time consensus problem of MASs based on the finite-time Lyapunov stability theory[12]. Rehman *et al.* investigated the consensus problem of leader-following MASs in both fixed undirected topology and fixed directed topology and proposed two distributed control protocols[13]. Liu *et al.* studied the positive consensus problem of MASs with directed communication topologies where all agents have identical continuous-time positive linear dynamics[14].

To handle the consensus problem, various control methods have been proposed including fuzzy control[15], robust H_∞ control[16], predictive control[17,18], adaptive control[19–21], sliding mode control (SMC)[22], and so on. Due to the strong robustness to external disturbance and parameter uncertainties, the sliding mode control method has been used widely in the MASs consensus research. For the leaderless MASs, Wang *et al.* designed a special SMC protocol for the consensus problem[23]. Cong *et al.* proposed a distributed nonsingular controller to deal with the consensus problem for a class of nonlinear single-integrator MASs with input uncertain dynamics[24]. Rahmani *et al.* proposed a projection recurrent neural network, which was suitable for robotic MASs, and designed a new optimal SMC technique to achieve consensus tracking[25].

However, a key feature of the aforementioned works is that the information can be transmitted accurately among agents. In practical MASs, a satisfying communication environment cannot be guaranteed under wireless transmission networks. As a result of the impact of amplitude attenuation and random interference, the wireless link communication among agents will suffer from the fading phenomenon, resulting in the distortion of the data. This unfavorable factor motivated some interesting research on consensus tracking of wireless MASs subject to channel fading. Oral *et al.*[26] considered link outages between agents and obtained the probability expression for MASs reaching consensus. Gu *et al.* designed a distributed SMC law to deal with the impact of the information fading phenomenon in communication channels[27]. Ding et al. investigated the finite-time consensus control for MASs with channel fading via SMC technique.[28]

Another adverse phenomenon in the wireless transmission network is the inevitable malicious attacks, thereby rendering the secure control of MASs fundamental significance[29]. Considering the different mechanisms and effects on the MASs consensus problem, cyber-attacks can be divided into various types, for example, deception attacks[30], replay attacks[31] and denial-of-service (DoS) attacks[32]. Among them, deception attacks may lead to erroneous information feedback by tampering with the real packets via injecting false data. Cui *et al.* investigated the consensus tracking problem of MASs, which may be subject to deception attacks randomly. Recently, SMC strategy combined with adaptive mechanism has shown promising performance for constrained systems, for example, Chen *et al.* constructed an adaptive sliding mode control law to deal with the effects of adversarial cyber injection attacks[33]. It is of great practical significance to investigate the consensus problem for MASs against deception attacks[34]. Meanwhile, it is challenging to design a feasible SMC law under unknown and time-varying deception attacks.

Inspired by the above discussion and based on the expanded research of ref.[28], this paper will be concerned with the secure consensus control problem for multi-agent systems with malicious attacks and channel fading via the adaptive sliding mode technique, and the main contributions are highlighted as follows: (1) Both the

position error and the velocity error are used to reflect the consistency of MASs, then the consensus tracking problem of MASs can be transformed into the stability problem of the tracking error system; (2) Coping with the effect of the fading channel between followers, the incomplete fading information received by the agent is introduced into the controller design; (3) An online estimation strategy is employed to estimate the unknown and time-varying attacks, based on which, an adaptive sliding mode controller is designed to attenuate the effect of the attacks on MASs; and (4) The distributed adaptive SMC strategy is designed to ensure the mean square consistency of MASs, despite the communication constraints.

Notation: $\mathbb{R}^n$ and $\mathbb{R}^{m\times n}$ mean the n dimension Euclidean space and the $m \times n$ real matrix set. The symbol $|\cdot|$ denotes the Euclidean norm and $\otimes$ denotes the Kronecker product. Denote $\text{sgn}(x)$ the sign symbolic function, $\mathbf{1}_N = [1, 1, \cdots, 1]^T$, $\mathbf{0}_N = [0, 0, \cdots, 0]^T$.

2. PROBLEM FORMULATION

2.1. Graph theory

Graph theory is an important tool to study MASs, which is a graph composed of several nodes and edges connecting the node. Each agent can be represented as a node, and the information interaction between agents can be denoted as an edge in graph theory. A directed weighted graph is represented by $G = \{\mathbb{V}, \mathbb{E}\}$. For MASs with one leader and N agents, the node-set $\mathbb{V} = \{v_1, v_2, \cdots, v_N\}$ indicates the set of all points on the graph and $\mathbb{E} = \{(i, j), i, j \in \mathbb{V}, i \neq j\}$ represents the set of all edges. $A = [a_{ij}] \in \mathbb{R}^{N\times N}$ is a non-negatively weighted adjacency matrix. If $a_{ij} > 0$, it means that agent i can receive information from agent j; conversely, if $a_{ij} = 0$, agent i cannot receive information from agent j. Define the matrix $B = \text{diag}(b_1, b_2, \cdots, b_N)$ to denote the communication between the leader and all followers, and the degree matrix $D = [d_{ii}]$ with $d_{ii} = \sum_{j=1}^{N} a_{ij}$. So, we can obtain the Laplace matrix $L = [l_{ij}]$ as:

$$L = D - A. \tag{1}$$

with

$$l_{ij} = \begin{cases} \sum_{k=1}^{N} a_{ik}, & i = j, \\ -a_{ij}, & i \neq j. \end{cases} \tag{2}$$

Lemma 1 [35] The matrix $L + B$ is invertible if the directed graph G has a directed spanning tree.

Definition 1 Consider a multi-agent system with N agents and let $x_i(t)$ represent the state of agent i. If $lim_{t\to\infty}\|x_i(t) - x_j(t)\| = 0$, for all $i, j = 1, 2, \cdots, N$, it is said that the multi-agent system can reach a consensus. Furthermore, if there exists a leader whose state is $x_0(t)$, then $lim_{t\to\infty}\|x_i(t) - x_0(t)\| = 0$, for all $i, j = 1, 2, \cdots, N$, means the tracking consensus is achieved.

2.2.System model

Consider a second-order MASs consisting of a leader labeled as node 0 and N followers indexed by $i \in \{1, 2, \cdots, N\}$, and the ith follower's dynamic is given as:

$$\begin{cases} \dot{x}_i(t) = v_i(t), \\ \dot{v}_i(t) = u_i(t), \end{cases} \tag{3}$$

where $x_i(t) \in \mathbb{R}^m$, $v_i(t) \in \mathbb{R}^m$, $u_i(t) \in \mathbb{R}^m$ represent the ith follower's position, velocity and the control input, respectively. According to equation (3), it is obvious that we are focused on double integrators.
The leader's dynamic is of the following form:

$$\begin{cases} \dot{x}_0(t) = v_0(t), \\ \dot{v}_0(t) = u_0(t), \end{cases} \tag{4}$$

with $x_0(t) \in \mathbb{R}^m$, $v_0(t) \in \mathbb{R}^m$ the leader's position and velocity, respectively, and $u_0(t) \in \mathbb{R}^m$ representing the control input.

Define the ith follower's consensus tracking errors as follows:

$$\begin{cases} e_{1i}(t) &= \sum_{j=1}^{N} a_{ij}\left(x_i(t) - x_j(t)\right) + b_i\left(x_i(t) - x_0(t)\right), \\ e_{2i}(t) &= \sum_{j=1}^{N} a_{ij}\left(v_i(t) - v_j(t)\right) + b_i\left(v_i(t) - v_0(t)\right), \end{cases} \tag{5}$$

with $e_{1i}(t)$ and $e_{2i}(t)$ the tracking error variables of position and velocity, a_{ij} represents the element of A, b_i determines whether there is information interaction between the leader and the followers, when $b_i > 0$, agent i can receive information from the leader, otherwise, $b_i = 0$.

The tracking errors can be rewritten in the compact form:

$$\begin{cases} e_1(t) &= (L+B) \otimes I_m \cdot (x(t) - \mathbf{1}_N \otimes x_0(t)), \\ e_2(t) &= (L+B) \otimes I_m \cdot (v(t) - \mathbf{1}_N \otimes v_0(t)), \end{cases} \tag{6}$$

with $e_1(t) \triangleq [e_{11}^T(t), \cdots, e_{1N}^T]^T$, $e_2(t) \triangleq \left[e_{21}^T(t), \cdots, e_{2N}^T(t)\right]^T$, $x(t) \triangleq \left[x_1^T(t), \cdots, x_N^T(t)\right]^T$, $v(t) \triangleq \left[v_1^T(t), \cdots, v_N^T(t)\right]^T$, $u(t) \triangleq \left[u_1^T(t), \cdots, u_N^T(t)\right]^T$, $B \triangleq \text{diag}\{b_1, b_2, \cdots, b_N\}$.

From the above definition, one can obtain the tracking error system as:

$$\begin{cases} \dot{e}_1(t) &= e_2(t), \\ \dot{e}_2(t) &= (L+B) \otimes I_m \cdot (u(t) - \mathbf{1}_N \otimes u_0(t)). \end{cases} \tag{7}$$

Now, the consensus tracking problem of MASs (3)-(4) converts to the stabilization problem of the tracking error system (7). The objective of this work is to achieve leader-follower consistency.

2.3. Fading channel

As stated in the Introduction, the transmission between followers may be inevitably suffered from the channel fading phenomenon. In this work, the network channel is considered as a continuous one with time-varying channel gain, the transmitted data will be modeled as the actually received information with random attenuation. Hence, introduce the following memoryless multiplicative fading model:

$$\begin{cases} x_{ij}(t) = \rho_{ij}(t) x_j(t), \\ v_{ij}(t) = \rho_{ij}(t) v_j(t), \end{cases} \tag{8}$$

where $x_{ij}(t)$ and $v_{ij}(t)$ are the fading position and speed signal of the jth agent received by the ith agent, and $x_j(t)$ and $v_j(t)$ are the signal and speed signal sent by the jth agent, respectively. The random coefficient $\rho_{ij}(t) \in (0, 1]$ are mutually independent random variables with mathematical expectation $\mathbb{E}\left(\rho_{ij}(t)\right) = \bar{\rho}$.

Assuming that fading occurs only in the channel between followers, the special case of channel fading from the leader to the followers is not considered in this work. Hence, based on the fading information (8), the tracking errors (5) are rewritten as:

$$\begin{cases} \bar{e}_{1i}(t) &= \sum_{j=1}^{N} a_{ij}\left(x_i(t) - \frac{1}{\bar{\rho}}\Lambda_{ij}(t) x_j(t)\right) + b_i\left(x_i(t) - x_0(t)\right), \\ \bar{e}_{2i}(t) &= \sum_{j=1}^{N} a_{ij}\left(v_i(t) - \frac{1}{\bar{\rho}}\Lambda_{ij}(t) v_j(t)\right) + b_i\left(v_i(t) - v_0(t)\right). \end{cases} \tag{9}$$

It can be seen that the tracking errors (9) involve the expectation of the random variable $\rho_{ij}(t)$, which is introduced to compute the consistent tracking error variable among the agents more accurately.

Define $\bar{e}_1(t) \triangleq [\bar{e}_{11}^T(t), \cdots, \bar{e}_{1N}^T(t)]^T$, $\bar{e}_2(t) \triangleq \left[\bar{e}_{21}^T(t), \cdots, \bar{e}_{2N}^T(t)\right]^T$. Then, the compact form of tracking errors (9) is of the following form:

$$\begin{cases} \bar{e}_1(t) &= \sum_{i=1}^{N} \alpha_i (A \otimes I_m) \cdot \frac{1}{\bar{\rho}}\Lambda_i(t) x(t) - (L+B) \otimes I_m \left(\mathbf{1}_n \otimes x_0(t)\right) \\ & \quad -(B+D) \otimes I_m \cdot x(t), \\ \bar{e}_2(t) &= \sum_{i=1}^{N} \alpha_i (A \otimes I_m) \cdot \frac{1}{\bar{\rho}}\Lambda_i(t) v(t) - (L+B) \otimes I_m \left(\mathbf{1}_n \otimes v_0(t)\right) \\ & \quad -(B+D) \otimes I_m \cdot v(t), \end{cases} \tag{10}$$

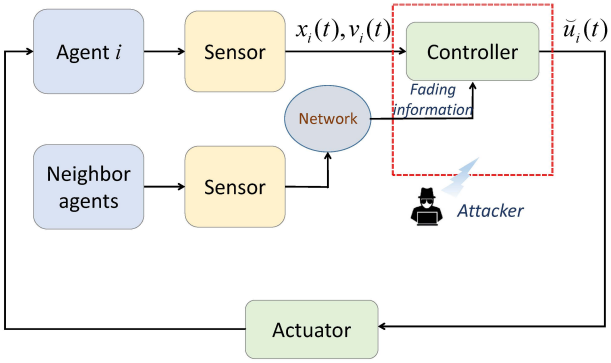

Figure 1. System over fading network subject to attacks on agent i.

where $\alpha_i \triangleq \text{diag}\{\delta_i^1, \delta_i^2, \ldots, \delta_i^N\}$, $\delta_i^k(\cdot)$ being the Kronecker delta function, which compares values of i and k and returns 0 when they are not equal; otherwise, it returns 1. $\Lambda_1(t) \triangleq \text{diag}\{0, \rho_{12}(t), \cdots, \rho_{1N}(t)\}$, $\cdots$, $\Lambda_N(t) \triangleq \text{diag}\{\rho_{N1}(t), \rho_{N2}(t), \cdots, 0\}$. Considering the effect of channel fading, since only faded data is available, accurate neighbors' information cannot be used for the controller design. In the following section 3.1, the SMC law will be designed based on the consensus tracking errors $\bar{e}_1(t)$ and $\bar{e}_2(t)$.

Remark 1. There are two special cases considered in the channel fading model (8): when $\rho_{ij}(t) = 0$, it means that there is no information interaction between agents and the communication channel is blocked, that is, the channel fading model is simplified to a packet loss model. In contrast, if $\rho_{ij}(t) = 1$, it indicates that the data transmission between agents is complete and without any attenuation.

2.4. Deception attacks

Among various cyber-attacks, the deception attack on controllers is a common form and usually satisfies the following assumptions: the hackers can steal the state information or measurement output of the agents to generate false data, which can then be injected into the controller. As shown in Figure 1, the hackers can attack the controller of agent i by injecting false data. Thus, the actual data received by the actuator of agent i is as follows:

$$\breve{u}_i(t) = u_i(t) + W(t)\Psi_a(x_i(t), t). \tag{11}$$

The compact form of expression (11) can be written as:

$$\breve{u}(t) = u(t) + W(t)\Psi_a(x(t), t). \tag{12}$$

where $u(t)$ is the designed control input and $W(t)\Psi_a(x(t), t)$ is the false data. The matrix $W(t)$ is an unknown and time-varying matrix that satisfies $\|W(t)\| \leq \mu(t)$ with $\mu(t)$ unknown and bounded, represents the injection patterns of the false data, for example, $W(t)$ may be a matrix composed of elements 0 and 1, that is, sometimes false data is injected, sometimes not, to confuse users. Thus, the attack is difficult to be detected by users. $\Psi_a(x(t), t)$ is a function of $x(t)$, which means the false data generated via the state $x(t)$, and satisfy $\|\Psi_a(x(t), t)\| \leq \psi(x(t), t)$ with $\psi(x(t), t)$ a known nonnegative function.

Remark 2. The deception attacks considered in this work focus on the controller, that is, $u(t)$ may be suffered from the false data injection, such as the problem considered in some literature [30,36] and so on. The deception attacks can also occur in the communication channel between agents, that is, $x(t)$ may be affected by false data injection during transmission [34].

3. MAIN RESULTS

3.1. Adaptive SMC law

To cope with the impact of the deception attacks, the information about the attack is usually utilized to design the controller. For example, when the upper bounds $\mu(t)$ and $\psi(x(t),t)$ of the attack are known, the design of the controller is relatively easy to implement, but the fixed upper bounds will inevitably lead to larger conservativeness. To overcome this problem, an online estimation strategy will be employed to estimate the time-varying and unknown attacks, based on which, an adaptive sliding mode controller will be designed to attenuate the effect of the unknown attacks on MASs.

Design the sliding function as follows:

$$s_i(t) = ce_{1i}(t) + e_{2i}(t), \tag{13}$$

with $c > 0$ the sliding gain, denoted $s(t) \triangleq \left[s_1^T(t), s_2^T(t), \cdots, s_N^T(t)\right]^T$, the compact form of sliding function (13) can be written as:

$$s(t) = ce_1(t) + e_2(t), \tag{14}$$

From (7), we can obtain the derivative of the sliding function:

$$\begin{aligned} \dot{s}(t) &= ce_2(t) + \dot{e}_2(t) \\ &= ce_2(t) + (L+B) \otimes I_m \cdot (\breve{u}(t) - I_N \otimes u_0(t)) . \end{aligned} \tag{15}$$

Under these constraints considered in this work, the ith agent cannot receive accurate and complete information from neighbor agents, the switching function (13) under fading channel is rewritten as:

$$\bar{s}_i(t) = c\bar{e}_{1i}(t) + \bar{e}_{2i}(t). \tag{16}$$

The compact form of expression (16) as:

$$\bar{s}(t) = c\bar{e}_1(t) + \bar{e}_2(t). \tag{17}$$

Then, construct the sliding mode controller as follow:

$$u(t) = u_a(t) + u_b(t), \tag{18}$$

where the robust term $u_a(t)$ is designed as :

$$u_a(t) = -(L+B)^{-1} \otimes I_m \cdot (k_1 \cdot \operatorname{sgn}(\bar{s}(t)) + c\bar{e}_2(t)) + I_N \otimes u_0(t), \tag{19}$$

with $k_1 > 0$, and the adaptive term $u_b(t)$ is designed as:

$$u_b(t) = -(L+B)^{-1} \otimes I_m \cdot (\|L+B\|\hat{\mu}(t)\psi(x(t),t) \cdot \operatorname{sgn}(\bar{s}(t))). \tag{20}$$

where $\hat{\mu}(t)$ is the estimation of $\mu(t)$ under the following adaptive law:

$$\dot{\hat{\mu}}(t) = \theta \|L+B\| \cdot \operatorname{Proj}(\hat{\mu}(t), \left\|\bar{s}^T(t)\right\| \psi(x(t),t)), \tag{21}$$

with θ an adaptive parameter, and Proj the smooth projection [37] as:

$$\begin{aligned} &\operatorname{Proj}(\hat{\mu}(t), \left\|s^T(t)\right\| \psi(x(t),t)) \\ &= \begin{cases} \left\|s^T(t)\right\| \psi(x(t),t), \text{ if } \varphi(\hat{\mu}(t)) \le 0, \\ \left\|s^T(t)\right\| \psi(x(t),t), \text{ if } \varphi(\hat{\mu}(t)) \ge 0 \text{ and } \varphi'(\hat{\mu}(t)) \left\|s^T(t)\right\| \psi(x(t),t) \le 0, \\ \left\|s^T(t)\right\| \psi(x(t),t) - \frac{\varphi(\hat{\mu}(t))\varphi'(\hat{\mu}(t))\left\|s^T(t)\right\|\psi(x(t),t)}{\|\varphi'(\hat{\mu}(t))\|'} \varphi'^T(\hat{\mu}(t)), \text{ otherwise}, \end{cases} \end{aligned} \tag{22}$$

where the continuous function $\varphi(\hat{\mu}(t))$ defined as:

$$\varphi(\hat{\mu}(t)) \triangleq \frac{2}{\delta}\left(\frac{\hat{\mu}^2(t)}{\hat{\mu}_{max}^2} - 1 + \delta\right) \tag{23}$$

with $\hat{\mu}_{max}$ the given bound of projection, and scalar $0 < \delta < 1$.

According to Imbedded Convex Sets Assumption [37], we obtain:

$$\left\|\text{Proj}\left(\hat{\mu}(t), \left\|s^T(t)\right\|\psi(x(t),t)\right)\right\| \leq \|s^T(t)\|\psi(x(t),t), \tag{24}$$

and

$$(\hat{\mu}(t)-\mu(t))(\text{Proj}(\hat{\mu}(t), \left\|s^T(t)\right\|\psi(x(t),t)) - \left\|s^T(t)\right\|\psi(x(t),t)) \leq 0 \tag{25}$$

and these two conditions will be used in the following derivation.

Remark 3. In some existing reliable control methods, the known bounds of attacks are usually utilized, which may inevitably yield larger conservativeness. To overcome this shortcoming, the online estimation mechanism for unknown attacks/faults was proposed in some related works [33,38]. Inspired by these works, the online estimation mechanism of the attack is integrated with the SMC technique in this work.

3.2. Consistence and Reachability

Theorem 1. Consider the MASs (3)-(4) with channel fading (8) and deception attacks (12), under the proposed SMC law (19)-(20), the reachability of the sliding surface $s(t) = 0$ can be guaranteed in the sense of mean square.

Proof. Choose the Lyapunov function as follows:

$$V(s,t) = \frac{1}{2}s^T(t)s(t) + \frac{1}{2}\theta^{-1}\tilde{\mu}^2(t), \tag{26}$$

where $\tilde{\mu}(t) = \hat{\mu}(t) - \mu(t)$ is the estimated error with $\dot{\tilde{\mu}}(t) = \dot{\hat{\mu}}(t)$.

Then, by the expressions (15) and (21), the derivative of $V_1(s,t)$ can be given as:

$$\begin{aligned}\dot{V}(s,t) =& s^T(t)\dot{s}(t) + \theta^{-1}\tilde{\mu}(t)\dot{\tilde{\mu}}(t)\\ =& s^T(t)(ce_2(t) - c\bar{e}_2(t) + (L+B)\otimes I_m \cdot W(t)\Psi_a(x(t),t))\\ &- \|L+B\|\cdot\hat{\mu}\psi(x(t),t)\cdot\text{sgn}(\bar{s}(t))) - k_1\,\text{sgn}(\bar{s}(t))) + \theta^{-1}\tilde{\mu}(t)\dot{\tilde{\mu}}(t).\end{aligned} \tag{27}$$

Taking mathematical expectation to the above expression (27), one has:

$$\begin{aligned}\mathbb{E}[\dot{V}(s,t)] =& s^T(t)[ce_2(t) - c\mathbb{E}(\bar{e}_2(t)) - k_1\mathbb{E}(\text{sgn}(\bar{s}(t))) + (L+B)\otimes I_m\\ &\cdot W(t)\Psi_a(x(t),t) - \|L+B\|\hat{\mu}\psi(x(t),t)\mathbb{E}(\text{sgn}(\bar{s}(t)))]\\ &+ \|L+B\|(\hat{\mu}(t)-\mu(t))\text{Proj}(\hat{\mu}(t), \left\|\bar{s}^T(t)\right\|\psi(x(t),t)).\end{aligned} \tag{28}$$

It can be easily verified from expressions (5) and (9) that $\mathbb{E}(e_1(t)) = \mathbb{E}(\bar{e}_1(t))$, $\mathbb{E}(e_2(t)) = \mathbb{E}(\bar{e}_2(t))$. Meanwhile, it follows from (14) and (17) that $\mathbb{E}(s(t)) = \mathbb{E}(\bar{s}(t))$. Then, one can obtain:

$$\begin{aligned}\mathbb{E}\left[\dot{V}(s,t)\right] =& -k_1 s^T(t)\,\text{sgn}(s(t)) + s^T(t)(L+B)\otimes I_m\cdot W(t)\Psi_a(x(t),t)\\ &+ \|L+B\|(\hat{\mu}(t)-\mu(t))\text{Proj}(\hat{\mu}(t), \left\|s^T(t)\right\|\psi(x(t),t))\\ &- s^T(t)\|L+B\|\hat{\mu}(t)\cdot\psi(x(t),t)\,\text{sgn}(s(t))\\ \leq& -k_1\|s^T(t)\| + \|L+B\|\|W(t)\|\,\|\Psi_a(x(t),t)\|\,\|s^T(t)\|\\ &+ \|L+B\|(\hat{\mu}(t)-\mu(t))\text{Proj}(\hat{\mu}(t), \|s^T(t)\|\cdot\psi(x(t),t))\\ &- \|L+B\|\hat{\mu}(t)\psi(x(t),t)\|s^T(t)\|.\end{aligned} \tag{29}$$

By the conditions $\|W(t)\| \leq \mu(t)$, $\|\Psi_a(x(t),t)\| \leq \psi(x(t),t)$, one has:

$$\begin{aligned}\mathbb{E}\left[\dot{V}(s,t)\right] \leq& -k_1\|s^T(t)\| + \|L+B\|(\mu(t)-\hat{\mu}(t))(\|s^T(t)\|\\ &\cdot\psi(x(t),t) - \text{Proj}(\hat{\mu}(t), \left\|s^T(t)\right\|\cdot\psi(x(t),t))).\end{aligned} \tag{30}$$

Then, it follows from (25) that:

$$\begin{aligned}\mathbb{E}\left[\dot{V}(s,t)\right] &\leq -k_1\|s^T(t)\| \\ &\leq 0.\end{aligned} \tag{31}$$

Hence, the reachability of the sliding surface $s(t) = 0$ can be ensured in the sense of mean square. □

Theorem 2. Considering the MASs (3)-(4) subject to deception attacks (12) and channel fading model (8), the consensus tracking for MASs (3)-(4) will be achieved under the proposed sliding surface (14) and the SMC law (19)-(20).

Proof. Select the Lyapunov function:

$$U(t) = \frac{1}{2}e_1(t)^T e_1(t) + \frac{1}{2}e_2(t)^T e_2(t), \tag{32}$$

Its derivative is given as:

$$\begin{aligned}\dot{U}(t) &= e_1^T(t)\dot{e}_1(t) + e_2^T(t)\dot{e}_2(t) \\ &= e_1^T(t)e_2(t) + e_2^T(t)\dot{e}_2(t).\end{aligned} \tag{33}$$

When the sliding surface $s(t) = 0$, it follows from (14) and (7) that $e_2(t) = -ce_1(t)$ and $\dot{e_2}(t) = -ce_2(t)$, then we can obtain:

$$\begin{aligned}\dot{U}(t) &= e_1^T(t)e_2(t) + e_2^T(t)\dot{e}_2(t) \\ &= -ce_1(t)^T e_1(t) - ce_2^T(t)e_2(t) \\ &= -c\left\|e_1(t)\right\|^2 - c\left\|e_2(t)\right\|^2 \\ &\leq 0.\end{aligned} \tag{34}$$

Combining the results of Theorem 1, the consensus tracking of MASs (3)-(4) can be ensured under the proposed sliding surface (14) and the SMC law (19)-(20). □

4. SIMULATION

Consider the second-order MASs with one leader and 4 followers, where the communication topology between agents is shown in Figure 2. The blue arrows indicate that the followers receive the complete information from the leader, while the red arrows indicate that the information interaction between followers is over fading channel. Thereby, follower 1 and follower 2 can receive accurate information from the leader, follower 3 can only receive the fading data from follower 1, and follower 4 can only receive the incomplete data from both follower 1 and follower 2. For simplicity, in this simulation example, the adjacency weights between neighbor agents are set as 1.

Then, according to the leader and followers' topology, we can get the adjacency matrix A, the diagonal matrix B, and the Laplace matrix L of these MASs as follows:

$$A = \begin{bmatrix}0 & 0 & 0 & 0\\ 0 & 0 & 0 & 0\\ 1 & 0 & 0 & 0\\ 1 & 1 & 0 & 0\end{bmatrix}, L = \begin{bmatrix}0 & 0 & 0 & 0\\ 0 & 0 & 0 & 0\\ -1 & 0 & 1 & 0\\ -1 & -1 & 0 & 2\end{bmatrix}, B = diag\left\{1 \quad 1 \quad 0 \quad 0\right\}.$$

In this simulation, the initial state of the leader's position, speed, and control input are set as $x_0 = [10, -10]^T$, $v_0 = [10, -10]^T$, $u_0 = [cos(t), sin(t)]^T$, the initial state of the followers' position and speed are set as $x_1 = [10, -2]^T$, $v_1 = [20, -2]^T$, $x_2 = [15, 15]^T$, $v_2 = [20, 3]^T$, $x_3 = [25, 5]^T$, $v_3 = [15, 0]^T$, $x_4 = [45, 15]^T$, $v_4 = [35, 0]^T$, and the injection packets $W(t)\Psi_a(x(t), t)$ set as $W(t) = [1, 1, 1, 1]$ and $\Psi_a(x(t), t) = 10x(t)sin(t)$.

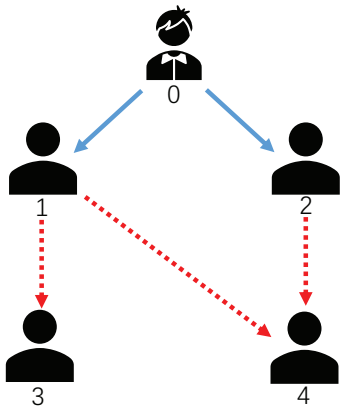

Figure 2. Communication topology diagram of MASs. MASs: multi-agent systems.

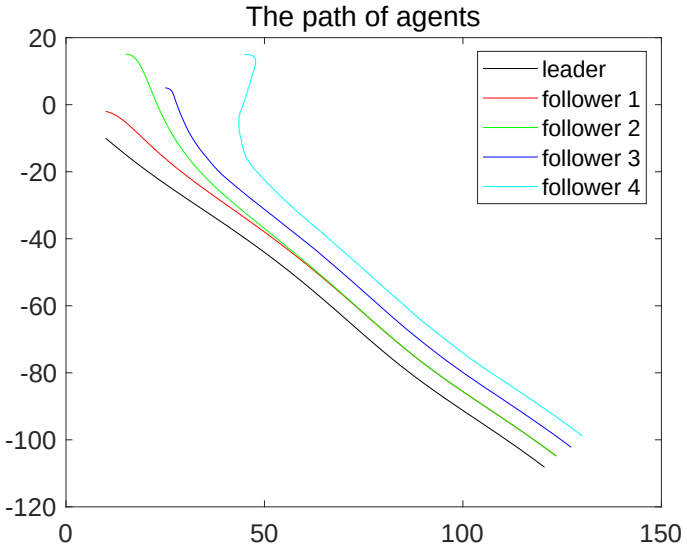

Figure 3. The trajectories of the MASs under the robust control term $u_a(t)$(19). MASs: multi-agent systems.

The sliding mode controller parameters are chosen as $c = 1$, $k_1 = 0.1$.

Simulation results are shown in Figures 3-7. Among them, Figure 3 shows the tracking trajectories of MASs under the robust control term $u_a(t)$ (19), and the horizontal and vertical axis represent the position state of different dimensions, respectively. As we can see from the Figure 3, the trajectories of the agents don't converge to a point, which indicates that the MASs under the robust control term $u_a(t)$ (19) can't achieve consensus under the deception attacks. For comparison, Figure 4 shows the tracking trajectories of the agents under the proposed adaptive SMC law (18), and it is shown that the closed-loop MASs under channel fading and deception attacks can achieve consensus tracking. Figures 5 and 6 show the position error $e_1(t)$ and velocity error $e_2(t)$ between followers respectively. Figure 7 shows the sliding variable $s(t)$ of the followers, respectively.

Remark 4. As shown in Figures 5-7, agents 1 and 2 have better consensus tracking performance with smaller amplitude oscillating and smoother curves, that is, because they can receive accurate information from the leader. In contrast, agents 3 and 4 perform worse because they cannot obtain information from the leader, but only from neighbor agents over fading channel (as shown in Figure 2). Even so, the proposed adaptive SMC scheme can still guarantee consensus tracking of all followers, as shown in Figure 4.

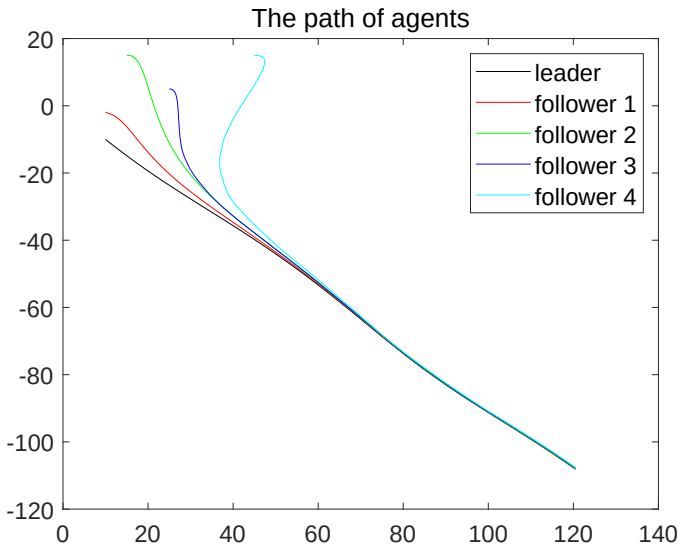

Figure 4. The trajectories of the MASs under the adaptive SMC law (18). SMC: sliding mode control.

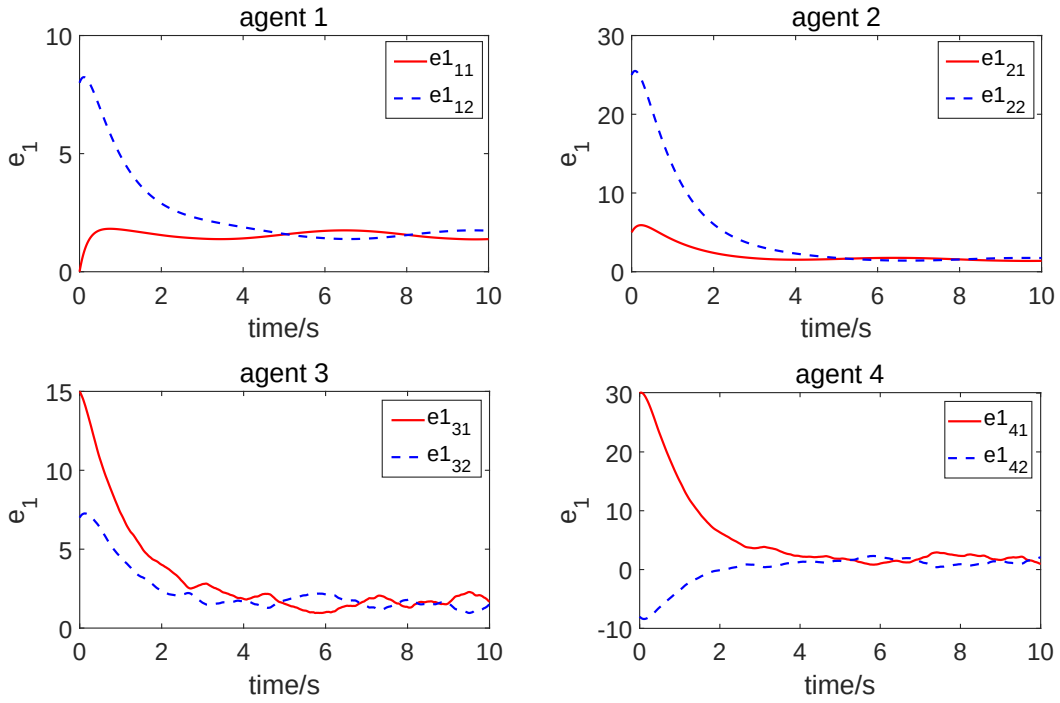

Figure 5. The position error $e_1(t)$ of the followers in Figure 5A-D. A: Position error of the 1st agent; B: Position error of the 2nd agent; C: Position error of the 3rd agent; D: Position error of the 4th agent.

5. CONCLUSION

This work considered the consensus control problem of MASs under deception attacks and fading channels. Due to the fading channels, the position and velocity errors cannot be calculated accurately. To solve this problem, the consensus tracking error variables have been designed based on the fading data received from neighbor agents. Meanwhile, the distributed adaptive SMC strategy via fading information has been proposed to deal with the time-varying and unknown deception attacks injected by the hacker. Utilizing the proposed

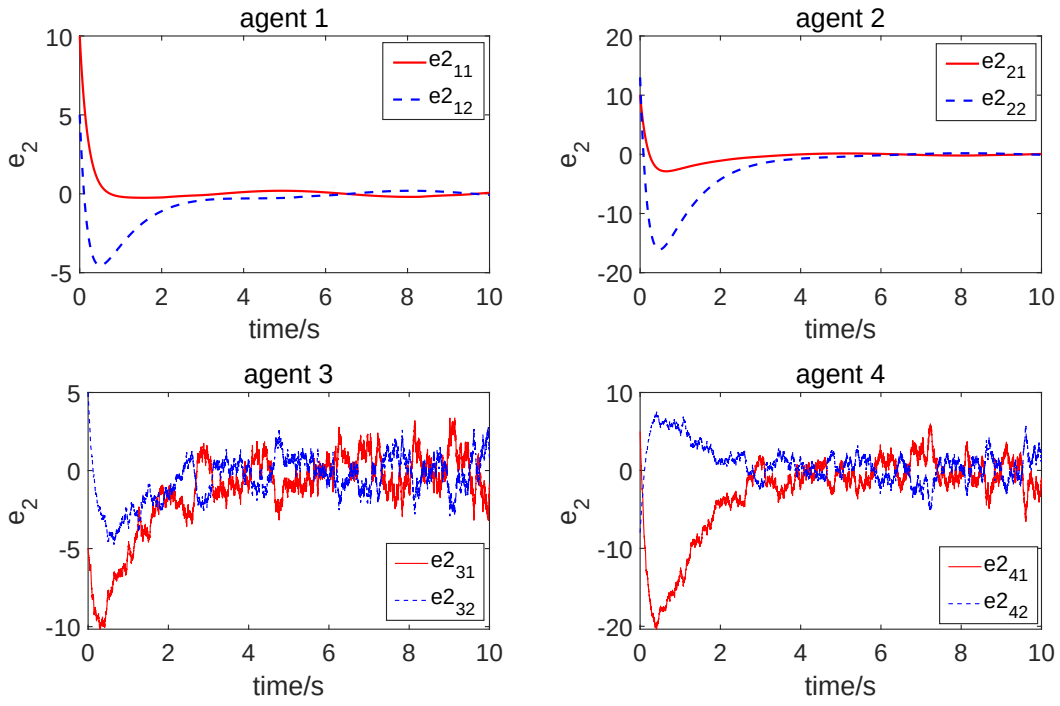

Figure 6. The velocity error $e_2(t)$ of the followers in Figure 6A-D. A: Velocity error of the 1st agent; B: Velocity error of the 2nd agent; C: Velocity error of the 3rd agent; D: Velocity error of the 4th agent.

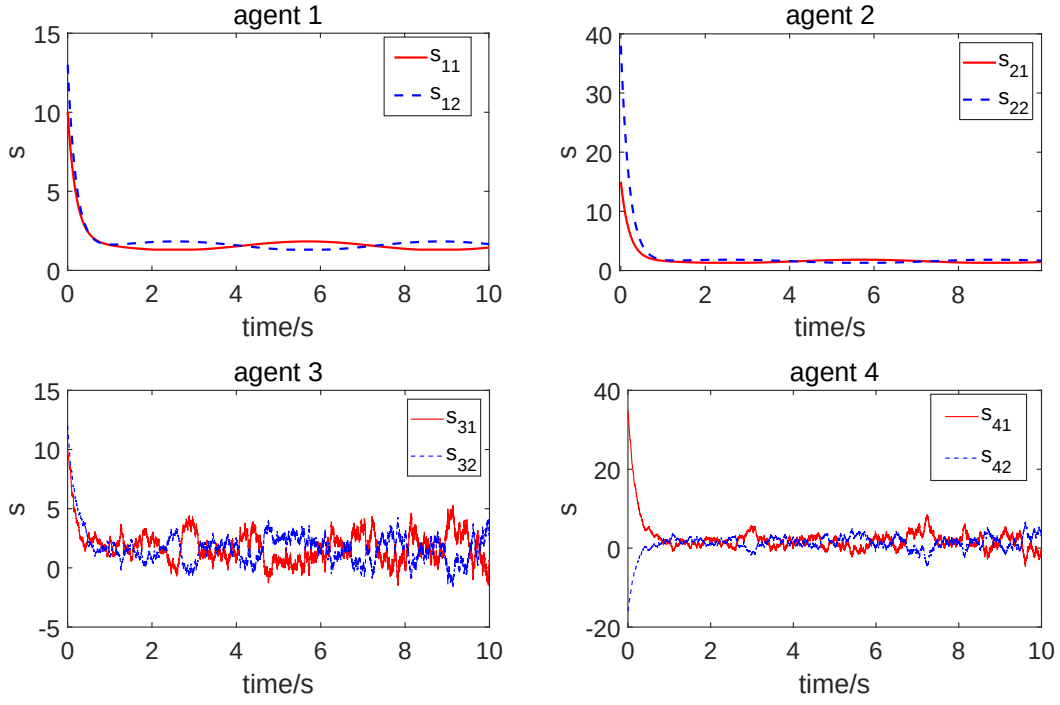

Figure 7. Sliding variables $s(t)$ of the followers in Figure 7A-D. A: Sliding variable $s(t)$ of the 1st agent; B: Sliding variable $s(t)$ of the 2nd agent; C: Sliding variable $s(t)$ of the 3rd agent; D: Sliding variable $s(t)$ of the 4th agent.

scheme, consensus tracking can be achieved. Only malicious attacks and channel fading have been considered in this work. In practical applications, there may coexist multiple constraints, such as actuator/sensor faults,

packet dropout, random noise[39,40], etc. Under these constraints, how to design a feasible consensus control method is worthy to research in future work.

DECLARATIONS

Acknowledgments
Special thanks to the School of Electronic and Electrical Engineering, Shanghai University of Engineering Science (China) for providing technical support for this research.

Authors' contributions
Methodology, software, validation, data curation, visualization, writing- original draft: Ding M
Conceptualization, riting-reviewing and editing, investigation: Chen B

Availability of data and materials
Not applicable.

Financial support and sponsorship
This work is supported in part by the NNSF of China (62173222, 61803255), Shanghai Science and Technology Innovation Action Plan (22S31903700, 21S31904200), and the National Key R&D Program of China (Grant No. 2020AAA0109301).

Conflicts of interest
Both authors declared that there are no conflicts of interest.

Ethical approval and consent to participate
Not applicable.

Consent for publication
Not applicable.

REFERENCES

1. Liao W, Wei XH, Lai JZ, Sun H. Formation control for multi-UAVs systems based on Kullback-Leibler divergence. *IEEE Trans Inst Meas Control* 2020;42:598-603. DOI
2. Dong X, Zhou Y, Ren Z, et al. Time-varying formation tracking for second-order multi-agent systems subjected to switching topologies with application to quadrotor formation flying. *IEEE Trans Ind Electron* 2016;64:5014-24. DOI
3. Belkacem K, Munawar K, Muhammad SS. Distributed cooperative control of autonomous multi-agent UAV systems using smooth control. *J Syst Eng Electron* 2021;31:1297-307. DOI
4. Ali S, Muhammad NM. Distributed observer for a team of autonomous underwater vehicles utilizing a beacon unit on the surface. In: 2017 IEEE 7th International Conference on Underwater System Technology: Theory and Applications 2017. DOI
5. Lv YK, Zhang H, Wang ZP, Yan HC. Distributed localization for dynamic multiagent systems with randomly varying trajectory lengths. *IEEE Trans Ind Electron* 2022;69:9298-308. DOI
6. Li X, Dong X, Li Q, Ren Z. Event-triggered time-varying formation control for general linear multi-agent systems. *J Frankl Inst* 2019;356:10179-95. DOI
7. Chai XF, Wang Q, Diao Q, Yu Y, Sun CY. Sampled-data-based dynamic event-triggered formation control for nonlinear multi-agent systems. *IEEE Trans Inst Meas Control* 2022;14:2719-28. DOI
8. Li Y, Jiao XY, Sun BQ, Yang JY. Multi-welfare-robot cooperation framework for multi-task assignment in healthcare facilities based on multi-agent system. In: 2021 IEEE International Conference on Intelligence and Safety for Robotics 2021. DOI
9. Das R, Dwivedi M. Multi agent dynamic weight based cluster trust estimation for hierarchical wireless sensor networks. *Peer-to-Peer Netw* 2022;15:1505-20. DOI

10. Abianeh AJ, Wan YH, Ferdowsi F, Mijatovic N, Dragicevic T. Vulnerability identification and remediation of FDI attacks in islanded DC microgrids using multiagent reinforcement learning. *IEEE Trans Ind Electron* 2022;37:6359-70. DOI
11. Hu HX, Wen GH, Yu WW, Huang TW, Cao JD. Distributed stabilization of multiple heterogeneous agents in the strong-weak competition network: a switched system approach. *IEEE Trans Cybern* 2021;51:5328-41. DOI
12. Yao DJ, Dou CX, Zhao N, Zhnag TJ. Finite-time consensus control for a class of multi-agent systems with dead-zone input. *J Frankl Inst* 2021;358:3512-29. DOI
13. Rehman AU, Rehan M, Iqbal N, Waris MZ. Leaderless adaptive output feedback consensus approach for one-sided Lipschitz multi-agents. *J Frankl Inst* 2020;357:8800-22. DOI
14. Liu JJR, Yang N, Kwok KW, Lam J. Positive consensus of directed multi-agent systems. *IEEE Trans Automat Contr* 2022;67:3641-6. DOI
15. Chen CLP, Wen GX, Liu YJ, Liu Z. Observer-based adaptive backstepping consensus tracking control for high-order nonlinear semi-strict-feedback multiagent systems. *IEEE Trans Cybern* 2016;46:1591-601. DOI
16. Sheng L, Wang Z, Zou L. Output-feedback H_2/H_∞ consensus control for stochastic time-varying multi-agent systems with (x, u, v)-dependent noises. *Syst Contr Lett* 2017;107:58-67. DOI
17. Yu D, Ji XY. Finite-time containment control of perturbed multi-agent systems based on sliding-mode control. *Int J Syst Sci* 2018;49:299-311. DOI
18. Zou Y, Sun X, Li S, Liu Y. Event-triggered distributed predictive control for asynchronous coordination of multi-agent systems. *Automatica* 2019;99:92-8. DOI
19. Yu WW, Chen GR, Cao M. Some necessary and sufficient conditions for second-order consensus in multi-agent dynamical systems. *Automatica* 2010;46:1089-95. DOI
20. Tao T, Roy S, Baldi S. Adaptive synchronization of uncertain complex networks under state-dependent a priori Interconnections". In: 2021 60th IEEE Conference on Decision and Control (CDC), Austin, TX, USA, 2021:1777-82. DOI
21. Tao T, Roy S, Baldi S. Adaptive single-stage control for uncertain nonholonomic Euler-Lagrange systems. In: 2022 IEEE 61st Conference on Decision and Control (CDC), Cancun, Mexico. 2022:2708-13. DOI
22. Zuo ZY. Nonsingular fixed-time consensus tracking for second-order multi-agent networks. *Automatica* 2015;54:305-9. DOI
23. Wang J, Zhang XR, Zhou JL. Chen YQ, Distribution consensus of nonlinear stochastic multi-agent systems based on sliding-mode control with probability density function compensation. *J Frankl Inst* 2020;357:9308-29. DOI
24. Cong YR, Feng ZG, Song HW, Wang SM. Containment control of singular heterogeneous multi-agent systems. *J Frankl Inst* 2018;55:4629-43. DOI
25. Rahmani R, Toshani H, Mobayen S. Consensus tracking of multi-agent systems using constrained neural-optimiser-based sliding mode control. *Int J Syst Sci* 2020;51:2653-74. DOI
26. Oral E, Schmeink A, Dartmann G, Ascheid G, Pusane AE. Consensus analysis of wireless multi-agent systems over fading channels. *IEEE Wireless Commun Lett* 2021;10:1528-31. DOI
27. Gu XW, Jia TG, Niu YG. Consensus tracking for multi-agent systems subject to channel fading: a sliding mode control method. *Int J Syst Sci* 2020;51:2703-11. DOI
28. Ding M, Chen B, Hu ZX and Zhang Y. Finite-time consensus control for multi-agent systems with channel fading via sliding mode technique. In: 2022 34th Chinese Control and Decision Conference (CCDC), Hefei, China. 2022:3706-11. DOI
29. He WL, Xu WY, Ge XH, Han QL, Du WL, Qian F. Secure control of multiagent systems against malicious attacks: a brief survey. *IEEE Trans Industr Inform* 2022;18:3595-608. DOI
30. Zhao L, Yang GH. Cooperative adaptive fault-tolerant control for multi-agent systems with deception attacks. *J Frankl Inst* 2020:357:3419-33. DOI
31. Tahoun AH, Arafa M. Cooperative control for cyber-physical multi-agent networked control systems with unknown false data-injection and replay cyber-attacks. *ISA Trans* 2021;110:1-14. DOI
32. Shang Y, Liu CL, Cao KC. Event-triggered consensus control of second-order nonlinear multi-agent systems under denial-of-service attacks . *IEEE Trans Inst Meas Control* 2021;10:2272-81. DOI
33. Chen B, Niu YG, Zou YY. Security control for Markov jump system with adversarial attacks and unknown transition rates via adaptive sliding mode technique. *J Frankl Inst* 2019;356:3333-52. DOI
34. Cui Y, Liu YR, Zhang WB, Alsaadi FE. Sampled-based consensus for nonlinear multiagent systems with deception attacks: the decoupled method. *IEEE Trans Syst Man Cybern Syst* 2018;51:561-73. DOI
35. Li W, Niu YG, Cao ZR. Event-triggered sliding mode control for multi-agent systems subject to channel fading. *Int J Syst Sci* 2021;53:1233-44. DOI
36. Chen B, Niu YG. Dynamic event-triggered sliding mode security control for Markovian jump systems: Learning-based iteration optimization method. *Int J Robust Nonlinear Control* 2021;32:2500-17. DOI
37. Pomet JB, Praly L. Adaptive nonlinear regulation:estimation from the Lyapunov equation. *IEEE Trans. Automat. Contr* 1992;37:729-40. DOI
38. Zou Z, Ho DWC, Wang Y. Fault tolerant control for singular systems with actuator saturation and nonlinear perturbation. *Automatica* 2010;46:569-76. DOI
39. Zhang QC, Zhou YY. Recent advances in non-gaussian stochastic systems control theory and its applications. *IJNDI* 2022;1:111-9. DOI
40. Ren MF, Zhang QC, Zhang JH. An introductory survey of probability density function control. *Syst Sci Contr Eng* 2019;7:158-70. DOI

Tan *et al*. *Complex Eng Syst* 2023;3:6
DOI: 10.20517/ces.2023.10

Complex Engineering Systems

Research Article

Open Access

Decentralized control for interconnected semi-markovian jump systems with partially accessible transition rates: a dynamic memory event-triggered mechanism

Yushun Tan[1], Xiaoming Cheng[1], Xinrui Li[1], Jie Bai[1], Jinliang Liu[2]

[1]School of Applied Mathematics, Nanjing University of Finance and Economics, Nanjing 210023, Jiangsu, China.
[2]School of Information Engineering, Nanjing University of Finance and Economics, Nanjing 210023, Jiangsu, China.

Correspondence to: Prof. Yushun Tan, School of Applied Mathematics, Nanjing University of Finance and Economics, Qi xia District, Nanjing 210023, Jiangsu, China. Email: tyshun994@163.com; ORCID:0000-0002-2944-0742

How to cite this article: Tan Y, Cheng X, Li X, Bai J, Liu J. Decentralized control for interconnected semi-markovian jump systems with partially accessible transition rates: a dynamic memory event-triggered mechanism. *Complex Eng Syst* 2023;3:6. http://dx.doi.org/10.20517/ces.2023.10

Received: 10 Mar 2023 **First Decision:** 31 Mar 2023 **Revised:** 12 Apr 2023 **Accepted:** 19 Apr 2023 **Published:** 17 May 2023

Academic Editor: Yurong Liu **Copy Editor:** Fanglin Lan **Production Editor:** Fanglin Lan

Abstract

This paper investigates the issue of decentralized control for interconnected semi-Markovian systems with partially accessible transition rates (TRs). Firstly, a dynamic system model with a memory event-triggered mechanism (METM) is designed, which can effectively improve the fault tolerance of the event-triggering mechanism by employing the historical trigger data. Then a state feedback control model with dynamic METM is constructed, in which the semi-Markovian parameters with completely unknown and partially known transition probabilities are considered. Some sufficient conditions that insure the stochastic stability of the interconnected semi-Markovian systems can be obtained by utilizing the Lyapunov function and suitable model transformations method. Meanwhile, the parameters and the controller gain matrices of dynamic METM are also solved simultaneously by applying the linear matrix inequalities (LMIs). Finally, a simulation example is given to verify the effectiveness of the proposed method.

Keywords: Decentralized control method, interconnected semi-Markovian jump systems, partially accessible transition rate, dynamic memory event-triggered mechanism.

1. INTRODUCTION

With the prompt development of modern industry, the requirements for system scale and control objectives are increasing. Many single systems improve their own characteristics through interconnection to meet local and global performance requirements[1]. Nowadays, interconnected systems are widely used in actual production and life, such as power systems[2], intelligent transportation systems[3], and network communication systems[4]. The interconnected systems are large-scale composite systems which are composed of several subsystems connected in a specific way. Interconnected systems usually have strong coupling, strong uncertainty, high dimensions, and other characteristics. Thus, the existing traditional control strategies designed for a single system are difficult to directly solve the analysis and control problems of interconnected systems[5,6]. Therefore, many scholars are devoted to the control analysis and design for this kind of large-scale system.

Recently, decentralized control methods have been applied to interconnected control systems, where the subsystem only uses its own information to achieve the control design. Due to its simple structure, low cost, and high reliability, the decentralized control method has drawn wide attention in the control design of large-scale complex systems, and numerous research results have emerged[7,8]. For example, a decentralized control strategy for the linearized power system with different load distributions was studied in[9]. A decentralized adaptive sliding mode control mechanism for the stability of large-scale semi-Markovian jump interconnected systems was proposed in[10,11], and a decentralized output feedback control for large-scale systems with communication delay and random shortcoming measurements was studied in[12]. Recently, it has also witnessed rapid growth in the application of decentralized control methodologies in the field of engineering. For instance, a decentralized Markovian jump H_∞ control routing strategy for mobile multi-agent networked systems were investigated in[13]. The adaptive fuzzy decentralized tracking control for large-scale interconnected nonlinear networked control systems was studied in[14,15], and a Lyapunov-function based event-triggered control was adopted to develop nonlinear discrete-time cyber-physical systems[16]. However, the decentralized control of interconnected systems is still an open field to be developed, and there are still many problems to be discussed.

It is noticed that most actual systems are often affected by some sudden changes during operation, and such systems can be represented by Markovian jump systems (MJSs). However, the residence time in MJSs follows exponential distribution and the distribution of residence time has no memory, that is, the transition rate is a random process independent of past modes, which brings some limitations to its application[17]. In comparison with MJSs, the dwell time of semi-Markovian jump systems (S-MJSs) can obey non-exponential distributions, such as Weibull distribution and Gaussian distribution. The S-MJSs release the limitation of the probability distribution function and reduce the conservatism of the system, thus they have wider application in practice[18]. In recent years, many important theoretical advances and practical significance for S-MJSs can be found. For example, the authors in[19] studied the dynamic output feedback control for a class of linear S-MJSs in the discrete-time domain. The stability of singular switching S-MJSs with uncertain TRs was developed in[20]. In[21], by using the LMI method, the authors studied the stochastic stability of linear S-MJSs, where TRs were divided into different parts. It is often difficult to fully know the jumping probability of modes when the system is modeled as a MJS or S-MJS. It is noticed that the TRs in S-MJSs are more complex because they stick to a more ordinary distribution instead of an exponential distribution[22,23]. Consequently, the study of different forms of TRs would increase the complexity of the process of control design. Recently, an estimation method has been proposed for nonlinear S-MJSs with partially unknown transition probability and output quantization, see[24] and the literature wherein. However, few related works involve exactly unknown and uncertain bounded transition rates of interconnected S-MJSs, which is one of the main motivations of this paper.

Additionally, the event-triggered mechanism (ETM) was drawn to avoid the waste of network resources. Compared with the periodic sampling method, the ETM can avoid the generation of data redundancy[25–27]. However, if the event-triggered threshold argument is a constant, it is difficult to fit in the variety of outside and

internal environments. The methods for solving this problem can be summarized as the following two types: the adaptive event-triggered mechanism and the dynamic event-triggered mechanism (DETM)[28,29]. For instance, the authors in[30] proposed an improved dynamic ETM to handle fault detections and isolation issues. And the authors in[31] studied the adaptive event-triggered problem of networked interconnected systems. It should be noted that the majority of triggering conditions are devised based on the diversity between the current sampling signal and the latest released packet[32]. In the above DETM methods, when the relative error between two sampled signals is faint, the current packet is unlikely to be released. Thus, the error message is not sufficient to reflex all dynamic characteristics. A sensitive DETM should consider more system trends in order to achieve a good balance between system performance and utilization of communication resources[33]. For instance, during the transient process, when the system dynamic curve achieves the response peak, the proportional error among two sampled signals is faint[34]. The DETM is unlikely to deliver the packet. However, we expect more sampled signals to be delivered in order to curtail the transient process. For this purpose, we design a weight-based dynamic METM on the base of the existing literature[35,36]. Applying some of the recently released information to ETM has shown to be effective in improving system performance. Obviously, the dynamic METM can appropriately release more packets and get better control performance under the same triggering parameters within a predefined limited time interval[37]. To our knowledge, there are few results on dynamic memory event-triggered control for the interconnected semi-Markovian jump systems, which is the second motivation that lead to our current study.

Enlightened by the viewpoints above, this paper focuses on the decentralized control for a dynamic memory event-triggered interconnected S-MJSs with partially accessible TRs. The main highlights of this paper are summarized below: (1) a decentralized control model for the S-MJSs with partially accessible transition rates is constructed, where a weight-based dynamic METM is first developed to reduce the signal communication burden and save limited broadband resources; (2) construct a semi-Markovian jump mode-depended Lyapunov-Krasovskii functional, and some sufficient conditions are deduced to guarantee the asymptotic stability of the considered system. The controller gain matrices and weighting matrices of dynamic METM are gained in terms of the LMIs technique. Meanwhile, the design scheme proposed is verified via a simulation example.

The rest of this paper is described as below: Interconnected semi-Markovian jump system models with memory event-triggered mechanisms are established in Section 2. Some main results are presented in Section 3. A simulation example is given in Section 4, and a concise conclusion is drawn in Section 5.

Notation: In this paper, $\mathbb{R}^n$ and $\mathbb{R}^{n\times m}$ represent the n-dimensional Euclidean space and the set of $n \times m$ real matrix respectively; the superscripts P^{T} and P^{-1} stand for transposition and inverse, respectively; $diag\{\cdots\}$ indicates a block diagonal matrix; $Q > 0 (\geq 0)$ denotes a positive matrix; $\mathbb{E}\{X\}$ submits the mathematical expectation of the stochastic variable X; the notation " $*$ " stands for the symmetric structure.

2. PROBLEM STATEMENT

2.1. System model description

Consider an interconnected semi-Markovian system, which is defined in a fixed probability space (X, F, P) and composed of N subsystems $X_i (i = 1, 2, \cdots, N)$. The dynamic description of the i th subsystem is as follows

$$\dot{x}_i(t) = \mathcal{A}_i(r_t)x_i(t) + \mathcal{B}_i(r_t)u_i(t) + \sum_{j=1, j\neq i}^{N} \mathcal{G}_{ji}(r_t)x_j(t), \tag{1}$$

where $x_i(t) \in \mathbb{R}^{n_i}$ and $u_i(t)$ represent the state vector of the i th subsystem and control input, respectively. The matrices $\mathcal{A}_i(r_t)$, $\mathcal{B}_i(r_t)$ are of proper dimensions. $\mathcal{G}_{ji}(r_t)$ denotes the interconnection matrix of the i th and j th subsystems; $\{r_t \geq 0\}$ defines a continuous time semi-Markovian process taking discrete values in a finite

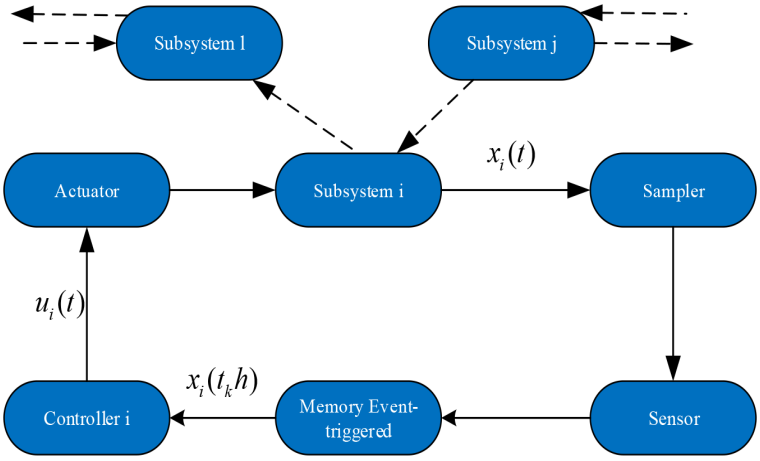

Figure 1. A framework of decentralized control system with METM.

set $S = \{1, 2, \cdots, s\}$ and the generator is given by

$$Pr\{r_{t+\delta} = l | r_t = m\} = \begin{cases} \pi_{ml}(\delta)\delta + o(\delta), m \neq l, \\ 1 + \pi_{mm}(\delta)\delta + o(\delta), m = l, \end{cases} \tag{2}$$

where $\delta > 0$ and $\lim_{\delta \to 0} \frac{o(\delta)}{\delta} = 0$, $\pi_{ml}(\delta) > 0$, $m \neq l$, denotes the transition rate from mode m at time t to mode l at time $t + \delta$, and satisfies $\pi_{mm}(\delta) = -\sum_{l=1, l\neq m}^{s} \pi_{ml}(\delta) < 0$, for each $r_t = m \in S$. More universal uncertain transition rates are taken into account with the following cases. (1) $\pi_{ml}(\delta)$ is completely unknown; (2) $\pi_{ml}(\delta)$ is not completely known but there are upper and lower bounds. In case (2), we assume that $\pi_{ml}(\delta) \in [\underline{\pi}_{ml}, \overline{\pi}_{ml}]$, in which $\underline{\pi}_{ml}$ and $\overline{\pi}_{ml}$ are known real constants meaning the lower and upper bounds of $\pi_{ml}(\delta)$ respectively. The parameter matrix of the system (1) can be abbreviated as $(\mathcal{A}_{im}, \mathcal{G}_{jim}, \mathcal{B}_{im})$. The TRs matrix can be described as

$$\begin{bmatrix} \pi_{11}(\delta) & ? & \pi_{13}(\delta) & \cdots & ? \\ ? & ? & \pi_{23}(\delta) & \cdots & \pi_{2s}(\delta) \\ \vdots & \vdots & \vdots & \vdots & \vdots \\ ? & \pi_{s2}(\delta) & ? & \cdots & \pi_{ss}(\delta) \end{bmatrix}$$

where "?" represents a completely unknown element of TRs. For brevity, $\forall m \in S$, let $\bigwedge_m = \bigwedge_{m,k} \bigcup \bigwedge_{m,uk}$, where $\bigwedge_{m,k} = \{l : \pi_{ml}(\delta)$ known upper and lower bounds for $l \in S\}$, $\bigwedge_{m,uk} = \{l : \pi_{ml}(\delta)$ completely unknown for $l \in S\}$.

2.2. Interconnected semi-Markovian jump systems with dynamic METM

To economize network resources and improve data transmission efficiency, here one introduces a dynamic METM. Unlike the other ETM, which only uses instantaneous system information, the proposed METM considers the historically triggered information. Suppose the event-triggered time of the current sampling data is $t_k h$, where $t_k (k = 1, 2, 3, \cdots)$ and h represent some positive integers satisfying $t_k \subset \{0, 1, 2, \cdots\}$ and the sampling period of the sensor, respectively. Define the difference between the latest released sampling data and the current sampling data

$$\Delta_{qi}^{(k)}(t) = x_i(t_{k-q+1}h) - x_i(t_k h + \epsilon h), q = 1, 2, \cdots, M, \tag{3}$$

where $\epsilon \in N_1 = \{1, 2, \cdots\}$, M denotes the memory length, and $t_k h$ indicates the event-triggered instant. The next releasing instant $t_{k+1}h$ is determined as follows

$$t_{k+1}h = t_k h + \min_{\epsilon \in N_1} \{\epsilon h | \sum_{q=1}^{M} \gamma_q (\Delta_{qi}^{(k)}(t))^{\mathrm{T}} \Omega_i \Delta_{qi}^{(k)}(t) > \theta_i(t) x_i^{\mathrm{T}}(t_k h + \epsilon h) \Omega_i x_i(t_k h + \epsilon h)\}, \tag{4}$$

where $\Omega_i > 0$ are the weighting matrix; $\gamma_q \in [0, 1]$ are the weighting parameters of the corresponding packet and satisfy $\sum_{q=1}^{M} \gamma_q = 1$. $\theta_i(t)$ are the memory event-triggered threshold and meet the following conditions

$$\dot{\theta}_i(t) = (\frac{1}{\theta_i^2(t)} - \frac{\theta_0}{\theta_i(t)}) \sum_{q=1}^{M} \gamma_q (\Delta_{qi}^{(k)}(t))^{\mathrm{T}} \Omega_i \Delta_{qi}^{(k)}(t), \tag{5}$$

where $\theta_i(t) \in (0, 1]$ and $\theta_0 > 0$ is used to regulate the release rate of sampling data. The framework of the decentralized control for interconnected semi-Markovian jump systems with a dynamic METM is shown in Figure 1.

Remark 1. From (5), we can obtain that the dynamic threshold $\theta_i(t)$ is related to the error variable $e_{qi}^{(k)}(t)$. When the error variable tends to zero, for instance, the system tends to be stable at the equilibrium, the dynamic threshold converges to a constant. When $\dot{\theta}_i(t) > 0$, $\theta_i(t)$ is monotonically increasing, which means that the release rate of data at the sampling time will reduce. On the contrary, when $\dot{\theta}_i(t) < 0$, $\theta_i(t)$ is monotonically decreasing, the release rate of data at the sampling time will increase. In particular, when $\dot{\theta}_i(t) \equiv 0$, the event-triggered condition becomes the traditional memory event-triggered condition [22].

Remark 2. By using the historical trigger signals, a memory-base event-triggered condition is proposed in (4), where the past events are assigned appropriate weighting values. This METM can not only save network resources but also can improve the fault tolerance of the event-triggering mechanism compared to the traditional design.

We divide the sampling time interval $[t_k h + \tau_k, t_{k+1} h + \tau_{k+1})$ into $\varepsilon_M + 1$ parts as follows:

$$[t_k h + \tau_k, t_{k+1} h + \tau_{k+1}) = \cup_{l=0}^{\varepsilon_M} I_l, \tag{6}$$

where $l = 0, 1, 2, \cdots, \varepsilon_M$, $\varepsilon_M = \min\{l | t_k h + (l+1)h + \tau_k \geq t_{k+1} h + \tau_{k+1}\}$ and $I_l = [t_k h + lh + \tau_k, t_{k+1} h + lh + h + \tau_{k+1})$, τ_k denotes the network induced delay. Define delay function $\tau_i(t) = t - (t_k h + \epsilon h)$, and we can get

$$0 \leq \tau_k \leq \tau_i(t) \leq \tau_k + h \leq \tau_M, t \in I_l. \tag{7}$$

Define the error variable $e_{qi}^{(k)}(t) = x_i(t_{k-q+1}h) - x_i(t_k h + \epsilon h)$, and combine the delay function $\tau_i(t) = t - (t_k h + \epsilon h)$, then we can obtain

$$x_i(t_{k-q+1}h) = e_{qi}^{(k)}(t) + x_i(t_k h + \epsilon h) = e_{qi}^{(k)}(t) + x_i(t - \tau_i(t)). \tag{8}$$

The control input $u_i(t)$ in system (1) can be designed as

$$u_i(t) = \sum_{q=1}^{M} K_i^q(r_t) x_i(t_{k-q+1}h) = \sum_{q=1}^{M} K_i^q(r_t)[e_{qi}^{(k)}(t) + x_i(t - \tau_i(t))], t \in I_l. \tag{9}$$

Based on the above analysis, system (1) can be rewritten as

$$\dot{x}_i(t) = \mathcal{A}_{im} x_i(t) + \mathcal{B}_{im} \sum_{q=1}^{M} K_{im}^q x_i(t - \tau_i(t)) + \mathcal{B}_{im} \sum_{q=1}^{M} K_{im}^q e_{qi}^{(k)}(t) + \sum_{j=1, j\neq i}^{N} \mathcal{G}_{jim} x_j(t), \tag{10}$$

where K_{im}^q is the controller gain matrix. Next, a definition and some lemmas will be innovated to deduce the subsequent results of this paper.

Definition 1([16]): Suppose $V(x(t), r_t, t \geq 0)$ is a functional candidate, then the infinitesimal operator $\Im V(t)$ is represented as

$$\Im V(x(t), r_t) = \lim_{\delta \to 0} \frac{E\{V(x(t+\delta), r_{t+\delta}) | x(t), r_t\} - V(x(t), r_t)}{\delta}. \tag{11}$$

Lemma 1([38]): For a given scalar $\mu_i \in (0,1)$, the continuous function $\tau_i(t) \in (0, \tau_M]$ and $\dot{x}_i(t) : [-\tau_M, 0) \to \mathbb{R}^{n_i}$, there exist positive symmetric matrices $\mathcal{R}_i \in \mathbb{R}^{n_i \times n_i}$ and $\mathcal{S}_i \in \mathbb{R}^{2n_i \times 2n_i}$ to make the inequality hold

$$\tau_M \int_{t-\tau_M}^{t} \dot{x}_i^{\mathrm{T}}(s)\mathcal{R}_i\dot{x}_i(s)ds \geq \omega_1^{\mathrm{T}}\tilde{\mathcal{R}}_{1i}\omega_1 + \omega_2^{\mathrm{T}}\tilde{\mathcal{R}}_{2i}\omega_2 + 2\omega_1^{\mathrm{T}}\mathcal{S}_i\omega_2, \tag{12}$$

where

$$\tilde{\mathcal{R}}_{1i} = \tilde{\mathcal{R}}_i + (1-\mu_i)(\tilde{\mathcal{R}}_i - \mathcal{S}_i\tilde{\mathcal{R}}_i^{-1}\mathcal{S}_i^{\mathrm{T}}), \tilde{\mathcal{R}}_{2i} = \tilde{\mathcal{R}}_i + \mu_i(\tilde{\mathcal{R}}_i - \mathcal{S}_i^{\mathrm{T}}\tilde{\mathcal{R}}_i^{-1}\mathcal{S}_i), \tilde{\mathcal{R}}_i = diag\{\mathcal{R}_i, 3\mathcal{R}_i\},$$
$$\omega_1 = \begin{bmatrix} x_i(t-\tau_i(t)) - x_i(t-\tau_M) \\ x_i(t-\tau_i(t)) + x_i(t-\tau_M) - 2\rho_{1i} \end{bmatrix}, \omega_2 = \begin{bmatrix} x_i(t) - x_i(t-\tau_i(t) \\ x_i(t) + x_i(t-\tau_i(t)) - 2\rho_{2i} \end{bmatrix},$$
$$\mathcal{S}_i = \begin{bmatrix} \mathcal{S}_{1i} & \mathcal{S}_{2i} \\ \mathcal{S}_{3i} & \mathcal{S}_{4i} \end{bmatrix}, \rho_{1i} = \frac{1}{\tau_i(t)}\int_{t-\tau_i(t)}^{t} x_i(s)ds, \rho_{2i} = \frac{1}{\tau_M - \tau_i(t)}\int_{t-\tau_M}^{t-\tau_i(t)} x_i(s)ds.$$

Lemma 2([39,40]): For a real scalar $\alpha_i > 0$, the matrices $W_i > 0$, $X_{im} > 0$, the following inequality holds

$$-X_{im}W_i^{-1}X_{im} \leq -2\alpha_i X_{im} + \alpha_i^2 W_i, m \in S. \tag{13}$$

3. MAIN RESULTS

Our purpose is to co-design the memory controller (9) and dynamic METM (4) so that system (10) with partially accessible transition rates is stochastically stable. By utilizing the Lyapunov function method, some sufficient conditions that insure the stochastic stability of the interconnected semi-Markovian system (10) are given. Then, a controller design scheme based on LMI is given in Theorem 2.

Theorem 1. For given positive real number $\tau_M > 0$, $\alpha_i > 0$, $\gamma > 0$, $\varepsilon_0 > 0$, $\varepsilon_{ij} > 0$ $(j = 1, 2, 3, \cdots, M+3)$, and $\mu_i \in (0,1)$, the interconnected semi-Markovian jump control system (10) is said to be randomly stable with partially accessible transition rates and dynamic METM if there are positive symmetric matrices $\mathcal{P}_{im} > 0$, $\mathcal{Q}_{im} > 0, \mathcal{Q}_i > 0, \mathcal{R}_i > 0, \Omega_i > 0$, and matrices K_{im}^q, $\mathcal{S}_{1i}, \mathcal{S}_{2i}, \mathcal{S}_{3i}$ and $\mathcal{S}_{4i}$ with proper dimensions, such that the following matrix inequalities hold:

Case 1. If $\bigwedge_{m,k} \neq \emptyset$ and $\bigwedge_{m,uk} \neq \emptyset$, $m \in \bigwedge_{m,k}$, for $\forall j \in \bigwedge_{m,uk}$, we have

$$\begin{bmatrix} \tilde{\Xi}_{im} & * & * & * & * & * & \cdots & * & * & * \\ \Gamma_{im}^{11} & -\check{\mathcal{P}}_{im} & * & * & * & * & \cdots & * & * & * \\ \Gamma_{im}^{21} & 0 & -\mathcal{R}_i & * & * & * & \cdots & * & * & * \\ \Gamma_{im}^{31} & 0 & 0 & -\varepsilon_{i2}\mathcal{R}_i & * & * & \cdots & * & * & * \\ \Gamma_{im}^{41} & 0 & 0 & 0 & -\varepsilon_{i3}\mathcal{R}_i & * & \cdots & * & * & * \\ \Gamma_{im}^{51} & 0 & 0 & 0 & 0 & -\varepsilon_{i4}\mathcal{R}_i & \cdots & * & * & * \\ \vdots & \vdots & \vdots & \vdots & \vdots & \vdots & \ddots & \vdots & \vdots & \vdots \\ \Gamma_{im}^{61} & 0 & 0 & 0 & 0 & 0 & \cdots & -\varepsilon_{i,M+3}\mathcal{R}_i & * & * \\ \Gamma_{im}^{71} & 0 & 0 & 0 & 0 & 0 & \cdots & 0 & -\check{\mathcal{R}}_i & * \\ \Gamma_{im}^{81} & 0 & 0 & 0 & 0 & 0 & \cdots & 0 & 0 & -\hat{\mathcal{R}}_i \end{bmatrix} < 0, \tag{14}$$

$$-\mathcal{Q}_i + \sum_{l \in \bigwedge_{m,k}} \pi_{ml}(h)(\mathcal{Q}_{il} - \mathcal{Q}_{ij}) < 0, \tag{15}$$

where

$$\tilde{\Xi}_{im} = \begin{bmatrix} \tilde{\Xi}_{im}^{11} & * & * & * & * & * & \cdots & * \\ \tilde{\Xi}_{im}^{21} & \tilde{\Xi}_{im}^{22} & * & * & * & * & \cdots & * \\ \tilde{\Xi}_{im}^{31} & \tilde{\Xi}_{im}^{32} & \tilde{\Xi}_{im}^{33} & * & * & * & \cdots & * \\ \tilde{\Xi}_{im}^{41} & \tilde{\Xi}_{im}^{42} & \tilde{\Xi}_{im}^{43} & \tilde{\Xi}_{im}^{44} & * & * & \cdots & * \\ \tilde{\Xi}_{im}^{51} & \tilde{\Xi}_{im}^{52} & -\mathcal{S}_{4i} & \mathcal{S}_{4i} & \tilde{\Xi}_{im}^{55} & * & \cdots & * \\ \tilde{\Xi}_{im}^{61} & 0 & 0 & 0 & 0 & \tilde{\Xi}_{im}^{66} & \cdots & * \\ \vdots & \vdots & \vdots & \vdots & \vdots & \vdots & \ddots & \vdots \\ \tilde{\Xi}_{im}^{M+5,1} & 0 & 0 & 0 & 0 & 0 & \cdots & \tilde{\Xi}_{im}^{M+5,M+5} \end{bmatrix},$$

$$\tilde{\Xi}_{im}^{11} = sym\{\mathcal{P}_{im}\mathcal{A}_{im}\} + \tau_M\mathcal{Q}_i - 4(1+\mu_i)\mathcal{R}_i + \mathcal{Q}_{im} + \sum_{l\in\bigwedge_{m,uk}} \frac{\pi_{ml}(h)}{-\lambda_k}[\sum_{l\in\bigwedge_{m,k}} \pi_{ml}(h)(\mathcal{P}_{il} - \mathcal{P}_{ij})].$$

Case 2. If $\bigwedge_{m,k} \neq \emptyset$ and $\bigwedge_{m,uk} \neq \emptyset$, $m \in \bigwedge_{m,uk}$, for $\forall j \in \bigwedge_{m,uk}$, we have

$$\begin{bmatrix} \hat{\Xi}_{im} & * & * & * & * & * & \cdots & * & * & * \\ \Gamma_{im}^{11} & -\check{\mathcal{P}}_{im} & * & * & * & * & \cdots & * & * & * \\ \Gamma_{im}^{21} & 0 & -\mathcal{R}_i & * & * & * & \cdots & * & * & * \\ \Gamma_{im}^{31} & 0 & 0 & -\varepsilon_{i2}\mathcal{R}_i & * & * & \cdots & * & * & * \\ \Gamma_{im}^{41} & 0 & 0 & 0 & -\varepsilon_{i3}\mathcal{R}_i & * & \cdots & * & * & * \\ \Gamma_{im}^{51} & 0 & 0 & 0 & 0 & -\varepsilon_{i4}\mathcal{R}_i & \cdots & * & * & * \\ \vdots & \vdots & \vdots & \vdots & \vdots & \vdots & \ddots & \vdots & \vdots & \vdots \\ \Gamma_{im}^{61} & 0 & 0 & 0 & 0 & 0 & \cdots & -\varepsilon_{i,M+3}\mathcal{R}_i & * & * \\ \Gamma_{im}^{71} & 0 & 0 & 0 & 0 & 0 & \cdots & 0 & -\check{\mathcal{R}}_i & * \\ \Gamma_{im}^{81} & 0 & 0 & 0 & 0 & 0 & \cdots & 0 & 0 & -\hat{\mathcal{R}}_i \end{bmatrix} < 0, \tag{16}$$

$$\mathcal{P}_{im} - \mathcal{P}_{ij} \geq 0, \mathcal{Q}_{im} - \mathcal{Q}_{ij} \geq 0, \tag{17}$$

$$-\mathcal{Q}_i + \sum_{l\in\bigwedge_{m,k}} \pi_{ml}(h)(\mathcal{Q}_{il} - \mathcal{Q}_{ij}) < 0, \tag{18}$$

where

$$\hat{\Xi}_{im} = \begin{bmatrix} \hat{\Xi}_{im}^{11} & * & * & * & * & * & \cdots & * \\ \tilde{\Xi}_{im}^{21} & \tilde{\Xi}_{im}^{22} & * & * & * & * & \cdots & * \\ \tilde{\Xi}_{im}^{31} & \tilde{\Xi}_{im}^{32} & \tilde{\Xi}_{im}^{33} & * & * & * & \cdots & * \\ \tilde{\Xi}_{im}^{41} & \tilde{\Xi}_{im}^{42} & \tilde{\Xi}_{im}^{43} & \tilde{\Xi}_{im}^{44} & * & * & \cdots & * \\ \tilde{\Xi}_{im}^{51} & \tilde{\Xi}_{im}^{52} & -\mathcal{S}_{4i} & \mathcal{S}_{4i} & \tilde{\Xi}_{im}^{55} & * & \cdots & * \\ \tilde{\Xi}_{im}^{61} & 0 & 0 & 0 & 0 & \tilde{\Xi}_{im}^{66} & \cdots & * \\ \vdots & \vdots & \vdots & \vdots & \vdots & \vdots & \ddots & \vdots \\ \tilde{\Xi}_{im}^{M+5,1} & 0 & 0 & 0 & 0 & 0 & \cdots & \tilde{\Xi}_{im}^{M+5,M+5} \end{bmatrix},$$

$$\hat{\Xi}_{im}^{11} = sym\{\mathcal{P}_{im}\mathcal{A}_{im}\} + \mathcal{Q}_{im} + \tau_M\mathcal{Q}_i - 4(1+\mu_i)\mathcal{R}_i$$
$$+ \sum_{l\in\bigwedge_{m,uk}} \frac{\pi_{ml}(h)}{-\pi_{mm}(h) - \lambda_k}[\sum_{l\in\bigwedge_{m,k}} \pi_{ml}(h)(\mathcal{P}_{il} - \mathcal{P}_{ij}) + \pi_{mm}(h)(\mathcal{P}_{il} - \mathcal{P}_{ij})].$$

Case 3. If $\bigwedge_{m,k} = \emptyset$, $\bigwedge_{m,uk} \neq \emptyset$, $m \in \bigwedge_{m,uk}$, and there exist $l \neq m$ and $l \in \bigwedge_{m,uk}$, we have

$$\begin{bmatrix} \check{\Xi}_{im} & * & * & * & * & * & \cdots & * & * & * \\ \Gamma_{im}^{11} & -\check{\mathcal{P}}_{im} & * & * & * & * & \cdots & * & * & * \\ \Gamma_{im}^{21} & 0 & -\mathcal{R}_i & * & * & * & \cdots & * & * & * \\ \Gamma_{im}^{31} & 0 & 0 & -\varepsilon_{i2}\mathcal{R}_i & * & * & \cdots & * & * & * \\ \Gamma_{im}^{41} & 0 & 0 & 0 & -\varepsilon_{i3}\mathcal{R}_i & * & \cdots & * & * & * \\ \Gamma_{im}^{51} & 0 & 0 & 0 & 0 & -\varepsilon_{i4}\mathcal{R}_i & \cdots & * & * & * \\ \vdots & \vdots & \vdots & \vdots & \vdots & \vdots & \ddots & \vdots & \vdots & \vdots \\ \Gamma_{im}^{61} & 0 & 0 & 0 & 0 & 0 & \cdots & -\varepsilon_{i,M+3}\mathcal{R}_i & * & * \\ \Gamma_{im}^{71} & 0 & 0 & 0 & 0 & 0 & \cdots & 0 & -\check{\mathcal{R}}_i & * \\ \Gamma_{im}^{81} & 0 & 0 & 0 & 0 & 0 & \cdots & 0 & 0 & -\hat{\mathcal{R}}_i \end{bmatrix} < 0, \tag{19}$$

where

$$\check{\Xi}_{im} = \begin{bmatrix} \check{\Xi}_{im}^{11} & * & * & * & * & * & \cdots & * \\ \tilde{\Xi}_{im}^{21} & \tilde{\Xi}_{im}^{22} & * & * & * & * & \cdots & * \\ \tilde{\Xi}_{im}^{31} & \tilde{\Xi}_{im}^{32} & \tilde{\Xi}_{im}^{33} & * & * & * & \cdots & * \\ \tilde{\Xi}_{im}^{41} & \tilde{\Xi}_{im}^{42} & \tilde{\Xi}_{im}^{43} & \tilde{\Xi}_{im}^{44} & * & * & \cdots & * \\ \tilde{\Xi}_{im}^{51} & \tilde{\Xi}_{im}^{52} & -\mathcal{S}_{4i} & \mathcal{S}_{4i} & \tilde{\Xi}_{im}^{55} & * & \cdots & * \\ \tilde{\Xi}_{im}^{61} & 0 & 0 & 0 & 0 & \tilde{\Xi}_{im}^{66} & \cdots & * \\ \vdots & \vdots & \vdots & \vdots & \vdots & \vdots & \ddots & \vdots \\ \tilde{\Xi}_{im}^{M+5,1} & 0 & 0 & 0 & 0 & 0 & \cdots & \tilde{\Xi}_{im}^{M+5,M+5} \end{bmatrix},$$

$$\check{\Xi}_{im}^{11} = sym\{\mathcal{P}_{im}\mathcal{A}_{im}\} + \mathcal{Q}_{im} + \tau_M\mathcal{Q}_i - 4(1+\mu_i)\mathcal{R}_i + a_m\pi_{ll}(h)(\mathcal{P}_{im} - \mathcal{P}_{ij}).$$

In addition, the other scalars are given as follows

$$\tilde{\Xi}_{im}^{21} = \sum_{q=1}^{M}(K_{im}^{q})^{\mathrm{T}}\mathcal{B}_{im}^{\mathrm{T}}\mathcal{P}_{im} - 2(1+\mu_i)\mathcal{R}_i - \mathcal{S}_{1i} - \mathcal{S}_{2i} - \mathcal{S}_{3i} - \mathcal{S}_{4i},$$
$$\tilde{\Xi}_{im}^{22} = -2(4+\mu_i)\mathcal{R}_i - 2\mathcal{S}_{1i} + 2\mathcal{S}_{2i} - 2\mathcal{S}_{3i} + 2\mathcal{S}_{4i} + \Omega_i, \tilde{\Xi}_{im}^{31} = -\mathcal{S}_{1i} - \mathcal{S}_{2i} + \mathcal{S}_{3i} + \mathcal{S}_{4i},$$
$$\tilde{\Xi}_{im}^{32} = -2(2-\mu_i)\mathcal{R}_i + \mathcal{S}_{1i} - \mathcal{S}_{2i} - \mathcal{S}_{3i} + \mathcal{S}_{4i}, \tilde{\Xi}_{im}^{33} = -\mathcal{Q}_{im} - 4(2-\mu_i)\mathcal{R}_i,$$
$$\tilde{\Xi}_{im}^{41} = -\mathcal{S}_{3i} - \mathcal{S}_{4i}, \tilde{\Xi}_{im}^{42} = \mathcal{S}_{3i} - \mathcal{S}_{4i} + 3(2-\mu_i)\mathcal{R}_i, \tilde{\Xi}_{im}^{43} = 3(2-\mu_i)\mathcal{R}_i, \tilde{\Xi}_{im}^{44} = -3(2-\mu_i)\mathcal{R}_i,$$
$$\tilde{\Xi}_{im}^{51} = 3(1+\mu_i)\mathcal{R}_i, \tilde{\Xi}_{im}^{52} = -\mathcal{S}_{2i} + 3(1+\mu_i)\mathcal{R}_i, \tilde{\Xi}_{im}^{55} = -3(1+\mu_i)\mathcal{R}_i,$$
$$\tilde{\Xi}_{im}^{61} = (K_{im}^{1})^{\mathrm{T}}\mathcal{B}_{im}^{\mathrm{T}}\mathcal{P}_{im}, \tilde{\Xi}_{im}^{66} = -\theta_0\gamma_1\Omega_i, \tilde{\Xi}_{im}^{M+5,1} = (K_{im}^{M})^{\mathrm{T}}\mathcal{B}_{im}^{\mathrm{T}}\mathcal{P}_{im}, \tilde{\Xi}_{im}^{M+5,M+5} = -\theta_0\gamma_M\Omega_i,$$
$$\Gamma_{im}^{11} = \begin{bmatrix}\mathcal{G}_{ijm}^{\mathrm{T}}\mathcal{P}_{im} & 0 & 0 & 0 & 0 & 0 & \cdots & 0\end{bmatrix},$$
$$\check{\mathcal{P}}_{im} = -(N-1)^{-1}diag\{\varepsilon_{i1}^{-1}\mathcal{P}_{im}, \cdots, \varepsilon_{j1}^{-1}\mathcal{P}_{jm, j\neq i}, \cdots, \varepsilon_{N1}^{-1}\mathcal{P}_{Nm}\},$$
$$\Gamma_{im}^{21} = \tau_M\mathcal{R}_i\begin{bmatrix}\mathcal{A}_{im} & \mathcal{B}_{im}\sum_{q=1}^{M}K_{im}^{q} & 0 & 0 & 0 & \mathcal{B}_{im}K_{im}^{1} & \cdots & \mathcal{B}_{im}K_{im}^{M}\end{bmatrix},$$
$$\Gamma_{im}^{31} = \tau_M\mathcal{R}_i\begin{bmatrix}\mathcal{A}_{im} & 0 & 0 & 0 & 0 & 0 & \cdots & 0\end{bmatrix},$$
$$\Gamma_{im}^{41} = \tau_M\mathcal{R}_i\begin{bmatrix}0 & \mathcal{B}_{im}\sum_{q=1}^{M}K_{im}^{q} & 0 & 0 & 0 & 0 & \cdots & 0\end{bmatrix},$$
$$\Gamma_{im}^{51} = \tau_M\mathcal{R}_i\begin{bmatrix}0 & 0 & 0 & 0 & 0 & \mathcal{B}_{im}K_{im}^{1} & \cdots & 0\end{bmatrix},$$
$$\Gamma_{im}^{61} = \tau_M\mathcal{R}_i\begin{bmatrix}0 & 0 & 0 & 0 & 0 & 0 & \cdots & \mathcal{B}_{im}K_{im}^{M}\end{bmatrix},$$
$$\Gamma_{im}^{71} = \tau_M\mathcal{R}_i\begin{bmatrix}\mathcal{G}_{ijm} & 0 & 0 & 0 & 0 & 0 & \cdots & 0\end{bmatrix},$$
$$\check{\mathcal{R}}_i = -(N-1)^{-1}diag\{(1+\varepsilon_{i2}+\varepsilon_{i3}+\cdots+\varepsilon_{i,M+3})^{-1}\mathcal{R}_1, \cdots, (1+\varepsilon_{j2}+\varepsilon_{j3}+\cdots+\varepsilon_{j,M+3})^{-1}\mathcal{R}_{j,j\neq i},$$
$$\cdots, (1+\varepsilon_{N2}+\varepsilon_{N3}+\cdots+\varepsilon_{N,M+3})^{-1}\mathcal{R}_N\},$$
$$\Gamma_{im}^{81} = \begin{bmatrix}0 & \mathcal{S}_{1i}+\mathcal{S}_{3i} & -\mathcal{S}_{1i}+\mathcal{S}_{3i} & -\mathcal{S}_{3i} & 0 & 0 & \cdots & 0\\ 0 & \mathcal{S}_{2i}+\mathcal{S}_{4i} & -\mathcal{S}_{2i}+\mathcal{S}_{4i} & -\mathcal{S}_{4i} & 0 & 0 & \cdots & 0\\ \mathcal{S}_{1i}+\mathcal{S}_{3i} & -\mathcal{S}_{1i}+\mathcal{S}_{3i} & 0 & 0 & -\mathcal{S}_{3i} & 0 & \cdots & 0\\ \mathcal{S}_{2i}+\mathcal{S}_{4i} & -\mathcal{S}_{2i}+\mathcal{S}_{4i} & 0 & 0 & -\mathcal{S}_{4i} & 0 & \cdots & 0\end{bmatrix},$$
$$\hat{\mathcal{R}}_i = diag\{-(1-\mu_i)^{-1}\mathcal{R}_i, -3(1-\mu_i)^{-1}\mathcal{R}_i, -\mu_i^{-1}\mathcal{R}_i, -3\mu_i^{-1}\mathcal{R}_i\}.$$

Proof: Define the following Lyapunov-Krasovskii functional $V(x(t), r_t)$:

$$V(x(t), r_t) = \sum_{i=1}^{N}[V_1(x_i(t), r_t) + V_2(x_i(t), r_t) + V_3(x_i(t), r_t) + V_4(x_i(t), r_t)], \tag{20}$$

where

$$V_1(x_i(t), r_t) = x_i^{\mathrm{T}}(t)\mathcal{P}_i(r_t)x_i(t),$$
$$V_2(x_i(t), r_t) = \int_{t-\tau_M}^{t}x_i^{\mathrm{T}}(s)\mathcal{Q}_i(r_t)x_i(s)ds + \int_{-\tau_M}^{0}\int_{t+\nu}^{t}x_i^{\mathrm{T}}(s)\mathcal{Q}_ix_i(s)dsd\nu,$$
$$V_3(x_i(t), r_t) = \tau_M\int_{-\tau_M}^{0}\int_{t+\nu}^{t}\dot{x}_i^{\mathrm{T}}(s)\mathcal{R}_i\dot{x}_i(s)dsd\nu,$$
$$V_4(x_i(t), r_t) = \frac{1}{2}\theta_i^2(t).$$

According to Definition 1, we can get

$$
\begin{aligned}
&\Im V_1(x_i(t), r_t) \\
&= \lim_{\delta\to 0^+}\frac{1}{\delta}\{[\sum_{l=1,l\neq m}^{s} Pr\{r_{t+\delta}=l|r_t=m\}x_i^{\mathrm{T}}(t+\delta)\mathcal{P}_{il}x_i(t+\delta)] \\
&+ [Pr\{r_{t+\delta}=m|r_t=m\}x_i^{\mathrm{T}}(t+\delta)\mathcal{P}_{im}x_i(t+\delta) - x_i^{\mathrm{T}}(t)\mathcal{P}_{im}x_i(t)]\} \\
&= \lim_{\delta\to 0^+}\frac{1}{\delta}[\sum_{l=1,l\neq m}^{s}\frac{Pr\{r_{t+\delta}=l, r_t=m\}}{Pr\{r_t=m\}}x_i^{\mathrm{T}}(t+\delta)\mathcal{P}_{il}x_i(t+\delta)] \\
&+ \lim_{\delta\to 0^+}\frac{1}{\delta}[\frac{Pr\{r_{t+\delta}=m, r_t=m\}}{Pr\{r_t=m\}}x_i^{\mathrm{T}}(t+\delta)\mathcal{P}_{im}x_i(t+\delta) - x_i^{\mathrm{T}}(t)\mathcal{P}_{im}x_i(t)] \\
&= \lim_{\delta\to 0^+}\frac{1}{\delta}[\sum_{l=1,l\neq m}^{s}\frac{\lambda_{ml}(\phi_m(h+\delta)-\phi_m(h))}{1-\phi_m(h)}x_i^{\mathrm{T}}(t+\delta)\mathcal{P}_{il}x_i(t+\delta)] \\
&+ \lim_{\delta\to 0^+}\frac{1}{\delta}[\frac{1-\phi_m(h+\delta)}{1-\phi_m(h)}x_i^{\mathrm{T}}(t+\delta)\mathcal{P}_{im}x_i(t+\delta) - x_i^{\mathrm{T}}(t)\mathcal{P}_{im}x_i(t)] \\
&= \lim_{\delta\to 0^+}\frac{1}{\delta}[\sum_{l=1,l\neq m}^{s}\frac{\lambda_{ml}(\phi_m(h+\delta)-\phi_m(h))}{1-\phi_m(h)}x_i^{\mathrm{T}}(t+\delta)\mathcal{P}_{il}x_i(t+\delta)] \\
&+ \lim_{\delta\to 0^+}\frac{1}{\delta}[\frac{1-\phi_m(h+\delta)}{1-\phi_m(h)}(x_i^{\mathrm{T}}(t+\delta) - x_i^{\mathrm{T}}(t))\mathcal{P}_{im}x_i(t+\delta)] \\
&+ \lim_{\delta\to 0^+}\frac{1}{\delta}[\frac{1-\phi_m(h+\delta)}{1-\phi_m(h)}x_i^{\mathrm{T}}(t)\mathcal{P}_{im}(x_i(t+\delta)-x_i(t)) - \frac{\phi_m(h+\delta)-\phi_m(h)}{1-\phi_m(h)}x_i^{\mathrm{T}}(t)\mathcal{P}_{im}x_i(t)],
\end{aligned}
\tag{21}
$$

where h is the dwell time when the system jumps from the previous mode to mode m, $\phi_m(h)$ represents the cumulative distribution function of residence time when the system (10) maintains in m th mode, λ_{ml} represents the probability density from mode m to mode l. Using the properties of cumulative distribution function, it can be seen that

$$
\lim_{\delta\to 0^+}\frac{1-\phi_m(h+\delta)}{1-\phi_m(h)} = 1, \lim_{\delta\to 0^+}\frac{1}{\delta}\frac{\phi_m(h+\delta)-\phi_m(h)}{1-\phi_m(h)} = \pi_m(h), \tag{22}
$$

where $\pi_m(h)$ represents the transition probability of the system in mode m. When $m \neq l$, we have $\pi_{ml}(h) = \lambda_{ml}\pi_m(h)$ and $\pi_{mm}(h) = -\sum_{l=1,l\neq m}^{s}\pi_{ml}(h)$, one derives that $\Im V_1(x_i(t), r_t) = x_i^{\mathrm{T}}(t)(\sum_{l=1,l\neq m}^{s}\pi_{ml}(h)\mathcal{P}_{il})x_i(t) + 2x_i^{\mathrm{T}}(t)\mathcal{P}_{im}\dot{x}_i(t)$.

According to[22], there is a scalar $\varepsilon_{i1}^{-1} \in (0, \varepsilon_0^{-1}]$, and we know that

$$
\sum_{i=1}^{N} 2x_i^{\mathrm{T}}(t)\mathcal{P}_{im}\sum_{j=1,j\neq i}^{N}\mathcal{G}_{jim}x_j(t) \leq \sum_{i=1}^{N}(\varepsilon_{i1}\sum_{j=1,j\neq i}^{N}x_j^{\mathrm{T}}(t)\mathcal{G}_{jim}^{\mathrm{T}}\mathcal{P}_{im}\sum_{j=1,j\neq i}^{N}\mathcal{G}_{jim}x_j(t) + \varepsilon_{i1}^{-1}x_i^{\mathrm{T}}(t)\mathcal{P}_{im}x_i(t)). \tag{23}
$$

Similarly, the $\Im V_2(x_i(t), r_t)$, $\Im V_3(x_i(t), r_t)$, $\Im V_4(x_i(t), r_t)$ can be written as

$$
\begin{aligned}
\Im V_2(x_i(t), r_t) &= x_i^{\mathrm{T}}(t)Q_{im}x_i(t) - x_i^{\mathrm{T}}(t-\tau_M)Q_{im}x_i(t-\tau_M) \\
&+ \tau_M x_i^{\mathrm{T}}(t)Q_i x_i(t) + \int_{t-\tau_M}^{t} x_i^{\mathrm{T}}(s)(-Q_i + \sum_{l=1}^{s}\pi_{ml}(h)Q_{il})x_i(s)ds, \\
\Im V_3(x_i(t), r_t) &= \tau_M^2\dot{x}_i^{\mathrm{T}}(t)\mathcal{R}_i\dot{x}_i(t) - \tau_M\int_{t-\tau_M}^{t}\dot{x}_i^{\mathrm{T}}(s)\mathcal{R}_i\dot{x}_i(s)ds, \\
\Im V_4(x_i(t), r_t) &= \frac{1}{\theta_i(t)}\sum_{q=1}^{M}\gamma_q(\Delta_{qi}^{(k)}(t))^{\mathrm{T}}\Omega_i\Delta_{qi}^{(k)}(t) - \theta_0\sum_{q=1}^{M}\gamma_q(\Delta_{qi}^{(k)}(t))^{\mathrm{T}}\Omega_i\Delta_{qi}^{(k)}(t) \\
&\leq x_i^{\mathrm{T}}(t-\tau_i(t))\Omega_i x_i(t-\tau_i(t)) - \theta_0\sum_{q=1}^{M}\gamma_q(e_{qi}^{(k)}(t))^{\mathrm{T}}\Omega_i e_{qi}^{(k)}(t).
\end{aligned}
$$

According to Lemma 1, one further comes to

$$-\tau_M \int_{t-\tau_M}^{t} \dot{x}_i^{\mathrm{T}}(s)\mathcal{R}_i\dot{x}_i(s)ds \le \xi_i^{\mathrm{T}}(t)\Xi_{im}\xi_i(t) + (1-\mu_i)\omega_1^{\mathrm{T}}\mathcal{S}_i\tilde{\mathcal{R}}_i^{-1}\mathcal{S}_i^{\mathrm{T}}\omega_1 + \mu_i\omega_2^{\mathrm{T}}\mathcal{S}_i^{\mathrm{T}}\tilde{\mathcal{R}}_i^{-1}\mathcal{S}_i\omega_2, \tag{24}$$

where

$$\xi_i^{\mathrm{T}}(t) = \left[x_i^{\mathrm{T}}(t) \quad x_i^{\mathrm{T}}(t-\tau_i(t)) \quad x_i^{\mathrm{T}}(t-\tau_M) \quad 2\rho_{1i}^{\mathrm{T}} \quad 2\rho_{2i}^{\mathrm{T}}\right],$$

$$\Xi_{im} = \begin{bmatrix} \Xi_{im}^{11} & * & * & * & * \\ \Xi_{im}^{21} & \Xi_{im}^{22} & * & * & * \\ \Xi_{im}^{31} & \Xi_{im}^{32} & \Xi_{im}^{33} & * & * \\ \Xi_{im}^{41} & \Xi_{im}^{42} & \Xi_{im}^{43} & \Xi_{im}^{44} & * \\ \Xi_{im}^{51} & \Xi_{im}^{52} & \Xi_{im}^{53} & \Xi_{im}^{54} & \Xi_{im}^{55} \end{bmatrix},$$

$$\Xi_{im}^{11} = -4(1+\mu_i)\mathcal{R}_i, \Xi_{im}^{21} = -2(1+\mu_i)\mathcal{R}_i - \mathcal{S}_{1i} - \mathcal{S}_{2i} - \mathcal{S}_{3i} - \mathcal{S}_{4i},$$

$$\Xi_{im}^{22} = -2(4+\mu_i)\mathcal{R}_i - 2\mathcal{S}_{1i} + 2\mathcal{S}_{2i} - 2\mathcal{S}_{3i} + 2\mathcal{S}_{4i}, \Xi_{im}^{31} = -\mathcal{S}_{1i} - \mathcal{S}_{2i} + \mathcal{S}_{3i} + \mathcal{S}_{4i},$$

$$\Xi_{im}^{32} = -2(2-\mu_i)\mathcal{R}_i + \mathcal{S}_{1i} - \mathcal{S}_{2i} - \mathcal{S}_{3i} + \mathcal{S}_{4i}, \Xi_{im}^{33} = -4(2-\mu_i)\mathcal{R}_i, \Xi_{im}^{41} = -\mathcal{S}_{3i} - \mathcal{S}_{4i},$$

$$\Xi_{im}^{42} = \mathcal{S}_{3i} - \mathcal{S}_{4i} + 3(2-\mu_i)\mathcal{R}_i, \Xi_{im}^{43} = 3(2-\mu_i)\mathcal{R}_i, \Xi_{im}^{44} = -3(2-\mu_i)\mathcal{R}_i,$$

$$\Xi_{im}^{51} = 3(1+\mu_i)\mathcal{R}_i, \Xi_{im}^{52} = -\mathcal{S}_{2i} + 3(1+\mu_i)\mathcal{R}_i, \Xi_{im}^{53} = -\mathcal{S}_{4i}, \Xi_{im}^{54} = \mathcal{S}_{4i}, \Xi_{im}^{55} = -3(1+\mu_i)\mathcal{R}_i.$$

And

$$\begin{aligned}
&\dot{x}_i^{\mathrm{T}}(t)\mathcal{R}_i\dot{x}_i(t) \\
&= (\mathcal{A}_{im}x_i(t) + \mathcal{B}_{im}\sum_{q=1}^{M} K_{im}^q x_i(t-\tau_i(t)) + \mathcal{B}_{im}\sum_{q=1}^{M} K_{im}^q e_{qi}^{(k)}(t))^{\mathrm{T}} \\
&\mathcal{R}_i(\mathcal{A}_{im}x_i(t) + \mathcal{B}_{im}\sum_{q=1}^{M} K_{im}^q x_i(t-\tau_i(t)) + \mathcal{B}_{im}\sum_{q=1}^{M} K_{im}^q e_{qi}^{(k)}(t)) \\
&+2x_i^{\mathrm{T}}(t)\mathcal{A}_{im}^{\mathrm{T}}\mathcal{R}_i\sum_{j=1,j\neq i}^{N}\mathcal{G}_{jim}x_j(t) + 2x_i^{\mathrm{T}}(t-\tau_i(t))\sum_{q=1}^{M} K_{im}^{q\ \mathrm{T}}\mathcal{B}_{im}^{\mathrm{T}}\mathcal{R}_i\sum_{j=1,j\neq i}^{N}\mathcal{G}_{jim}x_j(t) \\
&+2\sum_{q=1}^{M}(e_{qi}^{(k)}(t))^{\mathrm{T}}K_{im}^{q\ \mathrm{T}}\mathcal{B}_{im}^{\mathrm{T}}\mathcal{R}_i\sum_{j=1,j\neq i}^{N}\mathcal{G}_{jim}x_j(t) + \sum_{j=1,j\neq i}^{N} x_j^{\mathrm{T}}(t)\mathcal{G}_{jim}^{\mathrm{T}}\mathcal{R}_i\sum_{j=1,j\neq i}^{N}\mathcal{G}_{jim}x_j(t),
\end{aligned}$$

where

$$\sum_{i=1}^{N}(2x_i^{\mathrm{T}}(t)\mathcal{A}_{im}^{\mathrm{T}}\mathcal{R}_i\sum_{j=1,j\neq i}^{N}\mathcal{G}_{jim}x_j(t))$$
$$\leq\sum_{i=1}^{N}((N-1)\sum_{j=1,j\neq i}^{N}\varepsilon_{i2}x_i^{\mathrm{T}}(t)\mathcal{G}_{ijm}^{\mathrm{T}}\mathcal{R}_i\mathcal{G}_{ijm}x_i(t)+\varepsilon_{i2}^{-1}x_i^{\mathrm{T}}(t)\mathcal{A}_{im}^{\mathrm{T}}\mathcal{R}_i\mathcal{A}_{im}x_i(t)),$$
$$\sum_{i=1}^{N}(2x_i^{\mathrm{T}}(t-\tau_i(t))\sum_{q=1}^{M}K_{im}^{q\ \mathrm{T}}\mathcal{B}_{im}^{\mathrm{T}}\mathcal{R}_i\sum_{j=1,j\neq i}^{N}\mathcal{G}_{jim}x_j(t))$$
$$\leq\sum_{i=1}^{N}((N-1)\sum_{j=1,j\neq i}^{N}\varepsilon_{i3}x_i^{\mathrm{T}}(t-\tau_i(t))\mathcal{G}_{ijm}^{\mathrm{T}}\mathcal{R}_i\mathcal{G}_{ijm}x_i(t-\tau_i(t))$$
$$+\varepsilon_{i3}^{-1}x_i^{\mathrm{T}}(t-\tau_i(t))\sum_{q=1}^{M}K_{im}^{q\ \mathrm{T}}\mathcal{B}_{im}^{\mathrm{T}}\mathcal{R}_i\mathcal{B}_{im}\sum_{q=1}^{M}K_{im}^{q}x_i(t-\tau_i(t)),$$
$$\sum_{i=1}^{N}(2\sum_{q=1}^{M}(e_{qi}^{(k)}(t))^{\mathrm{T}}K_{im}^{q\ \mathrm{T}}\mathcal{B}_{im}^{\mathrm{T}}\mathcal{R}_i\sum_{j=1,j\neq i}^{N}\mathcal{G}_{jim}x_j(t))$$
$$\leq\sum_{i=1}^{N}((N-1)\sum_{j=1,j\neq i}^{N}\varepsilon_{i4}x_i^{\mathrm{T}}(t)\mathcal{G}_{ijm}^{\mathrm{T}}\mathcal{R}_i\mathcal{G}_{ijm}x_i(t)+\varepsilon_{i4}^{-1}\sum_{q=1}^{M}(e_{qi}^{(k)}(t))^{\mathrm{T}}K_{im}^{q\ \mathrm{T}}\mathcal{B}_{im}^{\mathrm{T}}\mathcal{R}_i\mathcal{B}_{im}\sum_{q=1}^{M}K_{im}^{q}e_{qi}^{(k)}(t)),$$
$$\sum_{i=1}^{N}(\sum_{j=1,j\neq i}^{N}x_j^{\mathrm{T}}(t)\mathcal{G}_{jim}^{\mathrm{T}}\mathcal{R}_i\sum_{j=1,j\neq i}^{N}\mathcal{G}_{jim}x_j(t))\leq\sum_{i=1}^{N}(N-1)\sum_{j=1,j\neq i}^{N}x_i^{\mathrm{T}}(t)\mathcal{G}_{ijm}^{\mathrm{T}}\mathcal{R}_i\mathcal{G}_{ijm}x_i(t).$$

Let $\eta_i(t)=\left[\xi_i^{\mathrm{T}}(t)\quad(e_{1i}^{(k)}(t))^{\mathrm{T}}\quad\cdots\quad(e_{Mi}^{(k)}(t))^{\mathrm{T}}\right]^{\mathrm{T}}$, then we obtain

$$\begin{aligned}\dot{V}(x(t),r_t)&\leq\sum_{i=1}^{N}\eta_i^{\mathrm{T}}(t)[\Gamma_{im}^{0}+(\Gamma_{im}^{11})^{\mathrm{T}}\mathcal{P}_{im}^{-1}\Gamma_{im}^{11}+(\Gamma_{im}^{21})^{\mathrm{T}}\mathcal{R}_i^{-1}\Gamma_{im}^{21}+\varepsilon_{i2}^{-1}(\Gamma_{im}^{31})^{\mathrm{T}}\mathcal{R}_i^{-1}\Gamma_{im}^{31}+\varepsilon_{i3}^{-1}(\Gamma_{im}^{41})^{\mathrm{T}}\mathcal{R}_i^{-1}\Gamma_{im}^{41}\\&\quad+\varepsilon_{i4}^{-1}(\Gamma_{im}^{51})^{\mathrm{T}}\mathcal{R}_i^{-1}\Gamma_{im}^{51}+\varepsilon_{i,M+1}^{-1}(\Gamma_{im}^{61})^{\mathrm{T}}\tilde{\mathcal{R}}_i^{-1}\Gamma_{im}^{61}+(\Gamma_{im}^{71})^{\mathrm{T}}\check{\mathcal{R}}_i^{-1}\Gamma_{im}^{71}(\Gamma_{im}^{81})^{\mathrm{T}}\hat{\mathcal{R}}_i^{-1}\Gamma_{im}^{81}]\eta_i(t)\\&=\sum_{i=1}^{N}\eta_i^{\mathrm{T}}(t)\Pi_{im}\eta_i(t),\end{aligned}$$

where $\Gamma_{im}^{0}=\tilde{\Xi}_{im}(case1)$, $\Gamma_{im}^{0}=\hat{\Xi}_{im}(case2)$, $\Gamma_{im}^{0}=\check{\Xi}_{im}(case3)$.

Therefore, if $\Pi_{im}<0$ and $-\mathcal{Q}_i+\sum_{l=1}^{s}\pi_{ml}(h)\mathcal{Q}_{il}<0$, the interconnected semi-Markovian control system (10) with partially accessible TRs and dynamic METM is stochastically stable. Considering the partially accessible transition rates, we will get the corresponding conclusion from the following three cases.

Case 1. If $\bigwedge_{m,k}\neq\emptyset$ and $\bigwedge_{m,uk}\neq\emptyset$, $m\in\bigwedge_{m,k}$, denote $\lambda_k=\sum_{l\in\bigwedge_{m,k}}\pi_{ml}(h)$. Since $\bigwedge_{m,uk}\neq\emptyset$, then one derives that $\lambda_k<0$, thus $\sum_{l=1}^{s}\pi_{ml}(h)\mathcal{P}_{il}$ can be presented as

$$\sum_{l=1}^{s}\pi_{ml}(h)\mathcal{P}_{il}=(\sum_{l\in\bigwedge_{m,k}}+\sum_{l\in\bigwedge_{m,uk}})\pi_{ml}(h)\mathcal{P}_{il}=\sum_{l\in\bigwedge_{m,k}}\pi_{ml}(h)\mathcal{P}_{il}-\lambda_k\sum_{l\in\bigwedge_{m,uk}}\frac{\pi_{ml}(h)}{-\lambda_k}\mathcal{P}_{il}.\tag{25}$$

Obviously, there exists $0\leq\frac{\pi_{ml}(h)}{-\lambda_k}\leq 1(l\in\bigwedge_{m,uk})$ and $\sum_{l\in\bigwedge_{m,uk}}\frac{\pi_{ml}(h)}{-\lambda_k}=1$. So for $\forall j\in\bigwedge_{m,uk}$, there is

$$\sum_{l=1}^{s}\pi_{ml}(h)\mathcal{P}_{il}=\sum_{l\in\bigwedge_{m,uk}}\frac{\pi_{ml}(h)}{-\lambda_k}(\sum_{l\in\bigwedge_{m,k}}\pi_{ml}(h)(\mathcal{P}_{il}-\mathcal{P}_{ij})).\tag{26}$$

According to Schur complement, it is inferred that (14) is equivalent to $\Pi_{im} < 0$ and (15) is equivalent to $-\mathcal{Q}_i + \sum_{l=1}^{s} \pi_{ml}(h)\mathcal{Q}_{il} < 0$.

Case 2. If $\bigwedge_{m,k} \neq \emptyset$ and $\bigwedge_{m,uk} \neq \emptyset$, $m \in \bigwedge_{m,uk}$, denote $\lambda_k = \sum_{l\in\bigwedge_{m,k}} \pi_{ml}(h)$. Since $\bigwedge_{m,k} \neq \emptyset$, we know that $\lambda_k > 0$, thus $\sum_{l=1}^{s} \pi_{ml}(h)\mathcal{P}_{il}$ can be presented as

$$\begin{aligned}\sum_{l=1}^{s} \pi_{ml}(h)\mathcal{P}_{il} &= \sum_{l\in\bigwedge_{m,k}} \pi_{ml}(h)\mathcal{P}_{il} + \pi_{mm}(h)\mathcal{P}_{im} + \sum_{l\in\bigwedge_{m,uk},l\neq m} \pi_{ml}(h)\mathcal{P}_{il} \\ &= \sum_{l\in\bigwedge_{m,k}} \pi_{ml}(h)\mathcal{P}_{il} + \pi_{mm}(h)\mathcal{P}_{im} - (\pi_{mm}(h) + \lambda_k) \sum_{l\in\bigwedge_{m,uk},l\neq m} \frac{\pi_{ml}(h)}{-\pi_{mm}(h) - \lambda_k}\mathcal{P}_{il}.\end{aligned} \tag{27}$$

It is obvious that $0 \leq \frac{\pi_{ml}(h)}{-\pi_{mm}(h)-\lambda_k} \leq 1 (l \in \bigwedge_{m,uk})$ and $\sum_{l\in\bigwedge_{m,uk}} \frac{\pi_{ml}(h)}{-\pi_{mm}(h)-\lambda_k} = 1$. So for $\forall j \in \bigwedge_{m,uk}, j \neq m$, there is

$$\sum_{l=1}^{s} \pi_{ml}(h)\mathcal{P}_{il} = \sum_{l\in\bigwedge_{m,uk},l\neq m} \frac{\pi_{ml}(h)}{-\pi_{mm}(h) - \lambda_k} (\sum_{l\in\bigwedge_{m,k}} \pi_{ml}(h)(\mathcal{P}_{il} - \mathcal{P}_{ij}) + \pi_{mm}(h)(\mathcal{P}_{il} - \mathcal{P}_{ij})). \tag{28}$$

By applying Schur complement and $\pi_{mm}(h) = -\sum_{l=1,l\neq m}^{s} \pi_{ml}(h)$, it is deduced that (16), (17) are equivalent to $\Pi_{im} < 0$ and (18) is equivalent to $-\mathcal{Q}_i + \sum_{l=1}^{s} \pi_{ml}(h)\mathcal{Q}_{il} < 0$.

Case 3. If $\bigwedge_{m,k} = \emptyset$ and $\bigwedge_{m,uk} \neq \emptyset$, $m \in \bigwedge_{m,uk}$, assume there exists $l \neq m$ and $l \in \bigwedge_{m,uk}$. Denote $\lambda_k = \pi_{mm}(h) = a_m\pi_{ll}(h)$. Noting that $\lambda_k < 0$, $\sum_{l=1}^{s} \pi_{ml}(h)\mathcal{P}_{il}$ can be presented as

$$\sum_{l=1}^{s} \pi_{ml}(h)\mathcal{P}_{il} = \pi_{mm}(h)\mathcal{P}_{im} + \sum_{l\in\bigwedge_{m,uk},l\neq m} \pi_{ml}(h)\mathcal{P}_{il} = \pi_{mm}(h)\mathcal{P}_{im} - \lambda_k \sum_{l\in\bigwedge_{m,uk},l\neq m} \frac{\pi_{ml}(h)}{-\lambda_k}\mathcal{P}_{il}. \tag{29}$$

It is obvious that $\sum_{l\in\bigwedge_{m,uk},l\neq m} \pi_{ml}(h) = -\pi_{mm}(h) = -\lambda_k > 0$. So for $\forall j \in \bigwedge_{m,uk}, j \neq m$, there is

$$\sum_{l=1}^{s} \pi_{ml}(h)\mathcal{P}_{il} = \sum_{l\in\bigwedge_{m,uk},l\neq m} \frac{\pi_{ml}(h)}{-\lambda_k}[\pi_{mm}(h)(\mathcal{P}_{im} - \mathcal{P}_{ij})] = \pi_{mm}(h)(\mathcal{P}_{im} - \mathcal{P}_{ij}) = a_m\pi_{ll}(h)(\mathcal{P}_{im} - \mathcal{P}_{ij}). \tag{30}$$

By applying Schur complement and $\pi_{mm}(h) = -\sum_{l=1,l\neq m}^{s} \pi_{ml}(h)$, we konw that (19) is equivalent to $\Pi_{im} < 0$.

In summary, if inequalities (14) – (19) hold, the interconnected semi-Markovian control system (10) with partially accessible TRs and dynamic METM is stochastically stable.

Remark 3. Theorem 1 designed sufficient conditions to ensure (10) is stochastically stable. However, it is difficult to directly use this result to acquire the controller gain matrices. Theorem 2 gives a LMI-based sufficient criterion for the solvability.

Theorem 2. For given a positive real number $\tau_M > 0$, $\alpha_i > 0$, $\gamma > 0$, $\varepsilon_0 > 0$, $\varepsilon_{ij} > 0$ ($j = 1, 2, 3, \cdots, M + 3$), $\mu_i \in (0, 1)$ and $\pi_{ml}(h) \in [\underline{\pi}_{ml}, \overline{\pi}_{ml}]$, the system (10) with partially accessible TRs and dynamic METM is stochastically stable if there are positive symmetric matrices $X_{im} > 0$, $Y_{im}^{q} > 0$, $\overline{\mathcal{Q}}_{im} > 0$, $\overline{\mathcal{Q}}_i > 0$,$\overline{\mathcal{R}}_i > 0$, $\overline{\Omega}_i > 0$, and matrices K_{im}^{q}, $\overline{\mathcal{S}}_{1i}$, $\overline{\mathcal{S}}_{2i}$, $\overline{\mathcal{S}}_{3i}$ and $\overline{\mathcal{S}}_{4i}$ with proper dimensions, such that the linear matrix inequalities hold:

Case 1. If $\bigwedge_{m,k} \neq \emptyset$ and $\bigwedge_{m,uk} \neq \emptyset$, $m \in \bigwedge_{m,k}$, for $\forall j \in \bigwedge_{m,uk}$, we have

$$\begin{bmatrix} \overline{\Xi}_{im,\overline{m}} & * & * & * & * & * & \cdots & * & * & * \\ \overline{\Gamma}_{im}^{11} & \overline{\Gamma}_{im}^{12} & * & * & * & * & \cdots & * & * & * \\ \overline{\Gamma}_{im}^{21} & 0 & \Phi(\overline{\mathcal{R}}_i) & * & * & * & \cdots & * & * & * \\ \overline{\Gamma}_{im}^{31} & 0 & 0 & \varepsilon_{i2}\Phi(\overline{\mathcal{R}}_i) & * & * & \cdots & * & * & * \\ \overline{\Gamma}_{im}^{41} & 0 & 0 & 0 & \varepsilon_{i3}\Phi(\overline{\mathcal{R}}_i) & * & \cdots & * & * & * \\ \overline{\Gamma}_{im}^{51} & 0 & 0 & 0 & 0 & \varepsilon_{i4}\Phi(\overline{\mathcal{R}}_i) & \cdots & * & * & * \\ \vdots & \vdots & \vdots & \vdots & \vdots & \vdots & \ddots & \vdots & \vdots & \vdots \\ \overline{\Gamma}_{im}^{61} & 0 & 0 & 0 & 0 & 0 & \cdots & \varepsilon_{i,M+3}\Phi(\overline{\mathcal{R}}_i) & * & * \\ \overline{\Gamma}_{im}^{71} & 0 & 0 & 0 & 0 & 0 & \cdots & 0 & -\breve{\overline{\mathcal{R}}}_i & * \\ \overline{\Gamma}_{im}^{81} & 0 & 0 & 0 & 0 & 0 & \cdots & 0 & 0 & -\hat{\overline{\mathcal{R}}}_i \end{bmatrix} < 0, \tag{31}$$

$$\begin{bmatrix} \overline{\Xi}_{im,\underline{m}} & * & * & * & * & * & \cdots & * & * & * \\ \overline{\Gamma}_{im}^{11} & \overline{\Gamma}_{im}^{12} & * & * & * & * & \cdots & * & * & * \\ \overline{\Gamma}_{im}^{21} & 0 & \Phi(\overline{\mathcal{R}}_i) & * & * & * & \cdots & * & * & * \\ \overline{\Gamma}_{im}^{31} & 0 & 0 & \varepsilon_{i2}\Phi(\overline{\mathcal{R}}_i) & * & * & \cdots & * & * & * \\ \overline{\Gamma}_{im}^{41} & 0 & 0 & 0 & \varepsilon_{i3}\Phi(\overline{\mathcal{R}}_i) & * & \cdots & * & * & * \\ \overline{\Gamma}_{im}^{51} & 0 & 0 & 0 & 0 & \varepsilon_{i4}\Phi(\overline{\mathcal{R}}_i) & \cdots & * & * & * \\ \vdots & \vdots & \vdots & \vdots & \vdots & \vdots & \ddots & \vdots & \vdots & \vdots \\ \overline{\Gamma}_{im}^{61} & 0 & 0 & 0 & 0 & 0 & \cdots & \varepsilon_{i,M+3}\Phi(\overline{\mathcal{R}}_i) & * & * \\ \overline{\Gamma}_{im}^{71} & 0 & 0 & 0 & 0 & 0 & \cdots & 0 & -\breve{\overline{\mathcal{R}}}_i & * \\ \overline{\Gamma}_{im}^{81} & 0 & 0 & 0 & 0 & 0 & \cdots & 0 & 0 & -\hat{\overline{\mathcal{R}}}_i \end{bmatrix} < 0, \tag{32}$$

$$-\overline{Q}_i + \textstyle\sum_{l \in \bigwedge_{m,k}} \overline{\pi}_{ml}(h)(\overline{Q}_{il} - \overline{Q}_{ij}) < 0, \tag{33}$$

$$-\overline{Q}_i + \textstyle\sum_{l \in \bigwedge_{m,k}} \underline{\pi} ml(h)(\overline{Q}_{il} - \overline{Q}_{ij}) < 0, \tag{34}$$

where

$$\overline{\Xi}_{im,\overline{m}} = \begin{bmatrix} \overline{\Xi}_{im,\overline{m}}^{11} & * & * & * & * & * & * & \cdots & * \\ 0 & \overline{\Xi}_{im,\overline{m}}^{22} & * & * & * & * & * & \cdots & * \\ \overline{\Xi}_{im}^{31} & 0 & \overline{\Xi}_{im}^{33} & * & * & * & * & \cdots & * \\ \overline{\Xi}_{im}^{41} & 0 & \overline{\Xi}_{im}^{43} & \overline{\Xi}_{im}^{44} & * & * & * & \cdots & * \\ \overline{\Xi}_{im}^{51} & 0 & \overline{\Xi}_{im}^{53} & \overline{\Xi}_{im}^{54} & \overline{\Xi}_{im}^{55} & * & * & \cdots & * \\ \overline{\Xi}_{im}^{61} & 0 & \overline{\Xi}_{im}^{63} & -\overline{\mathcal{S}}_{4i} & \overline{\mathcal{S}}_{4i} & \overline{\Xi}_{im}^{66} & * & \cdots & * \\ \overline{\Xi}_{im}^{71} & 0 & 0 & 0 & 0 & 0 & \overline{\Xi}_{im}^{77} & \cdots & * \\ \vdots & \vdots & \vdots & \vdots & \vdots & \vdots & \vdots & \ddots & \vdots \\ \overline{\Xi}_{im}^{M+6,1} & 0 & 0 & 0 & 0 & 0 & 0 & \cdots & \overline{\Xi}_{im}^{M+6,M+6} \end{bmatrix},$$

$$\underline{\overline{\Xi}}_{im,\underline{m}} = \begin{bmatrix} \underline{\overline{\Xi}}_{im,\underline{m}}^{11} & * & * & * & * & * & * & \cdots & * \\ 0 & \underline{\overline{\Xi}}_{im,\underline{m}}^{22} & * & * & * & * & * & \cdots & * \\ \underline{\overline{\Xi}}_{im}^{31} & 0 & \underline{\overline{\Xi}}_{im}^{33} & * & * & * & * & \cdots & * \\ \underline{\overline{\Xi}}_{im}^{41} & 0 & \underline{\overline{\Xi}}_{im}^{43} & \underline{\overline{\Xi}}_{im}^{44} & * & * & * & \cdots & * \\ \underline{\overline{\Xi}}_{im}^{51} & 0 & \underline{\overline{\Xi}}_{im}^{53} & \underline{\overline{\Xi}}_{im}^{54} & \underline{\overline{\Xi}}_{im}^{55} & * & * & \cdots & * \\ \underline{\overline{\Xi}}_{im}^{61} & 0 & \underline{\overline{\Xi}}_{im}^{63} & -\overline{\mathcal{S}}_{4i} & \overline{\mathcal{S}}_{4i} & \underline{\overline{\Xi}}_{im}^{66} & * & \cdots & * \\ \underline{\overline{\Xi}}_{im}^{71} & 0 & 0 & 0 & 0 & 0 & \underline{\overline{\Xi}}_{im}^{77} & \cdots & * \\ \vdots & \vdots & \vdots & \vdots & \vdots & \vdots & \vdots & \ddots & \vdots \\ \underline{\overline{\Xi}}_{im}^{M+6,1} & 0 & 0 & 0 & 0 & 0 & 0 & \cdots & \underline{\overline{\Xi}}_{im}^{M+6,M+6} \end{bmatrix},$$

$$\overline{\underline{\Xi}}_{im,\overline{m}}^{11} = sym\{\mathcal{A}_{im}X_{im}\} + \overline{\mathcal{Q}}_{im} + \tau_M\overline{\mathcal{Q}}_i - 4(1+\mu_i)\overline{\mathcal{R}}_i + \sum_{l\in\wedge_{m,k}} \overline{\pi}_{ml}(h)(X_{il} - X_{ij}),$$

$$\overline{\underline{\Xi}}_{im,\overline{m}}^{22} = sym\{\mathcal{A}_{im}X_{im}\} + \sum_{l\in\wedge_{m,k}} \overline{\pi}_{ml}(h)(X_{il} - X_{ij}),$$

$$\overline{\underline{\Xi}}_{im,\underline{m}}^{11} = sym\{\mathcal{A}_{im}X_{im}\} + \overline{\mathcal{Q}}_{im} + \tau_M\overline{\mathcal{Q}}_i - 4(1+\mu_i)\overline{\mathcal{R}}_i + \sum_{l\in\wedge_{m,k}} \underline{\pi}_{ml}(h)(X_{il} - X_{ij}),$$

$$\overline{\underline{\Xi}}_{im,\underline{m}}^{22} = sym\{\mathcal{A}_{im}X_{im}\} + \sum_{l\in\wedge_{m,k}} \underline{\pi}_{ml}(h)(X_{il} - X_{ij}).$$

Case 2. If $\wedge_{m,k} \neq \emptyset$ and $\wedge_{m,uk} \neq \emptyset$, $m \in \wedge_{m,uk}$, for$\forall j \in \wedge_{m,uk}$, we have

$$\begin{bmatrix} \ddot{\overline{\Xi}}_{im,\overline{m}} & * & * & * & * & * & \cdots & * & * & * \\ \overline{\Gamma}_{im}^{11} & \overline{\Gamma}_{im}^{12} & * & * & * & * & \cdots & * & * & * \\ \overline{\Gamma}_{im}^{21} & 0 & \Phi(\overline{\mathcal{R}}_i) & * & * & * & \cdots & * & * & * \\ \overline{\Gamma}_{im}^{31} & 0 & 0 & \varepsilon_{i2}\Phi(\overline{\mathcal{R}}_i) & * & * & \cdots & * & * & * \\ \overline{\Gamma}_{im}^{41} & 0 & 0 & 0 & \varepsilon_{i3}\Phi(\overline{\mathcal{R}}_i) & * & \cdots & * & * & * \\ \overline{\Gamma}_{im}^{51} & 0 & 0 & 0 & 0 & \varepsilon_{i4}\Phi(\overline{\mathcal{R}}_i) & \cdots & * & * & * \\ \vdots & \vdots & \vdots & \vdots & \vdots & \vdots & \ddots & \vdots & \vdots & \vdots \\ \overline{\Gamma}_{im}^{61} & 0 & 0 & 0 & 0 & 0 & \cdots & \varepsilon_{i,M+3}\Phi(\overline{\mathcal{R}}_i) & * & * \\ \overline{\Gamma}_{im}^{71} & 0 & 0 & 0 & 0 & 0 & \cdots & 0 & -\check{\overline{\mathcal{R}}}_i & * \\ \overline{\Gamma}_{im}^{81} & 0 & 0 & 0 & 0 & 0 & \cdots & 0 & 0 & -\hat{\overline{\mathcal{R}}}_i \end{bmatrix} < 0, \quad (35)$$

$$\begin{bmatrix} \ddot{\underline{\Xi}}_{im,\underline{m}} & * & * & * & * & * & \cdots & * & * & * \\ \overline{\Gamma}_{im}^{11} & \overline{\Gamma}_{im}^{12} & * & * & * & * & \cdots & * & * & * \\ \overline{\Gamma}_{im}^{21} & 0 & \Phi(\overline{\mathcal{R}}_i) & * & * & * & \cdots & * & * & * \\ \overline{\Gamma}_{im}^{31} & 0 & 0 & \varepsilon_{i2}\Phi(\overline{\mathcal{R}}_i) & * & * & \cdots & * & * & * \\ \overline{\Gamma}_{im}^{41} & 0 & 0 & 0 & \varepsilon_{i3}\Phi(\overline{\mathcal{R}}_i) & * & \cdots & * & * & * \\ \overline{\Gamma}_{im}^{51} & 0 & 0 & 0 & 0 & \varepsilon_{i4}\Phi(\overline{\mathcal{R}}_i) & \cdots & * & * & * \\ \vdots & \vdots & \vdots & \vdots & \vdots & \vdots & \ddots & \vdots & \vdots & \vdots \\ \overline{\Gamma}_{im}^{61} & 0 & 0 & 0 & 0 & 0 & \cdots & \varepsilon_{i,M+3}\Phi(\overline{\mathcal{R}}_i) & * & * \\ \overline{\Gamma}_{im}^{71} & 0 & 0 & 0 & 0 & 0 & \cdots & 0 & -\check{\overline{\mathcal{R}}}_i & * \\ \overline{\Gamma}_{im}^{81} & 0 & 0 & 0 & 0 & 0 & \cdots & 0 & 0 & -\hat{\overline{\mathcal{R}}}_i \end{bmatrix} < 0, \quad (36)$$

$$X_{im} - X_{ij} \geq 0, \overline{Q}_{im} - \overline{Q}_{ij} \geq 0, \tag{37}$$

$$-\overline{Q}_i + \sum_{l \in \wedge_{m,k}} \overline{\pi}_{ml}(h)(\overline{Q}_{il} - \overline{Q}_{ij}) < 0, \tag{38}$$

$$-\overline{Q}_i + \sum_{l \in \wedge_{m,k}} \underline{\pi}_{ml}(h)(\overline{Q}_{il} - \overline{Q}_{ij}) < 0, \tag{39}$$

where

$$\ddot{\Xi}_{im,\overline{m}} = \begin{bmatrix} \ddot{\Xi}^{11}_{im,\overline{m}} & * & * & * & * & * & * & \cdots & * \\ 0 & \ddot{\Xi}^{22}_{im,\overline{m}} & * & * & * & * & * & \cdots & * \\ \overline{\Xi}^{31}_{im} & 0 & \overline{\Xi}^{33}_{im} & * & * & * & * & \cdots & * \\ \overline{\Xi}^{41}_{im} & 0 & \overline{\Xi}^{43}_{im} & \overline{\Xi}^{44}_{im} & * & * & * & \cdots & * \\ \overline{\Xi}^{51}_{im} & 0 & \overline{\Xi}^{53}_{im} & \overline{\Xi}^{54}_{im} & \overline{\Xi}^{55}_{im} & * & * & \cdots & * \\ \overline{\Xi}^{61}_{im} & 0 & \overline{\Xi}^{63}_{im} & -\overline{\mathcal{S}}_{4i} & \overline{\mathcal{S}}_{4i} & \overline{\Xi}^{66}_{im} & * & \cdots & * \\ \overline{\Xi}^{71}_{im} & 0 & 0 & 0 & 0 & 0 & \overline{\Xi}^{77}_{im} & \cdots & * \\ \vdots & \vdots & \vdots & \vdots & \vdots & \vdots & \vdots & \ddots & \vdots \\ \overline{\Xi}^{M+6,1}_{im} & 0 & 0 & 0 & 0 & 0 & 0 & \cdots & \overline{\Xi}^{M+6,M+6}_{im} \end{bmatrix},$$

$$\ddot{\Xi}_{im,\underline{m}} = \begin{bmatrix} \ddot{\Xi}^{11}_{im,\underline{m}} & * & * & * & * & * & * & \cdots & * \\ 0 & \ddot{\Xi}^{22}_{im,\underline{m}} & * & * & * & * & * & \cdots & * \\ \overline{\Xi}^{31}_{im} & 0 & \overline{\Xi}^{33}_{im} & * & * & * & * & \cdots & * \\ \overline{\Xi}^{41}_{im} & 0 & \overline{\Xi}^{43}_{im} & \overline{\Xi}^{44}_{im} & * & * & * & \cdots & * \\ \overline{\Xi}^{51}_{im} & 0 & \overline{\Xi}^{53}_{im} & \overline{\Xi}^{54}_{im} & \overline{\Xi}^{55}_{im} & * & * & \cdots & * \\ \overline{\Xi}^{61}_{im} & 0 & \overline{\Xi}^{63}_{im} & -\overline{\mathcal{S}}_{4i} & \overline{\mathcal{S}}_{4i} & \overline{\Xi}^{66}_{im} & * & \cdots & * \\ \overline{\Xi}^{71}_{im} & 0 & 0 & 0 & 0 & 0 & \overline{\Xi}^{77}_{im} & \cdots & * \\ \vdots & \vdots & \vdots & \vdots & \vdots & \vdots & \vdots & \ddots & \vdots \\ \overline{\Xi}^{M+6,1}_{im} & 0 & 0 & 0 & 0 & 0 & 0 & \cdots & \overline{\Xi}^{M+6,M+6}_{im} \end{bmatrix},$$

$$\ddot{\Xi}^{11}_{im,\overline{m}} = sym\{\mathcal{A}_{im}X_{im}\} + \overline{Q}_{im} + \tau_M\overline{Q}_i - 4(1+\mu_i)\overline{\mathcal{R}}_i + \sum_{l \in \wedge_{m,k}} \overline{\pi}_{ml}(h)(X_{il} - X_{ij}) + \overline{\pi}_{mm}(h)(X_{im} - X_{ij}),$$

$$\ddot{\Xi}^{22}_{im,\overline{m}} = sym\{\mathcal{A}_{im}X_{im}\} + \sum_{l \in \wedge_{m,k}} \overline{\pi}_{ml}(h)(X_{il} - X_{ij}) + \overline{\pi}_{mm}(h)(X_{im} - X_{ij}),$$

$$\ddot{\Xi}^{11}_{im,\underline{m}} = sym\{\mathcal{A}_{im}X_{im}\} + \overline{Q}_{im} + \tau_M\overline{Q}_i - 4(1+\mu_i)\overline{\mathcal{R}}_i + \sum_{l \in \wedge_{m,k}} \underline{\pi}_{ml}(h)(X_{il} - X_{ij}) + \underline{\pi}_{mm}(h)(X_{im} - X_{ij}),$$

$$\ddot{\Xi}^{22}_{im,\underline{m}} = sym\{\mathcal{A}_{im}X_{im}\} + \sum_{l \in \wedge_{m,k}} \underline{\pi}_{ml}(h)(X_{il} - X_{ij}) + \underline{\pi}_{mm}(h)(X_{im} - X_{ij}).$$

Case 3. If $\bigwedge_{m,k} = \emptyset$, $\bigwedge_{m,uk} \neq \emptyset$, $m \in \bigwedge_{m,uk}$, and there exist $l \neq m$ and $l \in \bigwedge_{m,uk}$, we have

$$\begin{bmatrix} \breve{\Xi}_{im,m} & * & * & * & * & * & \cdots & * & * & * \\ \overline{\Gamma}_{im}^{11} & \overline{\Gamma}_{im}^{12} & * & * & * & * & \cdots & * & * & * \\ \overline{\Gamma}_{im}^{21} & 0 & \Phi(\overline{\mathcal{R}}_i) & * & * & * & \cdots & * & * & * \\ \overline{\Gamma}_{im}^{31} & 0 & 0 & \varepsilon_{i2}\Phi(\overline{\mathcal{R}}_i) & * & * & \cdots & * & * & * \\ \overline{\Gamma}_{im}^{41} & 0 & 0 & 0 & \varepsilon_{i3}\Phi(\overline{\mathcal{R}}_i) & * & \cdots & * & * & * \\ \overline{\Gamma}_{im}^{51} & 0 & 0 & 0 & 0 & \varepsilon_{i4}\Phi(\overline{\mathcal{R}}_i) & \cdots & * & * & * \\ \vdots & \vdots & \vdots & \vdots & \vdots & \vdots & \ddots & \vdots & \vdots & \vdots \\ \overline{\Gamma}_{im}^{61} & 0 & 0 & 0 & 0 & 0 & \cdots & \varepsilon_{i,M+3}\Phi(\overline{\mathcal{R}}_i) & * & * \\ \overline{\Gamma}_{im}^{71} & 0 & 0 & 0 & 0 & 0 & \cdots & 0 & -\breve{\overline{\mathcal{R}}}_i & * \\ \overline{\Gamma}_{im}^{81} & 0 & 0 & 0 & 0 & 0 & \cdots & 0 & 0 & -\hat{\overline{\mathcal{R}}}_i \end{bmatrix} < 0, \tag{40}$$

where

$$\breve{\Xi}_{im,m} = \begin{bmatrix} \breve{\Xi}_{im,m}^{11} & * & * & * & * & * & * & \cdots & * \\ 0 & \breve{\Xi}_{im,m}^{22} & * & * & * & * & * & \cdots & * \\ \overline{\Xi}_{im}^{31} & 0 & \overline{\Xi}_{im}^{33} & * & * & * & * & \cdots & * \\ \overline{\Xi}_{im}^{41} & 0 & \overline{\Xi}_{im}^{43} & \overline{\Xi}_{im}^{44} & * & * & * & \cdots & * \\ \overline{\Xi}_{im}^{51} & 0 & \overline{\Xi}_{im}^{53} & \overline{\Xi}_{im}^{54} & \overline{\Xi}_{im}^{55} & * & * & \cdots & * \\ \overline{\Xi}_{im}^{61} & 0 & \overline{\Xi}_{im}^{63} & -\overline{\mathcal{S}}_{4i} & \overline{\mathcal{S}}_{4i} & \overline{\Xi}_{im}^{66} & * & \cdots & * \\ \overline{\Xi}_{im}^{71} & 0 & 0 & 0 & 0 & 0 & \overline{\Xi}_{im}^{77} & \cdots & * \\ \vdots & \vdots & \vdots & \vdots & \vdots & \vdots & \vdots & \ddots & \vdots \\ \overline{\Xi}_{im}^{M+6,1} & 0 & 0 & 0 & 0 & 0 & 0 & \cdots & \overline{\Xi}_{im}^{M+6,M+6} \end{bmatrix},$$

$$\begin{aligned} \breve{\Xi}_{im,m}^{11} &= sym\{\mathcal{A}_{im}X_{im}\} + \overline{\mathcal{Q}}_{im} + \tau_M\overline{\mathcal{Q}}_i - 4(1+\mu_i)\overline{\mathcal{R}}_i + a_m\pi_{ll}(h)(X_{im} - X_{ij}), \\ \breve{\Xi}_{im,m}^{22} &= sym\{\mathcal{A}_{im}X_{im}\} + a_m\pi_{ll}(h)(X_{im} - X_{ij}). \end{aligned}$$

In addition, the other scalars are given as follows

$$\begin{aligned}
&\overline{\Xi}_{im}^{31} = \sum_{q=1}^{M}(Y_{im}^{q})^{\mathrm{T}}\mathcal{B}_{im}^{\mathrm{T}} - 2(1+\mu_i)\overline{\mathcal{R}}_i - \overline{\mathcal{S}}_{1i} - \overline{\mathcal{S}}_{2i} - \overline{\mathcal{S}}_{3i} - \overline{\mathcal{S}}_{4i},\\
&\overline{\Xi}_{im}^{33} = -2(4+\mu_i)\overline{\mathcal{R}}_i + 2\overline{\mathcal{S}}_{1i} - 2\overline{\mathcal{S}}_{2i} + 2\overline{\mathcal{S}}_{3i} - 2\overline{\mathcal{S}}_{4i}, \overline{\Xi}_{im}^{41} = \overline{\mathcal{S}}_{1i} + \overline{\mathcal{S}}_{2i} - \overline{\mathcal{S}}_{3i} - \overline{\mathcal{S}}_{4i},\\
&\overline{\Xi}_{im}^{43} = -2(2-\mu_i)\overline{\mathcal{R}}_i - \overline{\mathcal{S}}_{1i} + \overline{\mathcal{S}}_{2i} + \overline{\mathcal{S}}_{3i} - \overline{\mathcal{S}}_{4i}, \overline{\Xi}_{im}^{44} = -\overline{\mathcal{Q}}_{im} - 4(2-\mu_i)\overline{\mathcal{R}}_i,\\
&\overline{\Xi}_{im}^{51} = \overline{\mathcal{S}}_{3i} + \overline{\mathcal{S}}_{4i}, \tilde{\Xi}_{im}^{53} = -\overline{\mathcal{S}}_{3i} + \overline{\mathcal{S}}_{4i} + 3(2-\mu_i)\overline{\mathcal{R}}_i, \overline{\Xi}_{im}^{54} = 3(2-\mu_i)\overline{\mathcal{R}}_i, \overline{\Xi}_{im}^{55} = -3(2-\mu_i)\overline{\mathcal{R}}_i,\\
&\overline{\Xi}_{im}^{61} = 3(1+\mu_i)\overline{\mathcal{R}}_i, \overline{\Xi}_{im}^{62} = \overline{\mathcal{S}}_{2i} + 3(1+\mu_i)\overline{\mathcal{R}}_i, \overline{\Xi}_{im}^{66} = -3(1+\mu_i)\overline{\mathcal{R}}_i,\\
&\overline{\Xi}_{im}^{71} = Y_{im}^{1\ \mathrm{T}}\mathcal{B}_{im}^{\mathrm{T}}, \overline{\Xi}_{im}^{77} = -\theta_0\gamma_1\overline{\Omega}_i, \overline{\Xi}_{im}^{M+6,1} = Y_{im}^{M\mathrm{T}}\mathcal{B}_{im}^{\mathrm{T}}, \overline{\Xi}_{im}^{M+6,M+6} = -\theta_0\gamma_M\overline{\Omega}_i,\\
&\overline{\Gamma}_{im}^{11} = \begin{bmatrix} X_{im}\mathcal{G}_{ijm}^{\mathrm{T}} & 0 & 0 & 0 & 0 & 0 & 0 & \cdots & 0 \end{bmatrix},\\
&\overline{\Gamma}_{im}^{12} = -(N-1)^{-1}diag\{\varepsilon_{i1}^{-1}X_{im}, \cdots, \varepsilon_{j1}^{-1}X_{im,j\neq i}, \cdots, \varepsilon_{N1}^{-1}X_{im}\},\\
&\overline{\Gamma}^{21} = \tau_M \begin{bmatrix} \mathcal{A}_{im}X_{im} & 0 & \mathcal{B}_{im}\sum_{q=1}^{M}Y_{im}^{q} & 0 & 0 & 0 & \mathcal{B}_{im}Y_{im}^{1} & \cdots & \mathcal{B}_{im}Y_{im}^{M} \end{bmatrix},\\
&\overline{\Gamma}_{im}^{31} = \tau_M \begin{bmatrix} \mathcal{A}_{im}X_{im} & 0 & 0 & 0 & 0 & 0 & 0 & \cdots & 0 \end{bmatrix},\\
&\overline{\Gamma}_{im}^{41} = \tau_M \begin{bmatrix} 0 & 0 & \mathcal{B}_{im}\sum_{q=1}^{M}Y_{im}^{q} & 0 & 0 & 0 & 0 & \cdots & 0 \end{bmatrix},\\
&\overline{\Gamma}_{im}^{51} = \tau_M \begin{bmatrix} 0 & 0 & 0 & 0 & 0 & 0 & \mathcal{B}_{im}Y_{im}^{1} & \cdots & 0 \end{bmatrix},\\
&\overline{\Gamma}_{im}^{61} = \tau_M \begin{bmatrix} 0 & 0 & 0 & 0 & 0 & 0 & 0 & \cdots & \mathcal{B}_{im}Y_{im}^{M} \end{bmatrix},\\
&\overline{\Gamma}_{im}^{71} = \tau_M \begin{bmatrix} \mathcal{G}_{ijm}X_{im} & 0 & 0 & 0 & 0 & 0 & 0 & \cdots & 0 \end{bmatrix},
\end{aligned}$$

$$\begin{aligned}
&\breve{\overline{\mathcal{R}}}_i = -(N-1)^{-1}diag\{(1+\varepsilon_{i2}+\varepsilon_{i3}+\cdots+\varepsilon_{i,M+3})^{-1}\Phi(\overline{\mathcal{R}}_1), \cdots, (1+\varepsilon_{j2}+\varepsilon_{j3}+\cdots+\varepsilon_{j,M+3})^{-1}\Phi(\overline{\mathcal{R}}_j), j\neq i,\\
&\cdots, (1+\varepsilon_{N2}+\varepsilon_{N3}+\cdots+\varepsilon_{N,M+3})^{-1}\Phi(\overline{\mathcal{R}}_N)\},\\
&\Phi(\overline{\mathcal{R}}_l) = -2\alpha_i X_{im} + \alpha_i^2\overline{\mathcal{R}}_l, l = \{1, \cdots, j(j\neq i), \cdots, N\},\\
&\overline{\Gamma}_{im}^{81} = \begin{bmatrix} 0 & 0 & \overline{\mathcal{S}}_{1i}+\overline{\mathcal{S}}_{3i} & -\overline{\mathcal{S}}_{1i}+\overline{\mathcal{S}}_{3i} & -\overline{\mathcal{S}}_{3i} & 0 & 0 & \cdots & 0\\ 0 & 0 & \overline{\mathcal{S}}_{2i}+\overline{\mathcal{S}}_{4i} & -\overline{\mathcal{S}}_{2i}+\overline{\mathcal{S}}_{4i} & -\overline{\mathcal{S}}_{4i} & 0 & 0 & \cdots & 0\\ \overline{\mathcal{S}}_{1i}+\overline{\mathcal{S}}_{3i} & 0 & -\overline{\mathcal{S}}_{1i}+\overline{\mathcal{S}}_{3i} & 0 & 0 & -\overline{\mathcal{S}}_{3i} & 0 & \cdots & 0\\ \overline{\mathcal{S}}_{2i}+\overline{\mathcal{S}}_{4i} & 0 & -\overline{\mathcal{S}}_{2i}+\overline{\mathcal{S}}_{4i} & 0 & 0 & -\overline{\mathcal{S}}_{4i} & 0 & \cdots & 0 \end{bmatrix},\\
&\hat{\overline{\mathcal{R}}}_i = diag\{-(1-\mu_i)^{-1}\overline{\mathcal{R}}_i, -3(1-\mu_i)^{-1}\overline{\mathcal{R}}_i, -\mu_i^{-1}\overline{\mathcal{R}}_i, -3\mu_i^{-1}\overline{\mathcal{R}}_i\}.
\end{aligned}$$

Furthermore, the memory controller gain matrix is $K_{im}^{q} = Y_{im}^{q}X_{im}^{-1}$.

Proof: Define $X_{im} = \mathcal{P}_{im}^{-1}$, then pre-multiplying and post-multiplying (15),(17),(20) with $diag\{X_{im}, \cdots, X_{im}, \mathcal{R}_i^{-1}$ $\mathcal{R}_i^{-1}, \mathcal{R}_i^{-1}, \mathcal{R}_i^{-1}, \mathcal{R}_i^{-1}, \mathcal{R}_i^{-1}, X_{im}, X_{im}, X_{im}, X_{im}\}$ respectively, and define $Y_{im} = K_{im}X_{im}, \overline{\mathcal{R}}_{im} = X_{im}\mathcal{R}_{im}X_{im}, \overline{\mathcal{Q}}_{im} = X_{im}\mathcal{Q}_{im}X_{im}, \overline{\mathcal{S}}_{1i} = X_{im}\mathcal{S}_{1i}X_{im}, \overline{\mathcal{S}}_{2i} = X_{im}\mathcal{S}_{2i}X_{im}, \overline{\mathcal{S}}_{3i} = X_{im}\mathcal{S}_{3i}X_{im}, \overline{\mathcal{S}}_{4i} = X_{im}\mathcal{S}_{4i}X_{im}, \overline{\mathcal{Q}}_i = X_{im}\mathcal{Q}_iX_{im}, \overline{\Omega}_i = X_{im}\Omega_iX_{im}$. According to Schur complement and Lemma 2, and considering $\pi_{ml}(h) \in [\underline{\pi}_{ml}(h), \overline{\pi}_{ml}(h)]$, (31), (32), (35), (36), (40) can be obtained. This completes the proof.

Remark 4. For a given dwell time h, the TR $\pi_{ml}(h)$ can be regarded as a linear combination of its upper and lower bounds, namely $\pi_{ml}(h) = \beta_1\overline{\pi}_{ml}(h) + \beta_2\underline{\pi}_{ml}(h)$, where $\beta_1 + \beta_2 = 1$ and $\beta_1 > 0, \beta_2 > 0$. We can change β_1 and β_2 to get the corresponding value of $\pi_{ml}(h)$.

Remark 5. Theorem 2 presents a solution algorithm in terms of linear matrix inequality to obtain the controller gains. However, the transition probability in Case 3 is completely unknown. We introduce $a_m\pi_{ll}(h)$ to

replace the unknown $\pi_{mm}(h)$, in which a_m is a parameter to be estimated. If this case exists, we can obtain the estimation value of parameter a_m by employing the optimization algorithm in [24].

4. SIMULATION EXAMPLE

This section will give an example to verify the feasibility of the above theoretical results. We consider a semi-Markovian interconnected system composed of three subsystems, and the relevant parameters are as follows[23]:

$$\mathcal{A}_{11} = \begin{bmatrix} 0 & 5 \\ -9.81 & -1 \end{bmatrix}, \mathcal{A}_{12} = \begin{bmatrix} 0 & 5 \\ -0.31 & -1 \end{bmatrix}, \mathcal{A}_{21} = \begin{bmatrix} 0 & 5 \\ -9.81 & -1.4 \end{bmatrix}, \mathcal{A}_{22} = \begin{bmatrix} 0 & 5 \\ -0.31 & -1.4 \end{bmatrix},$$
$$\mathcal{A}_{31} = \begin{bmatrix} 0 & 5 \\ -9.81 & -0.5 \end{bmatrix}, \mathcal{A}_{32} = \begin{bmatrix} 0 & 5 \\ -0.31 & -0.5 \end{bmatrix}, \mathcal{B}_{11} = \mathcal{B}_{12} = \begin{bmatrix} 0 \\ 0.5 \end{bmatrix}, \mathcal{B}_{21} = \mathcal{B}_{22} = \begin{bmatrix} 0 \\ 0.4 \end{bmatrix},$$
$$\mathcal{B}_{31} = \mathcal{B}_{32} = \begin{bmatrix} 0 \\ 0.33 \end{bmatrix}, \mathcal{G}_{121} = \begin{bmatrix} 0 & 0 \\ 1 & 0 \end{bmatrix}, \mathcal{G}_{122} = \begin{bmatrix} 0 & 0 \\ 1 & 0 \end{bmatrix}, \mathcal{G}_{211} = \begin{bmatrix} 0 & 0 \\ 0.8 & 0 \end{bmatrix}, \mathcal{G}_{212} = \begin{bmatrix} 0 & 0 \\ 0.8 & 0 \end{bmatrix},$$
$$\mathcal{G}_{311} = \begin{bmatrix} 0 & 0 \\ 0.5 & 0 \end{bmatrix}, \mathcal{G}_{312} = \begin{bmatrix} 0 & 0 \\ 0.5 & 0 \end{bmatrix}.$$

The transition probability matrix of system (10) is $\begin{bmatrix} ? & ? \\ \pi_{21}(h) & \pi_{22}(h) \end{bmatrix}$, where "?" represents a completely unknown transition probability, and $\pi_{21}(h) \in [0.4, 0.7], \pi_{22}(h) \in [-0.6, -0.3]$. The scalars and positive matrix are chosen as $\tau_M = 0.1, a_m = 0.5, \gamma = 0.8, \varepsilon_{i1} = \varepsilon_{i2} = \varepsilon_{i3} = \varepsilon_{i4} = 1, \gamma_q = 20$ and $R_i = I$, respectively. By solving LMIs in Theorem 2, the weighting matrices in equation (4) are $\Omega_1 = 0.3844, \Omega_2 = 0.3839, \Omega_3 = 0.3792$, and the corresponding controller gains are

$$K_{11}^1 = \begin{bmatrix} 0.1456 & -0.2717 \end{bmatrix}, K_{11}^2 = \begin{bmatrix} -0.2089 & -0.3153 \end{bmatrix},$$
$$K_{12}^1 = \begin{bmatrix} -3.5900 & -15.3939 \end{bmatrix}, K_{12}^2 = \begin{bmatrix} -3.6974 & -15.8393 \end{bmatrix},$$
$$K_{21}^1 = \begin{bmatrix} 0.1452 & -0.2697 \end{bmatrix}, K_{21}^2 = \begin{bmatrix} -0.2548 & -0.3342 \end{bmatrix},$$
$$K_{22}^1 = \begin{bmatrix} -2.6929 & -12.1132 \end{bmatrix}, K_{22}^2 = \begin{bmatrix} -2.7779 & -12.4794 \end{bmatrix},$$
$$K_{31}^1 = \begin{bmatrix} 0.2304 & -0.2927 \end{bmatrix}, K_{31}^2 = \begin{bmatrix} -0.1659 & -0.3184 \end{bmatrix},$$
$$K_{32}^1 = \begin{bmatrix} -1.9339 & -12.7768 \end{bmatrix}, K_{32}^2 = \begin{bmatrix} -1.9851 & -13.0934 \end{bmatrix}.$$

The initial conditions are given as $x_1(0) = \begin{bmatrix} -0.45 & 0.85 \end{bmatrix}^{\mathrm{T}}, x_2(0) = \begin{bmatrix} 0.5 & -0.5 \end{bmatrix}^{\mathrm{T}}, x_3(0) = \begin{bmatrix} -0.95 & 0.55 \end{bmatrix}^{\mathrm{T}}$. Figure 2 shows the states response of dynamic METM with M=2. To illustrate the effectiveness of the designed method, Figure 3 presents the state's response without control input. Figure 4 plots the control input of the systems. Figure 5 shows the switching states of the semi-Markovian process. Figure 6 depicts the data-releasing instants and intervals of dynamic METM with M=2. Figure 7 describes the instants and intervals of memoryless ETM (the case of M = 1). From Figure 6 and Figure 7, we can see that the event-triggered times for M=2 are significantly less than the case of M=1, which illustrates that the dynamic METM has more advantages in reducing the number of released signals.

5. CONCLUSION

In this paper, a dynamic METM has been drawn for the decentralized control of interconnected semi-Markovian systems with partially accessible TRs. Considering both the dynamic METM and partially accessible TRs, a new kind of interconnected semi-Markovian system model has been designed. By applying the Lyapunov function theory and the LMI techniques, some sufficient conditions have been obtained to ensure the proposed system is asymptotical stability. Meanwhile, the controller gain matrices and the parameters of dynamic METM are also solved simultaneously. Finally, a simulation example has been used to verify the effectiveness

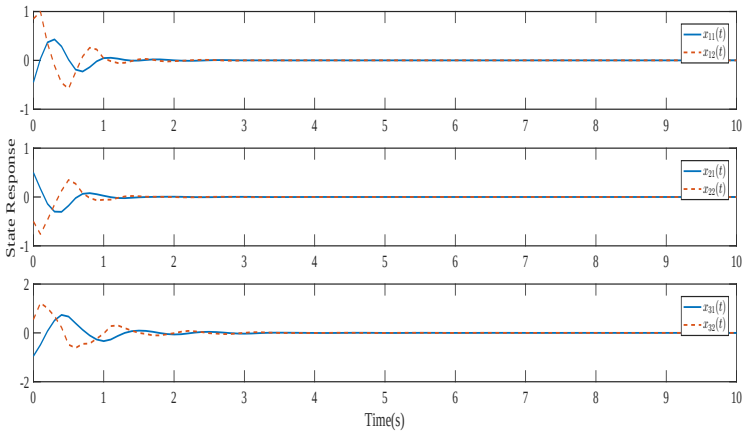

Figure 2. The state's response of dynamic METM with M = 2. METM: memory event-triggered mechanism.

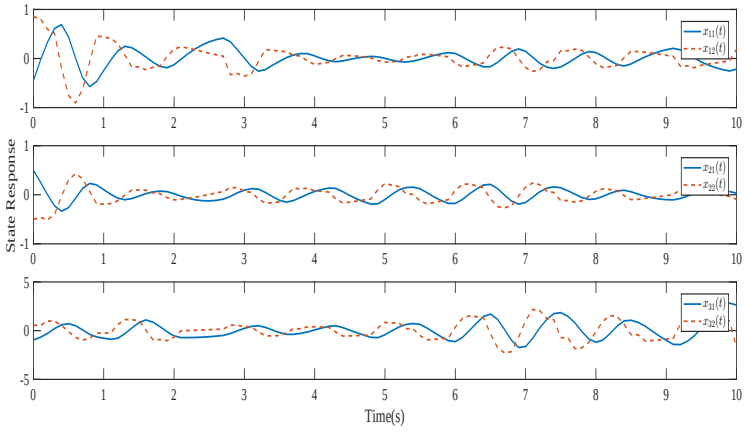

Figure 3. The state's response without control input.

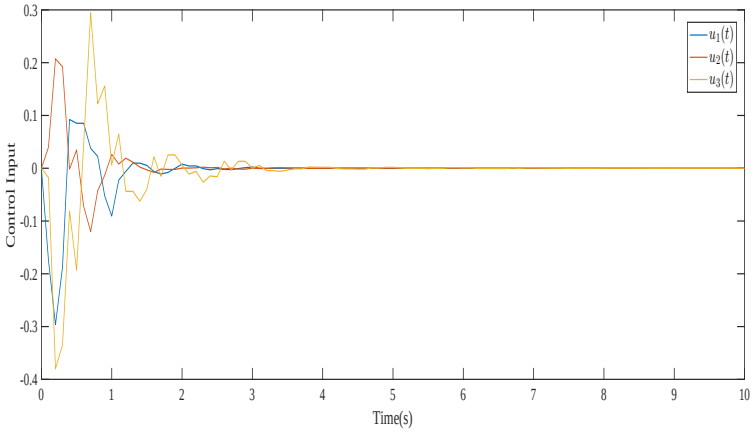

Figure 4. The control input of the three systems.

of the developed method, which illustrates the proposed dynamic METM can save more network resources

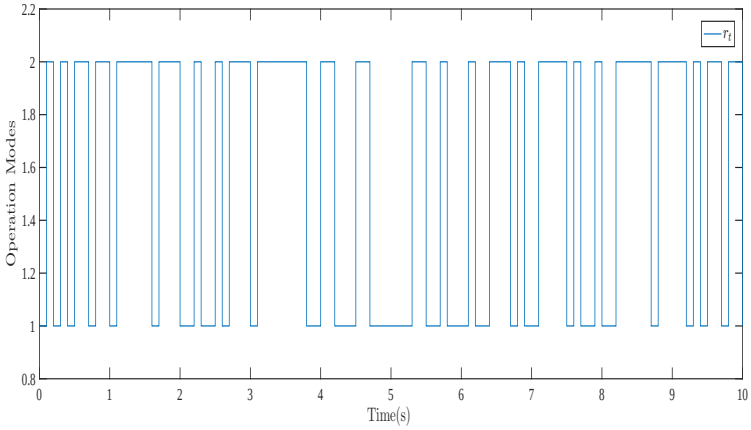

Figure 5. The switching state of the semi-Markovian process.

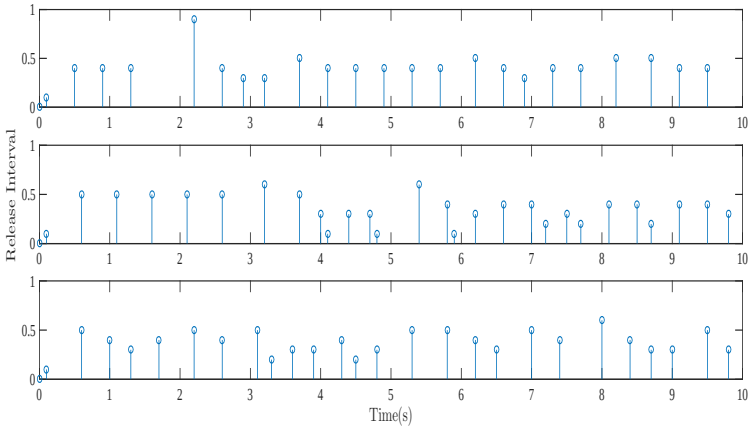

Figure 6. The data-releasing instants and intervals of dynamic METM with M = 2. METM: memory event-triggered mechanism.

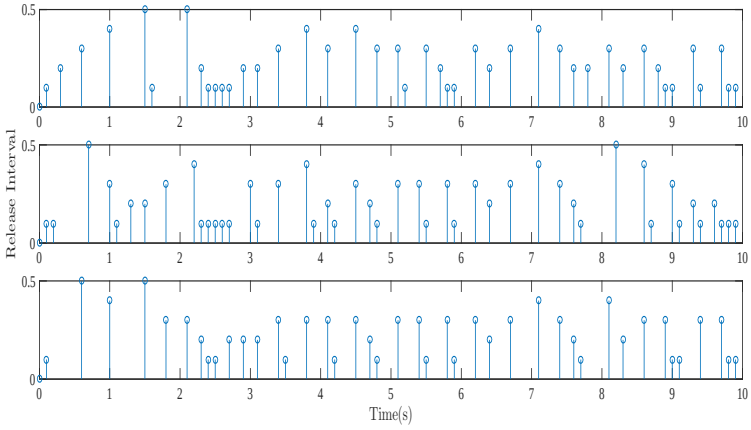

Figure 7. The instants and intervals of memoryless ETM (the case of M = 1). ETM: event-triggered mechanism.

than the memoryless event-triggered mechanism.

In the future, we will pay attention to the distributed memory event-triggered control design for interconnected systems via the observer method. Moreover, the memory event-triggered security control problem for the interconnected Markovian jump systems with cyber attacks is also an interesting issue, which is left to be developed.

DECLARATIONS

Acknowledgments
The authors are grateful to the Guest Editors and anonymous reviewers for their constructive comments based on which the presentation of this paper has been greatly improved.

Authors' contributions
Made substantial contributions to the conception and design of the study and performed data analysis and interpretation: Tan Y, Cheng X, Li X, Bai J
Performed data acquisition, as well as providing administrative, technical, and material support: Tan Y, Liu J

Availability of data and materials
Not applicable.

Financial support and sponsorship
None.

Conflicts of interest
All authors declared that there are no conflicts of interest.

Ethical approval and consent to participate
Not applicable.

Consent for publication
Not applicable.

REFERENCES

1. Zhang CZ, Gang F, Gao HJ, Qiu JB. H_∞ filtering for nonlinear discrete-time systems subject to quantization and packet dropouts. *IEEE Trans Fuzzy Syst* 2011;19:353-65. DOI
2. Shoukry Y, Tabuada P. Event-triggered state observers for sparse sensor noise attacks. *IEEE Trans Automat Contr* 2016;61:2079-91. DOI
3. Liu D, Hao F. Decentralized event-triggered control strategy in distributed networked systems with delays. *Int J Control Autom Syst* 2013;11:33-40. DOI
4. Guo XG, Zhang DY, Wang JL, Ahn CK. Adaptive memory event-triggered observer-based control for nonlinear MASs under DOS attacks. *IEEE/CAA J Autom Sinica* 2021;8:1644-56. DOI
5. Wei YL, Wang M, Karimi HR, Qiu JB. H_∞ control for two-dimensional Markovian jump systems with state-delays and defective mode information. *Math Probl Eng* 2013;5:1-11. DOI
6. Tong SC, Huo BY, Li YM. Observer-Based adaptive decentralized fuzzy fault-tolerant control of nonlinear large-scale systems with actuator failures. *IEEE Trans Fuzzy Syst* 2014;22:1-15. DOI
7. Huang XQ, Lin W, Yang B. Global finite-time stabilization of a class of uncertain nonlinear systems. *Automatica* 2005;41:881-8. DOI
8. Qi WH, Zong GD, Zheng WX. Adaptive event-triggered SMC for stochastic switching systems with semi-Markov process and application to boost converter circuit model. *IEEE Trans Circuits Syst I* 2021;68:786-96. DOI
9. Liu YZ, Chen Y. Dynamic memory event-triggered adaptive control for a class of strict-feedback nonlinear systems. *IEEE Trans Circuits Syst II* 2022;69:3470-4. DOI
10. He SP, Liu F. Observer-based finite-time control of time-delayed jump systems. *Appl Math Comput* 2010;217:2327-38. DOI

11. Zhong ZX, Zhu YZ. Observer-based output-feedback control of large-scale networked fuzzy systems with two-channel event-triggering. *Franklin Inst* 2017;354:5398-420. DOI
12. Zhang ZY, Lin Chong, Chen B. New decentralized H_∞ filter design for nonlinear interconnected systems based on takagi-sugeno fuzzy models. *IEEE Trans Cybern* 2015;45:2914-24. DOI
13. Wang CL, Wen CG, Lin Y, Wang W. Decentralized adaptive tracking control for a class of interconnected nonlinear systems with input quantization. *Automatica* 2017;81:359-368. DOI
14. Lin D, Wang XY. Observer-based decentralized fuzzy neural sliding mode control for interconnected unknown chaotic systems via network structure adaptation. *Fuzzy Sets & Systems* 2010;161:2066-80. DOI
15. Yu ZM, Sun Y, Dai X, Su XJ. Decentralized time-delay control using partial variables with measurable states for a class of interconnected systems with time delays. *IEEE Trans Cybern* 2020;52:10882-94. DOI
16. Du BZ, Lam J, Zou Y, Shu Z. Stability and stabilization for Markovian jump time-delay systems with partially unknown transition rates. *IEEE Trans Circuits Syst I* 2013;60:341-351. DOI
17. An LW, Yang GH. Decentralized adaptive fuzzy secure control for nonlinear uncertain interconnected systems against intermittent DoS attacks. *IEEE Trans Cybern* 2019;49:827-38. DOI
18. Zhang YQ, Shi P, Nguang SK, Karimi HR. Observer-based finite-time fuzzy H_∞ control for discrete-time systems with stochastic jumps and time-delays. *Signal Processing* 2014;97:252–61. DOI
19. Polyakov A, Efimov D, Perruquetti W. Finite-time and fixed-time stabilization: implicit Lyapunov function approach. *IEEE Trans Automat Contr* 2015;51:332-40. DOI
20. Zhang Z, Zhang ZX, Zhang H, Zheng B, Karimi HR. Finite-time stability analysis and stabilization for linear discrete-time system with time-varying delay. *J Franklin Inst* 2014;351:3457-76. DOI
21. Wang TC, Tong SC. Observer-based fuzzy adaptive optimal stabilization control for completely unknown nonlinear interconnected systems. *Neurocomputing* 2018;313:415-25. DOI
22. Li F, Fu J, Du D. A novel decentralised event-triggered control for network control systems with communication delays. *Int J Syst Sci* 2016;47:1-18. DOI
23. Tan YS, Liu QY, Du DS, Niu B, Fei SM. Observer-based finite-time H_∞ control for interconnected fuzzy systems with quantization and random network attacks. *IEEE Trans Fuzzy Syst* 2021;29:674-685. DOI
24. Tan YS, Liu QY, Liu JL, Xie XP, Fei SM. Observer-based security control for interconnected semi-Markovian jump systems with unknown transition probabilities. *IEEE Trans Cybern* 2022;52:9013-25. DOI
25. Liang BY, Zheng SQ, Ahn CK, Liu F. Adaptive fuzzy control for fractional-order interconnected systems with unknown control directions. *IEEE Trans Fuzzy Syst* 2022;30:75-87. DOI
26. Wang XD, Fei ZY, Yu JinY, Wang GQ. Adaptive memory-based event-triggered fault detection for networked stochastic systems. *IEEE Trans Circuits Syst II* 2023;70:201-205. DOI
27. Wang X, Sun J, Wang G, Allgöwer F, Chen J. Data-driven control of distributed event-triggered network systems. *IEEE/CAA J Autom Sinica* 2023;10:351-64. DOI
28. Cao ZR, Niu YG, Lam HK, Zhao JC. Sliding mode control of Markovian jump fuzzy systems: a dynamic event-triggered method. *IEEE Trans Fuzzy Syst* 2021;29:2902-15. DOI
29. Jiang BP, Gao CC. Decentralized adaptive sliding mode control of large-scale semi-Markovian jump interconnected systems with dead-zone input. *IEEE Trans Automat Contr* 2022;67:1521-28. DOI
30. Zhang LC, Liang HJ, Sun YH, Ahn CK. Adaptive event-triggered fault detection scheme for semi-Markovian jump systems with output quantization. *IEEE Trans Syst Man Cybern, Syst* 2021;51:2370-81. DOI
31. Wang FL, Long LJ. Decentralized dynamic event-triggered adaptive fuzzy control for switched nonlinear systems with unstable inverse dynamics. *IEEE Trans Syst Man Cybern, Syst* 2023;53:357-68. DOI
32. Tian E, Peng C. Memory-based event-triggering H_∞ load frequency control for power systems under deception attacks. *IEEE Trans Cybern* 2020;50:4610-8. DOI
33. Wang J, Ru TT, Xia JW, Shen H, Sreeram V. Asynchronous event-triggered sliding mode control for semi-Markov jump systems within a finite-time interval. *IEEE Trans Circuits Syst I* 2021;68:458-68. DOI
34. Abdollahi F, Khorasani K. A decentralized Markovian jump H_∞ control routing strategy for mobile multi-agent networked systems. *IEEE Trans Contr Syst Technol* 2011;19:269-83. DOI
35. Ma M, Wang T, Qiu JB, Karimi HR. Adaptive fuzzy decentralized tracking control for large-scale interconnected nonlinear networked control systems. *IEEE Trans Fuzzy Syst* 2021;29:3186-91. DOI
36. Zhan YL, Sui S, Tong SC. Adaptive fuzzy decentralized dynamic surface control for fractional-order nonlinear large-scale systems. *IEEE Trans Fuzzy Syst* 2022;30:3373-83. DOI
37. Yan S, Gu Zh, Park JH. Lyapunov-function-based event-triggered control of nonlinear discrete-time cyber-physical systems. *IEEE Trans Circuits Syst II* 2021;68:458-468. DOI
38. Zhou J. Decentralized adaptive control for large-scale time-delay systems with dead-zone input. *Automatica* 2008;44:1790-99. DOI
39. Vadivel R, Hammachukiattikul P, Gunasekaran N, Saravanakumar R, Dutta H. Strict dissipativity synchronization for delayed static neural networks: an event-triggered scheme. *Chaos, Solitons & Fractals* 2021;150:111212. DOI
40. Wu YB, Wang Y, Gunasekaran N, Vadivel R. Almost sure consensus of multi-agent systems: an intermittent noise. *IEEE Trans Circuits Syst II* 2022; 69:2897-2901. DOI

AUTHOR INSTRUCTIONS

1. Submission Overview

Before you decide to publish with *Complex Engineering Systems* (*CES*), please read the following items carefully and make sure that you are well aware of Editorial Policies and the following requirements.

1.1 Topic Suitability

The topic of the manuscript must fit the scope of the journal. Please refer to Aims and Scope for more information.

1.2 Open Access and Copyright

The journal adopts Gold Open Access publishing model and distributes content under the Creative Commons Attribution 4.0 International License. Copyright is retained by authors. Please make sure that you are well aware of these policies.

1.3 Publication Fees

CES is an open access journal. When a paper is accepted for publication, authors are required to pay Article Processing Charges (APCs) to cover its editorial and production costs. The APC for each submission is $600. There are no additional charges based on color, length, figures, or other elements. For more details, please refer to OAE Publication Fees.

1.4 Language Editing

All submissions are required to be presented clearly and cohesively in good English. Authors whose first language is not English are advised to have their manuscripts checked or edited by a native English speaker before submission to ensure the high quality of expression. A well-organized manuscript in good English would make the peer review even the whole editorial handling more smoothly and efficiently.

If needed, authors are recommended to consider the language editing services provided by Charlesworth to ensure that the manuscript is written in correct scientific English before submission. Authors who publish with OAE journals enjoy a special discount for the services of Charlesworth via the following two ways.
Submit your manuscripts directly at http://www.charlesworthauthorservices.com/~OAE;
Open the link http://www.charlesworthauthorservices.com/, and enter Promotion Code “OAE” when you

1.5 Work Funded by the National Institutes of Health

If an accepted manuscript was funded by National Institutes of Health (NIH), the author may inform editors of the NIH funding number. The editors are able to deposit the paper to the NIH Manuscript Submission System on behalf of the author.

2. Submission Preparation

2.1 Cover Letter

A cover letter is required to be submitted accompanying each manuscript. Here is a guideline of a cover letter for authors’ consideration:

List the highlights of the current manuscript and no more than 5 short sentences;

All authors have read the final manuscript, have approved the submission to the journal, and have accepted full responsibilities pertaining to the manuscript’s delivery and contents;

Clearly state that the manuscript is an original work on its own merit, that it has not been previously published in whole or in part, and that it is not being considered for publication elsewhere;

No materials are reproduced from another source (if there is material in your manuscript that has been reproduced from another source, please state whether you have obtained permission from the copyright holder to use them);

Conflicts of interest statement;

If the manuscript is contributed to a Special Issue, please also mention it in the cover letter;

If the manuscript was presented partly or entirely in a conference, the author should clearly state the background information of the event, including the conference name, time, and place in the cover letter.

2.2 Types of Manuscripts

There is no restriction on the length of manuscripts, number of figures, tables and references, provided that the manuscript is concise and comprehensive. The journal publishes Research Article, Review, Technical Note, *etc*. For more details about paper type, please refer to the following table.

Manuscript Type	Definition	Word Limit	Abstract	Keywords	Main Text Structure
Research Article	A Research Article is a seminal and insightful research study and showcases that often involves modern techniques or methodologies. Authors should justify that their work is of novel findings	8000 max	The abstract should state briefly the purpose of the research, the principal results and major conclusions. No more than 250 words	3-8 keywords	The main content should include four sections: Introduction, Methods, Results and Discussion
Review	A Review should be an authoritative, well balanced, and critical survey of recent progress in an attractive or a fundamental research field	10000 max	Unstructured abstract. No more than 250 words	3-8 keywords	The main text may consist of several sections with unfixed section titles. We suggest that the author include an "Introduction" section at the beginning, several sections with unfixed titles in the middle part, and a "Conclusions" section at the end
Technical Note	A Technical Note is a short article giving a brief description of a specific development, technique, or procedure, or it may describe a modification of an existing technique, procedure or device applied in research	3500 max	Unstructured abstract. No more than 250 words	3-8 keywords	/
Editorial	An Editorial is a short article describing news about the journal or opinions of senior Editors or the publisher	1000 max	None required	None required	/
Commentary	A Commentary is to provide comments on a newly published article or an alternative viewpoint on a certain topic	2500 max	Unstructured abstract. No more than 250 words	3-8 keywords	/
Perspective	A Perspective provides personal points of view on the state-of-the-art of a specific area of knowledge and its future prospects	2000 max	Unstructured abstract. No more than 250 words	3-8 keywords	/

2.3 Manuscript Structure

2.3.1 Front Matter

2.3.1.1 Title

The title of the manuscript should be concise, specific and relevant, with no more than 16 words if possible.

2.3.1.2 Authors and Affiliations

Authors' full names should be listed. The initials of middle names can be provided. The affiliations and email addresses for all authors should be listed. At least one author should be designated as the corresponding author. In addition, corresponding authors are suggested to provide their Open Researcher and Contributor ID upon submission. Please note that any change to authorship is not allowed after manuscript acceptance. The authors' affiliations should be provided in this format: department, institution, city, postcode, country.

2.3.1.3 Abstract

The abstract should be a single paragraph with word limitation and specific structure requirements (for more details please refer to Types of Manuscripts). It usually describes the main objective(s) of the study, explains how the study was done, including any model organisms used, without methodological detail, and summarizes the most important results and their significance. The abstract must be an objective representation of the study: it is not allowed to contain results that are not presented and substantiated in the manuscript, or exaggerate the main conclusions. Citations should not be included in the abstract.

2.3.1.4 Graphical Abstract

The graphical abstract is essential as this can catch first view of your publication by readers. We recommend you submit an eye-catching figure. It should summarize the content of the article in a concise graphical form. It is recommended to use it because this can make online articles get more attention.

The graphical abstract should be submitted as a separate document in the online submission system. Please provide an image with a minimum of 531 × 1,328 pixels (h × w) or proportionally more. The image should be readable at a size of 5 cm × 13 cm using a regular screen resolution of 96 dpi. Preferred file types: TIFF, PSD, AI, JPEG, and EPS files.

2.3.1.5 Keywords

Three to eight keywords should be provided, which are specific to the article, yet reasonably common within the subject discipline.

Sections 2.3.1.1 and 2.3.1.2 should appear in all manuscript types.

2.3.2 Main Text

Manuscripts of different types are structured with different sections of content. Please refer to Types of Manuscripts to make sure which sections should be included in the manuscripts.

2.3.2.1 Introduction

The introduction should contain background that puts the manuscript into context, allow readers to understand why the study is important, include a brief review of key literature, and conclude with a brief statement of the overall aim of the work and a comment about whether that aim was achieved. Relevant controversies or disagreements in the field should be introduced as well.

2.3.2.2 Methods

The methods should contain sufficient details to allow others to fully replicate the study. New methods and protocols should be described in detail while well-established methods can be briefly described or appropriately cited. Statistical terms, abbreviations, and all symbols used should be defined clearly. Protocol documents for clinical trials, observational studies, and other non-laboratory investigations may be uploaded as supplementary materials.

2.3.2.3 Results

This section contains the findings of the study. Results of statistical analysis should also be included either as text or as tables or figures if appropriate. Authors should emphasize and summarize only the most important observations. Data on all primary and secondary outcomes identified in the section Methods should also be provided. Extra or supplementary materials and technical details can be placed in supplementary documents.

2.3.2.4 Discussion

This section should discuss the implications of the findings in context of existing research and highlight limitations of the study. Future research directions may also be mentioned.

2.3.2.5 Conclusion

It should state clearly the main conclusions and include the explanation of their relevance or importance to the field.

2.3.3 Back Matter

The following sections should appear in all manuscript types.

2.3.3.1 Acknowledgments

Anyone who contributed towards the article but does not meet the criteria for authorship, including those who provided professional writing services or materials, should be acknowledged. Authors should obtain permission to acknowledge from all those mentioned in the Acknowledgments section. This section is not added if the author does not have anyone to acknowledge.

2.3.3.2 Authors' Contributions

Each author is expected to have made substantial contributions to the conception or design of the work, or the acquisition, analysis, or interpretation of data, or the creation of new software used in the work, or have drafted the work or substantively revised it.

Please use Surname and Initial of Forename to refer to an author's contribution. For example: made substantial contributions to conception and design of the study and performed data analysis and interpretation: Salas H, Castaneda WV; performed data acquisition, as well as providing administrative, technical, and material support: Castillo N, Young V.

If an article is single-authored, please include "The author contributed solely to the article." in this section.

2.3.3.3 Availability of Data and Materials

In order to maintain the integrity, transparency and reproducibility of research records, authors should include this section in their manuscripts, detailing where the data supporting their findings can be found. Data can be deposited into data repositories or published as supplementary information in the journal. Authors who cannot share their data should state that the data will not be shared and explain it. If a manuscript does not involve such issues, please state "Not applicable." in this section.

2.3.3.4 Financial Support and Sponsorship

All sources of funding for the study reported should be declared. The role of the funding body in the experiment design, collection, analysis and interpretation of data, and writing of the manuscript should be declared. Any relevant grant numbers and the link of funder's website should be provided if any. If the study is not involved with this issue, state "None." in this section.

2.3.3.5 Conflicts of Interest

Authors must declare any potential conflicts of interest that may be perceived as inappropriately influencing the representation or interpretation of reported research results. If there are no conflicts of interest, please state "All authors declared that there are no conflicts of interest." in this section. Some authors may be bound by confidentiality agreements. In such cases, in place of itemized disclosures, we will require authors to state "All authors declared that they are bound by confidentiality agreements that prevent them from disclosing their conflicts of interest in this work.". If authors are unsure whether conflicts of interest exist, please refer to the "Conflicts of Interest" of *Complex Engineering Systems* (*CES*) Editorial Policies for a full explanation.

2.3.3.6 Ethical Approval and Consent to Participate

Research involving human subjects, human material or human data must be performed in accordance with the Declaration of Helsinki and approved by an appropriate ethics committee. An informed consent to participate in the study should also be obtained from participants, or their parents or legal guardians for children under 16. A statement detailing the name of the ethics committee (including the reference number where appropriate) and the informed consent obtained must appear in the manuscripts reporting such research.

Studies involving animals and cell lines must include a statement on ethical approval. More information is available at Editorial Policies.

If the manuscript does not involve such issues, please state "Not applicable." in this section.

2.3.3.7 Consent for Publication

Manuscripts containing individual details, images or videos, must obtain consent for publication from that person, or in the case of children, their parents or legal guardians. If the person has died, consent for publication must be obtained from the next of kin of the participant. Manuscripts must include a statement that written informed consent for publication was obtained. Authors do not have to submit such content accompanying the manuscript. However, these documents must be available if requested. If the manuscript does not involve this issue, state "Not applicable." in this section.

2.3.3.8 Copyright

Authors retain copyright of their works through a Creative Commons Attribution 4.0 International License that clearly states how readers can copy, distribute, and use their attributed research, free of charge. A declaration "© The Author(s) 2023." will be added to each article. Authors are required to sign a License to Publish before formal publication.

2.3.3.9 References

References should be numbered in order of appearance at the end of manuscripts. In the text, reference numbers should be placed in square brackets and the corresponding references are cited thereafter. List all authors when the number of authors

is less than or equal to six, if there are more than six authors, only the first three authors' names should be listed, other authors' names should be omitted and replaced with "et al.". The journal's name should be required to be italicized and the journal references should have corresponding DOI numbers. Information from manuscripts accepted but not published should be cited in the text as "Unpublished material" with written permission from the source. Journal names should be abbreviated according to the List of Title Word Abbreviations.

References should be described as follows, depending on the types of works:

Types	**Examples**
Journal articles by individual authors	Cao MS, Pan LX, Gao YF, et al. Neural network ensemble-based parameter sensitivity analysis in civil engineering systems. *Neural Comput Applic* 2017;28:1583-90. [DOI: 10.1007/s00521-015-2132-4]
Organization as author	Diabetes Prevention Program Research Group. Hypertension, insulin, and proinsulin in participants with impaired glucose tolerance. *Hypertension* 2002;40:679-86. [DOI: 10.1161/01.hyp.0000035706.28494.09]
Both personal authors and organization as author	Vallancien G, Emberton M, Harving N, van Moorselaar RJ; Alf-One Study Group. Sexual dysfunction in 1,274 European men suffering from lower urinary tract symptoms. *J Urol* 2003;169:2257-61. [DOI: 10.1097/01.ju.0000067940.76090.73]
Journal articles not in English	Mao X, Ding YK. Sentiment feature analysis and harmonic sense evaluation of images. *J Electronic* 2001;29:23-7. (in Chinese)
Journal articles ahead of print	Albasir A, Hu Q, Naik K, Naik N. Unsupervised detection of security threats in cyberphysical system and IoT devices based on power fingerprints and RBM autoencoders. *J Surveill Secur Saf* 2021; Epub ahead of print [DOI: 10.20517/jsss.2020.19]
Books	Gaydon AG, Wolfhard HG. Flames. 2nd ed. London: Chapman and Hall Ltd.; 1960. pp. 10-20.
Book chapters	Chothia T, Smirnov V. A traceability attack against e-passports. In: Sion R, Editor. Financial cryptography. Lecture notes in computer science. Springer; 2010. pp. 20-34..
Online resource	Intel Technology Journal. Developing smart toys - from idea to product. Available from: https://www.intel.com/content/dam/www/public/us/en/documents/research/2001-vol05-iss-4-intel-technology-journal.pdf. [Last accessed on 20 Feb 2021]
Conference proceedings	Harnden P, Joffe JK, Jones WG, Editors. Germ cell tumours V. Proceedings of the 5th Germ Cell Tumour Conference; 2001 Sep 13-15; Leeds, UK. New York: Springer; 2002..
Conference paper	Christensen S, Oppacher F. An analysis of Koza's computational effort statistic for genetic programming. In: Foster JA, Lutton E, Miller J, Ryan C, Tettamanzi AG, Editors. Genetic programming. EuroGP 2002: Proceedings of the 5th European Conference on Genetic Programming; 2002 Apr 3-5; Kinsdale, Ireland. Berlin: Springer; 2002. pp. 182-91.
Unpublished material	Tian D, Araki H, Stahl E, Bergelson J, Kreitman M. Signature of balancing selection in Arabidopsis. Proc Natl Acad Sci U S A. Forthcoming 2002.

The journal also recommends that authors prepare references with a bibliography software package, such as EndNote to avoid typing mistakes and duplicated references.

2.3.3.10 Supplementary Materials

Additional data and information can be uploaded as Supplementary Materials to accompany the manuscripts. The supplementary materials will also be available to the referees as part of the peer-review process. Any file format is acceptable, such as data sheet (word, excel, csv, cdx, fasta, pdf or zip files), presentation (powerpoint, pdf or zip files), image (cdx, eps, jpeg, pdf, png or tiff), table (word, excel, csv or pdf), audio (mp3, wav or wma) or video (avi, divx, flv, mov, mp4, mpeg, mpg or wmv). All information should be clearly presented. Supplementary materials should be cited in the main text in numeric order (e.g., Supplementary Figure 1, Supplementary Figure 2, Supplementary Table 1, Supplementary Table 2, *etc*.). The style of supplementary figures or tables complies with the same requirements on figures or tables in main text. Videos and audios should be prepared in English, and limited to a size of 500 MB.

2.4 Manuscript Format

2.4.1 File Format

Manuscript files can be in DOC and DOCX formats and should not be locked or protected.

Manuscript prepared in LaTex must be collated into one ZIP folder (including all source files and images, so that the Editorial Office can recompile the submitted PDF).

When preparing manuscripts in different file formats, please use the corresponding Manuscript Templates.

2.4.2 Length

There are no restrictions on paper length, number of figures, or number of supporting documents. Authors are encouraged

to present and discuss their findings concisely.

2.4.3 Language

Manuscripts must be written in English.

2.4.4 Multimedia Files

The journal supports manuscripts with multimedia files. The requirements are listed as follows:

Video or audio files are only acceptable in English. The presentation and introduction should be easy to understand. The frames should be clear, and the speech speed should be moderate;
A brief overview of the video or audio files should be given in the manuscript text;
The video or audio files should be limited to a size of up to 500 MB;
Please use professional software to produce high-quality video files, to facilitate acceptance and publication along with the submitted article. Upload the videos in mp4, wmv, or rm format (preferably mp4) and audio files in mp3 or wav format.

2.4.5 Figures

Figures should be cited in numeric order (e.g., Figure 1, Figure 2) and placed after the paragraph where it is first cited;

Figures can be submitted in format of TIFF, PSD, AI, EPS or JPEG, with resolution of 300-600 dpi;

Figure caption is placed under the Figure;

Diagrams with describing words (including, flow chart, coordinate diagram, bar chart, line chart, and scatter diagram, *etc.*) should be editable in word, excel or powerpoint format. Non-English information should be avoided;

Labels, numbers, letters, arrows, and symbols in figure should be clear, of uniform size, and contrast with the background;

Symbols, arrows, numbers, or letters used to identify parts of the illustrations must be identified and explained in the legend;

Internal scale (magnification) should be explained and the staining method in photomicrographs should be identified;

All non-standard abbreviations should be explained in the legend;

Permission for use of copyrighted materials from other sources, including re-published, adapted, modified, or partial figures and images from the internet, must be obtained. It is authors' responsibility to acquire the licenses, to follow any citation instruction requested by third-party rights holders, and cover any supplementary charges.

2.4.6 Tables

Tables should be cited in numeric order and placed after the paragraph where it is first cited;

The table caption should be placed above the table and labeled sequentially (e.g., Table 1, Table 2);

Tables should be provided in editable form like DOC or DOCX format (picture is not allowed);

Abbreviations and symbols used in table should be explained in footnote;

Explanatory matter should also be placed in footnotes;

Permission for use of copyrighted materials from other sources, including re-published, adapted, modified, or partial tables from the internet, must be obtained. It is authors' responsibility to acquire the licenses, to follow any citation instruction requested by third-party rights holders, and cover any supplementary charges.

2.4.7 Abbreviations

Abbreviations should be defined upon first appearance in the abstract, main text, and in figure or table captions and used consistently thereafter. Non-standard abbreviations are not allowed unless they appear at least three times in the text. Commonly-used abbreviations, such as DNA, RNA, ATP, *etc.*, can be used directly without definition. Abbreviations in titles and keywords should be avoided, except for the ones which are widely used.

2.4.8 Italics

General italic words like vs., et al., etc., in vivo, in vitro; t test, F test, U test; related coefficient as r, sample number as n, and probability as P; names of genes; names of bacteria and biology species in Latin.

2.4.9 Units

SI Units should be used. Imperial, US customary and other units should be converted to SI units whenever possible. There is a space between the number and the unit (i.e., 23 mL). Hour, minute, second should be written as h, min, s.

2.4.10 Numbers

Numbers appearing at the beginning of sentences should be expressed in English. When there are two or more numbers in a paragraph, they should be expressed as Arabic numerals; when there is only one number in a paragraph, number < 10 should be expressed in English and number > 10 should be expressed as Arabic numerals. 12345678 should be written as 12,345,678.

2.4.11 Equations

Equations should be editable and not appear in a picture format. Authors are advised to use either the Microsoft Equation Editor or the MathType for display and inline equations.

Display equations should be numbered consecutively, using Arabic numbers in parentheses;
Inline equations should not be numbered, with the same/similar size font used for the main text.

2.4.12 Headings

In the main body of the paper, three different levels of headings may be used.

Level one headings: they should be in bold, and numbered using Arabic numbers, such as 1. INTRODUCTION, and 2. METHODS, with all letters capitalized;
Level two headings: they should be in bold and numbered after the level one heading, such as 2.1 Statistical analyses, 2.2 ..., 2.3..., *etc*., with the first letter capitalized;
Level three headings: they should be italicized, and numbered after the level two heading, such as 2.1.1 Data distributions,and 2.1.2 outliers and linear regression, with the first letter capitalized.

2.4.13 Text Layout

As the electronic submission will provide the basic material for typesetting, it is important to prepare papers in the general editorial style of the journal.

The font is Times New Roman;
The font size is 12pt;
Single column, 1.5x line spacing;
Insert one line break (one Return) before the heading and paragraph, if the heading and paragraph are adjacent, insert a line break before the heading only;
No special indentation;
Alignment is left end;
Insert consecutive line numbers;
For other details please refer to the Manuscript Templates.

2.5 Submission Link

Submit an article via https://oaemesas.com/login?JournalId=comengsys.

3. Research and Publication Ethics

3.1 Research Involving Human Subjects

All studies involving human subjects must be in accordance with the Helsinki Declaration and seek approval to conduct the study from an independent local, regional, or national review body (e.g., ethics committee, institutional review board, *etc*.). Such approval, including the names of the ethics committee, institutional review board, *etc*., must be listed in a declaration statement of Ethical Approval and Consent to Participate in the manuscript. If the study is judged exempt from ethics approval, related information (e.g., name of the ethics committee granting the exemption and the reason for the exemption) must be listed. Further documentation on ethics should also be prepared, as Editors may request more detailed information. Manuscripts with suspected ethical problems will be investigated according to COPE Guidelines.

3.1.1 Consent to Participate

For all studies involving human subjects, informed consent to participate in the studies must be obtained from participants, or their parents or legal guardians for children under 16. Statements regarding consent to participate should be included in a declaration statement of Ethical Approval and Consent to Participate in the manuscript. If informed consent is not required, the name of the ethics committee granting the exemption and the reason for the exemption must be listed. If any ethical violation is found at any stage of publication, the issue will be investigated seriously based on COPE Guidelines.

3.1.2 Consent for Publication

All articles published by OAE are freely available on the Internet. All manuscripts that include individual participants' data in any form (i.e., details, images, videos, *etc.*) will not be published without Consent for Publication obtained from that person(s), or for children, their parents, or legal guardians. If the person has died, Consent for Publication must be obtained from the next of kin. Authors must add a declaration statement of Consent for Publication in the manuscript, specifying written informed consent for publication has been obtained.

3.1.3 Trial Registration

OAE requires all authors to register all relevant clinical trials that are reported in manuscripts submitted. OAE follows the World Health Organization (WHO)'s definition of clinical trials: "A clinical trial is any research study that prospectively assigns human participants or groups of humans to one or more health-related interventions to evaluate the effects on health outcomes. Interventions include but are not restricted to drugs, cells, other biological products, surgical procedures, radiologic procedures, devices, behavioral treatments, process-of-care changes, preventive care, *etc.*".

In line with International Committee of Medical Journal Editors (ICMJE) Recommendations, OAE requires the registration of clinical trials in a public trial registry at or before the time of first patient enrollment. OAE accepts publicly accessible registration in any registry that is a primary register of the WHO International Clinical Trials Registry Platform or in ClinicalTrials.gov. The trial registration number should be listed at the end of the Abstract section.

Secondary data analyses of primary (parent) clinical trials should not be registered as a new clinical trial, but rather reference the trial registration number of the primary trial.

Editors of OAE journals will consider carefully whether studies failed to register or had an incomplete trial registration. Because of the importance of prospective trial registration, if there is an exception to this policy, trials must be registered and the authors should indicate in the publication when registration was completed and why it was delayed. Editors will publish a statement indicating why an exception was allowed. Please note such exceptions should be rare, and authors failing to prospectively register a trial risk its inadmissibility to OAE journals.

Authors who are not sure whether they need trial registration may refer to ICMJE FAQs for further information.

3.2 Research Involving Animals

Experimental research on animals should be approved by an appropriate ethics committee and must comply with institutional, national, or international guidelines. OAE encourages authors to comply with the AALAS Guidelines, the ARRIVE Guidelines, and/or the ICLAS Guidelines, and obtain prior approval from the relevant ethics committee. Manuscripts must include a statement indicating that the study has been approved by the relevant ethical committee and the whole research process complies with ethical guidelines. If a study is granted an exemption from requiring ethics approval, the name of the ethics committee granting the exemption and the reason(s) for the exemption should be detailed. Editors will take account of animal welfare issues and reserve the right to reject a manuscript, especially if the research involves protocols that are inconsistent with commonly accepted norms of animal research.

3.3 Research Involving Cell Lines

Authors must describe what cell lines are used and their origin so that the research can be reproduced. For established cell lines, the provenance should be stated and references must also be given to either a published paper or to a commercial source. For de novo cell lines derived from human tissue, appropriate approval from an institutional review board or equivalent ethical committee, and consent from the donor or next of kin, should be obtained. Such statements should be listed on the Declaration section of Ethical Approval and Consent to Participate in the manuscript.

Further information is available from the International Cell Line Authentication Committee (ICLAC). OAE recommends that authors check the NCBI database for misidentification and contamination of human cell lines.

3.4 Research Involving Plants

Experimental research on plants (either cultivated or wild), including collection of plant material, must comply with institutional, national, or international guidelines. Field studies should be conducted in accordance with local legislation, and the manuscript should include a statement specifying the appropriate permissions and/or licenses. OAE recommends that authors comply with the IUCN Policy Statement on Research Involving Species at Risk of Extinction and the Convention on the Trade in Endangered Species of Wild Fauna and Flora.

For each submitted manuscript, supporting genetic information and origin must be provided for plants that were utilized. For research manuscripts involving rare and non-model plants (other than, e.g., Arabidopsis thaliana, Nicotiana benthamiana, Oriza sativa, or many other typical model plants), voucher specimens must be deposited in a public herbarium or other public collections providing access to deposited materials.

3.5 Publication Ethics Statement

OAE is a member of the Committee on Publication Ethics (COPE). We fully adhere to its Code of Conduct and to its Best Practice Guidelines.

The Editors of this journal enforce a rigorous peer-review process together with strict ethical policies and standards to guarantee to add high-quality scientific works to the field of scholarly publication. Unfortunately, cases of plagiarism, data falsification, image manipulation, inappropriate authorship credit, and the like, do arise. The Editors of *CES* take such publishing ethics issues very seriously and are trained to proceed in such cases with zero tolerance policy.

Authors wishing to publish their papers in *CES* must abide by the following:

The author(s) must disclose any possibility of a conflict of interest in the paper prior to submission;
The authors should declare that there is no academic misconduct in their manuscript in the cover letter;
Authors should accurately present their research findings and include an objective discussion of the significance of their findings;
Data and methods used in the research need to be presented in sufficient detail in the manuscript so that other researchers can replicate the work;
Authors should provide raw data if referees and the Editors of the journal request;
Simultaneous submission of manuscripts to more than one journal is not tolerated;
Republishing content that is not novel is not tolerated (for example, an English translation of a paper that is already published in another language will not be accepted);
The manuscript should not contain any information that has already been published. If you include already published figures or images, please get the necessary permission from the copyright holder to publish under the CC-BY license;
Plagiarism, data fabrication and image manipulation are not tolerated;
Plagiarism is not acceptable in OAE journals.

Plagiarism involves the inclusion of large sections of unaltered or minimally altered text from an existing source without appropriate and unambiguous attribution, and/or an attempt to misattribute original authorship regarding ideas or results, and copying text, images, or data from another source, even from your own publications, without giving credit to the source. As to reusing the text that is copied from another source, it must be between quotation marks and the source must be cited. If a study's design or the manuscript's structure or language has been inspired by previous studies, these studies must be cited explicitly.

If plagiarism is detected during the peer-review process, the manuscript may be rejected. If plagiarism is detected after publication, we may publish a Correction or retract the paper.

Falsification is manipulating research materials, equipment, or processes, or changing or omitting data or results so that the findings are not accurately represented in the research record.

Image files must not be manipulated or adjusted in any way that could lead to misinterpretation of the information provided by the original image.

Irregular manipulation includes: introduction, enhancement, moving, or removing features from the original image; grouping of images that should be presented separately, or modifying the contrast, brightness, or color balance to obscure, eliminate, or enhance some information.

If irregular image manipulation is identified and confirmed during the peer-review process, we may reject the manuscript. If irregular image manipulation is identified and confirmed after publication, we may publish a Correction or retract the paper.

OAE reserves the right to contact the authors' institution(s) to investigate possible publication misconduct if the Editors find conclusive evidence of misconduct before or after publication. OAE has a partnership with iThenticate, which is the most trusted similarity checker. It is used to analyze received manuscripts to avoid plagiarism to the greatest extent possible. When plagiarism becomes evident after publication, we will retract the original publication or require modifications, depending on the degree of plagiarism, context within the published article, and its impact on the overall integrity of the published study. Journal Editors will act under the relevant COPE guidelines.

4. Authorship

Authorship credit of *CES* should be solely based on substantial contributions to a published study, as specified in the

following four criteria:

1. Substantial contributions to the conception or design of the work, or the acquisition, analysis, or interpretation of data for the work;
2. Drafting the work or revising it critically for important intellectual content;
3. Final approval of the version to be published;
4. Agreement to be accountable for all aspects of the work in ensuring that questions related to the accuracy or integrity of any part of the work are appropriately investigated and resolved.

All those who meet these criteria should be identified as authors. Authors must specify their contributions in the section Authors'' Contributions of their manuscripts. Contributors who do not meet all the four criteria (like only involved in acquisition of funding, general supervision of a research group, general administrative support, writing assistance, technical editing, language editing, proofreading, *etc*.) should be acknowledged in the section of Acknowledgement in the manuscript rather than being listed as authors.

If a large multiple-author group has conducted the work, the group ideally should decide who will be authors before the work starts and confirm authors before submission. All authors of the group named as authors must meet all the four criteria for authorship.

AI and AI-assisted technologies should not be listed as an author or co-author.

5. Reviewers Exclusions

You are welcome to exclude a limited number of researchers as potential Editors or reviewers of your manuscript. To ensure a fair and rigorous peer review process, we ask that you keep your exclusions to a maximum of three people. If you wish to exclude additional referees, please explain or justify your concerns—this information will be helpful for Editors when deciding whether to honor your request.

6. Editors and Journal Staff as Authors

Editorial independence is extremely important and OAE does not interfere with Editorial decisions. Editorial staff or Editors shall not be involved in processing their own academic work. Submissions authored by Editorial staff/Editors will be assigned to at least three independent outside reviewers. Decisions will be made by the Editor-in-Chief, including Special Issue papers. Journal staff are not involved in the processing of their own work submitted to any OAE journals.

7. Policy of the Use of AI and AI-assisted Technologies in Scientific Writing

Generative AI and AI-assisted technologies (e.g., large language models) are expected to be increasingly used to create content. In the writing process of manuscripts, using AI and AI-assisted technologies to complete key researcher work, such as producing scientific insights, analyzing and interpreting data or drawing scientific conclusions, is not allowed, and they should only be used to improve the readability and language of manuscripts.

AI and AI-assisted technologies should be used under human control and supervision as they may generate incorrect or prejudiced output, and they should not be listed as an author or co-author, nor cited as an author.

The use of AI and AI-assisted technologies should be disclosed by authors in their manuscripts, and a statement will be required in the final publication.

OAE will keep monitoring the development and adjust the policy when necessary.

8. Conflict of Interests

OAE journals require authors to declare any possible financial and/or non-financial conflicts of interest at the end of their manuscript and in the cover letter, as well as confirm this point when submitting their manuscript in the submission system. If no conflicts of interest exist, authors need to state "All authors declared that there are no conflicts of interest". We also recognize that some authors may be bound by confidentiality agreements, in which cases authors need to state "All authors declared that they are bound by confidentiality agreements that prevent them from disclosing their competing interests in this work".OAE will keep monitoring the development and adjust the policy when necessary.

9. Editorial Process

9.1 Pre-Check

New submissions are initially checked by the Managing Editor from the perspectives of originality, suitability, structure and formatting, conflicts of interest, background of authors, *etc*. Poorly prepared manuscripts may be rejected at this stage. If your manuscript does not meet one or more of these requirements, we will return it for further revisions.

Once your manuscript has passed the initial check, it will be assigned to the Assistant Editor, and then the Editor-in-Chief, or an Associate Editor in the case of a conflict of interest, will be notified of the submission and invited to review. Regarding Special Issue paper, after passing the initial check, the manuscript will be successively assigned to the Assistant Editor, and then to the Editor-in-Chief, or an Associate Editor in the case of conflict of interest for the Editor-in-Chief to review. The Editor-in-Chief, or the Associate Editor may reject manuscripts that they deem highly unlikely to pass peer review without further consultation. Once your manuscript has passed the Editorial assessment, the Associate Editor will start to organize peer-review.

All manuscripts submitted to *CES* are screened using CrossCheck powered by iThenticate to identify any plagiarized content. Your study must also meet all ethical requirements as outlined in our Editorial Policies. If the manuscript does not pass any of these checks, we may return it to you for further revisions or decline to consider your study for publication.

9.2 Peer Review

CES operates a single-blind review process, which means that reviewers know the names of authors, but the names of the reviewers are hidden from the authors. The scientific quality of the research described in the manuscript is assessed by a minimum of three independent expert reviewers. The Editor-in-Chief is responsible for the final decision regarding acceptance or rejection of the manuscript.

All information contained in your manuscript and acquired during the review process will be held in the strictest confidence.

9.3 Decisions

Your research will be judged on scientific soundness only, not on its perceived impact as judged by Editors or referees. There are three possible decisions: Accept (your study satisfies all publication criteria), Invitation to Revise (more work is required to satisfy all criteria), and Reject (your study fails to satisfy key criteria and it is highly unlikely that further work can address its shortcomings). All of the following publication criteria must be fulfilled to enable your manuscript to be accepted for publication:

Originality

The study reports original research and conclusions.

Data availability

All data to support the conclusions either have been provided or are otherwise publicly available.

Statistics

All data have been analyzed through appropriate statistical tests and these are clearly defined.

Methods

The methods are described in sufficient detail to be replicated.

Citations

Previous work has been appropriately acknowledged.

Interpretation

The conclusions are a reasonable extension of the results.

Ethics

The study design, data presentation, and writing style comply with our Editorial Policies.

9.4 Revisions

Authors are required to submit the revised manuscript within one week if minor revision is recommended while two weeks if major revision recommended or one month if additional experiments are needed. If authors need more than one month to revise their manuscript, we usually require the authors to resubmit their paper. We request that a document of point-to-point response to all comments of reviewers and the Editor-in-Chief or the Associate Editor should be supplied along with the revised manuscript to allow quick assessment of your revised manuscript. This document should outline in detail how each of the comments was addressed in the revised manuscript or should provide a rebuttal to the criticism. Manuscripts may or may not be sent to reviewers after revision, dependent on whether the reviewer requested to see the revised version. Apart from in exceptional circumstances, *CES* only supports a round of major revision per manuscript.

10. Contact Us

Journal Contact
Complex Engineering Systems Editorial Office
Suite 1504, Tower A, Xi'an National Digital Publishing Base, No. 996 Tiangu 7th Road, Gaoxin District, Xi'an 710077, Shaanxi, China.

Wen Zhang
Managing Editor
editorial@comengsys.com

Last updated on 2 June, 2023

www.oaepublish.com

Complex Engineering Systems
(*CES*)
Los Angeles Office
245 E Main Street Ste 107, Alhambra,
CA 91801, USA
E-mail: editorial@comengsys.com
Website: www.comengsys.com.